Improving Performance of Differential Space-Time Block Codes

by

Poramate Tarasak
B.Eng. , Chulalongkorn University, 1997
M.Eng., Asian Institute of Technology, 1999

A Dissertation Submitted in Partial Fulfillment of the Requirements
for the Degree of

DOCTOR OF PHILOSOPHY

in the Department of Electrical and Computer Engineering

Supervisor: Dr. Vijay K. Bhargava

ABSTRACT

Differential space-time block code (DSTBC) has its advantage in achieving spatial diversity without channel knowledge. This is particularly useful in multiple antenna systems where complicated multiple-input multiple-output (MIMO) channel estimation is bypassed. The objective of this research is to study a few ways to improve the performance of DSTBC at both transmit antenna and receive antenna sides. DSTBC formally originated in year 2000 has become one of the main research interests in the field of space-time coding. While much early research focused on the design of the DSTBC, many related research problems have remained.

This thesis investigates the peak-to-power average ratio (PAPR) problem inherent in DSTBC. Although the constellation input has constant modulus property (phase-shifted keying (PSK)-typed), the transmission constellation does not retain this property. When DSTBC is applied in practice, high PAPR may cause the nonlinear amplifier to operate in a nonlinear region which causes amplitude clipping or distortion. This thesis proposes some constraints on DSTBC mapping to avoid constellation expansion by trading-off data rate. The DSTBC without constellation expansion achieves full spatial diversity and trade-off between data rate and performance while it retains PSK transmission constellation. This thesis also introduces $\pi/4-DQPSK-STBC$ as an alternative way to tackle PAPR problem. The $\pi/4-DQPSK-STBC$ scheme, which extends naturally from $\pi/4-DQPSK$ applied in single antenna systems, achieves full spatial diversity with low complexity suboptimal decoder as well as PAPR reduction.

Conventional differential detection of DSTBC has about 3-dB performance degradation compared to coherent detection in quasi-static fading channels. The concept of multiple symbol differential detection (MSDD) in single antenna systems is borrowed to explore its use in DSTBC. Since MSDD for DSTBC has extremely high complexity, two low complexity schemes: multiple differential feedback detection (MDFD) and reduced search de-

tection (RSD) have been presented. They enable a larger observation length than MSDD and have higher performance gain with lower complexity.

Since an irreducible error floor exists with differential detection of DSTBC in time-varying channels and MSDD in quasi-static fading channels fails to operate, a receiver based on maximum-likelihood (ML) receiver is studied. An approximate ML receiver has been derived in the literature and shows significant error floor reduction. Nevertheless, the ML receiver was based on the assumption of fixed channel gains during one transmission block interval and some error floor still exists. In this thesis, an approximate ML receiver is scrutinized and an improved receiver has been proposed which outperforms the existing receiver by taking the previously mentioned assumption into account. A further reduction of error has been achieved. Extension to a soft-output receiver is studied on a concatenated coding scheme as well.

When transmit antenna spacing is not enough, there exists spatial correlation which leads to loss in diversity and hence performance degradation. This thesis proposes a modification of the approximate ML receiver to take into account the spatial correlation. A small improvement in performance gain and error floor reduction has been shown with this new receiver.

DSTBC alone does not provide coding gains. To achieve better performance, a concatenated coding scheme is a viable option. In this thesis, a concatenated coding scheme of trellis-coded modulation (TCM) and DSTBC has been studied. The design criteria have been derived and the concept of quasiregularity has been extended. Several new TCM schemes have been presented which outperform the existing TCM schemes designed for additive white Gaussian noise (AWGN) and fading channels.

Table of Contents

List of Tables

List of Figures

List of Abbreviations

AWGN	additive white Gaussian noise
BER	bit error rate
CR	conventional receiver
CSI	channel state information
DD	differential detection
DSTBC	differential space-time block codes
FER	frame error rate
IBI	intrablock interference
PSK	phase shifted keying
STBC	space-time block codes
MIMO	multiple-input multiple-output
ML	maximum-likelihood
MDFD	multiple differential feedback detection
MR	multistage receiver
MSDD	multiple symbol differential detection
PEP	pairwise error probability
RSD	reduced search detection
SNR	signal to noise ratio
TCM	trellis-coded modulation
VR	Viterbi receiver
VR-IBIC	Viterbi receiver with intrablock interference cancellation

List of Principal Symbols

a	channel gain
b	prediction coefficient
d	data symbol
$\boldsymbol{D}$	Alamouti's transmission matrix
$f_d T$	normalized Doppler frequency
L	observation length/error event length
N	frame length (in block interval)
p	eigenvalue
Q	prediction order
ρ	cross correlation between two channels
r	received symbol
R	autocorrelation
σ_w^2	noise variance
s	transmitted symbol
w	noise
y	channel plus noise process
z	combined value

Acknowledgement

I would like to express my deepest gratitude to my supervisor, Professor Vijay K. Bhargava, for his constant support, guidance and encouragement. I would also like to thank specially to Dr. Hlaing Minn for his helpful discussions and contributions on my work. Many thanks are due to my friends in the communication lab for lots of help. Finally, I am grateful to the UVic-Anand Fund for financial support during my first year of study and from the Natural Sciences and Engineering Research Council of Canada (NSERC) for financial support throughout the program.

Dedication

To My Parents

Chapter 1

Introduction

Emerging wireless applications such as mobile internet and multimedia service require future generations of mobile system to accommodate high data rate transmission with satisfactory performance. Due to limited resources and the hostile characteristics of mobile channels, design of efficient mobile communication systems remains a challenging task. Apart from fundamental limitations, which are bandwidth and power, communication via mobile channels experiences additional problems such as fading, intersymbol interference, time variation, and interference from the environment or other users.

Multipath propagation causes several signal paths to combine destructively at the receiver, i.e., fading. When the signal is in deep fade, the receiver can hardly detect the signal. If this situation exists for a long time, signal loss or severe bit-error rate (BER) performance will occur. This worst-case scenario can only be counteracted by providing an alternative communication channel which transfers the same information. This is referred to as diversity.

History suggests time diversity via an error control coding to deal with the detection error caused by mostly random noises. However, since deep fade can prolong the low SNR situation, burst errors will occur and may be beyond the correcting capability of the error control coding. Other forms of diversity techniques are needed. Frequency diversity is widely exploited in the context of orthogonal division multiplexing (OFDM) where it works effectively in frequency-selective fading channels. However if the channel is frequency flat, OFDM will not be able to provide frequency diversity. More recently, spatial diversity

achieved by using multiple antennas at the transmitter and/or receiver has become a popular approach. Since spatial diversity provides more than one physical communication channel, if one channel is in deep fade the receiver can still obtain the same information from other channels without the need for extra bandwidth or power.

Receive diversity employs multiple receive antennas and performs selection or maximum ratio combining to obtain best average signal-to-noise ratio (SNR) output. If two receive antennas have enough separation, receive diversity can provide a significant improvement. Receive diversity has been well-established in the literature and has been used in an uplink transmission where there are multiple receive antennas receiving signals from a single antenna at the mobile.

Recently, space-time coding which combines coding, modulation and multiple transmit antennas is one of the most popular techniques to achieve both time and spatial diversities. The information is encoded such that it spans both the time and space dimensions. Since space-time coding transmits the same information via multiple transmit antennas at the same time, it aims at providing diversity rather than providing higher data transmission rate.

Early space-time coding research assumed the availability of channel state information (CSI) at the receiver. From this assumption, Tarokh et. al. derived the design criteria for space-time codes in frequency-flat fading channels [1]. The codes have trellis representations and therefore Viterbi algorithm is used in the decoding. These codes are usually referred to as space-time trellis codes which provide diversity and coding gains. However, the codes suffer from the receiver complexity, which is exponential with the number of transmit antennas. There is another important class of space-time codes referred to as space-time block code (STBC) which have linear complexity receivers. STBC is proposed by Alamouti in [2] in which the code lies on the orthogonal matrix. Extensions of both classes of space-time codes are common to accommodate more than two transmit antennas and to other environments.

The assumption of the availability of the CSI at the receiver is questionable when the

mobile moves at high speed. In this situation, the channel condition changes rapidly and channel estimation becomes difficult or requires too many training symbols. There have been recent efforts to forego channel estimation by introducing differential schemes for multiple transmit antennas [3], [4], [5]. Since the transmission is in blocks, differential space-time block codes (DSTBC) or differential space-time modulation (DSTM) is referred to these schemes interchangeably.

Differential detection of DSTBC suffers 3-dB performance degradation compared to coherent detection in quasi-static fading channels with perfect CSI. The performance degrades more if the channel is time-varying and an irreducible error floor exists. Therefore, an efficient receiver design or a more complicated coding scheme is an important issue to improve the performance of a DSTBC system.

1.1 Previous Results

The following summarizes the main papers relevant to the research problems. More citations are included in each chapter.

Hughes proposed DSTM for two transmit antennas [5]. This paper provides a complete design criteria and code construction for two transmit antennas from group theory. The paper mentions a problem of constellation expansion occurring in DSTBC from [3] but provides no solution for such schemes directly. Instead, the paper adopts the notion of group codes using the symbols from PSK constellation in which constellation expansion does not occur.

Multiple symbol detection for DSTBC under quasi-static fading channels was proposed in [6]. The performance of DSTBC has been slightly improved due to increasing in the observation length but the paper does not extend to higher modulation schemes or more than two transmit antennas due to very high complexity.

Chiavaccini and Vitetta attacked the problem of detection of DSTBC under time-varying fading channels [7]. An irreducible error floor is substantially decreased by about an order

of magnitude in slow fading channels. However, the receiver is designed based on the assumption of fixed channel fading gains within a transmission block. This assumption leads to large performance degradation in fast fading channels.

Concatenated coding with space-time coding is an alternative to improve the performance of transmit diversity schemes. Trellis coded modulation (TCM) is considered as an outer code to concatenate with STBC in [8]. Design criteria have been derived but only a few hand-designed TCM codes were given. There is no comment on whether these TCM schemes can be used in the situation where CSI is absent.

1.2 Objectives

This study focuses on improving the performance of DSTBC at both transmitter and receiver sides. At the transmitter side, the problem of high peak-to-average power ratio (PAPR) is studied. Also, the design of a concatenated coding scheme of TCM and DSTBC is discussed. At the receiver side, the modified receiver scheme is studied under some environments such as time-varying and spatial correlation channels. The objectives are to:

1. present the problem of PAPR existing in DSTBC and propose ways of tackling it;
2. extend and analyze the existing DSTBC receiver and propose improved DSTBC receivers in order to further reduce the irreducible error floor;
3. design TCM schemes concatenated with DSTBC to further improve the performance of the system.

1.3 Contribution of This Thesis

The following contributions are made in this study.

1. A constraint mapping of DSTBC is introduced to avoid constellation expansion. The resultant codes use only phase-shifted keying (PSK) signal constellation and therefore reduces the PAPR. The connection of DSTBC without constellation expansion

and DSTM from groups is discussed. These schemes offer trade-offs between data rate and performance while ensuring that the signals are only in the PSK constellation.

2. As it is known that if the signal envelopes cross the zero points, nonlinear amplification will cause a spectral sidelobe resulting in deterioration of the performance. A modulation scheme whose signal envelope avoids crossing the zero point is preferable in practice. In single antenna systems, $\pi/4 - DPSK$ is a such scheme. In this thesis, a similar idea to $\pi/4 - DPSK$ is applied to DSTBC. This results in a novel transmission scheme called $\pi/4 - DQPSK - STBC$ which provides full spatial diversity and avoids the signal crossing the zero point at the same time. In addition, a suboptimum receiver is proposed in which very low complexity is achieved while providing almost the same performance as an optimal receiver.
3. Multiple symbol differential detection (MSDD) of STBC has been extended to longer observation lengths. Since it is known that the complexity of MSDD of STBC is prohibitively complex, two reduced complexity versions of MSDD are presented. One is decision feedback differential detection and the other is reduced search detection. Both schemes provide performance enhancement by enabling longer observation lengths which is almost impossible to do with MSDD. The schemes work on quasi-static fading channels while they collapse in fast time-varying channels.
4. For time-varying channels, a thorough analysis of the existing receiver which is an approximate maximum-likelihood (ML) receiver is given. An upper bound on the bit error rate (BER) performance is derived based on the standard union-Chernoff bounding of the pairwise error probability. The bound is evaluated by a residue theorem which possibly yields further insight to the behavior of DSTBC with this receiver. A new multistage receiver is proposed to tackle the assumption of fixed channel gains during a transmission block. The receiver applies the concept of multistage channel estimation and detection to deal with the varying channel gains which are viewed as intrablock interference. An outer convolutional code is also considered

with the multistage receiver. Soft-output information from the DSTBC multistage receiver is derived and its performance is compared with the hard-output multistage receiver.

5. The assumption of independent transmission paths between transmission antennas is relaxed. This means there exists spatial correlation which leads to performance degradation due to the loss in diversity. This thesis proposes an extension of an approximate ML receiver to take into account the spatial correlation. The new receiver exploits spatial correlation information in order to improve the BER performance. Further analysis for this type of receiver is extended as well.
6. Design criteria for TCM concatenated with DSTBC have been derived. The concept of quasiregular codes with respect to these criteria is extended. Based on these results, several new TCM schemes have been searched and are shown to outperform existing TCM schemes which are designed to be optimum for fading or AWGN channels.

1.4 Thesis Outline

The subsequent chapters are organized as follows. Chapter 2 presents the basic concept of DSTBC encoding and decoding for two or more transmit antennas as well as other related codes. The problem of PAPR with DSTBC is shown. In addition, DSTBC without constellation expansion and $\pi/4 - DQPSK - STBC$ are also proposed in this chapter.

Chapter 3 extends the application of MSDD of DSTBC for longer observation lengths and proposes two reduced complexity versions of MSDD.

Chapter 4 focuses on an approximate ML receiver and provides a thorough analysis. A multistage receiver is proposed and compared with existing receivers. In addition, soft-output multistage receiver is derived and compared with the hard-output receiver in a concatenated scheme with outer convolutional code.

Chapter 5 extends the receiver in Chapter 4 to accommodate the spatial correlation in

the channel. An analysis is also extended for this new receiver. The receiver is compared with an approximated ML receiver without spatial correlation.

Chapter 6 derives the design criteria of TCM concatenated with DSTBC under perfect interleaving and noninterleaving conditions. Several new TCM schemes which outperform the existing schemes are presented.

Chapter 7 proposes extensions and future work which include extensions to more than two transmit antennas, an optimal receiver for DSTBC in frequency-flat and frequency-selective fading channels and iterative decoding of the concatenated coding with DSTBC schemes.

Appendix A provides a detailed derivation of the upper bound on the bit error rate and the pairwise error probability of an approximate ML receiver by applying the residue theorem.

Chapter 2

Differential Space-Time Block Codes

2.1 Introduction

The purpose of this chapter is to explain the basic concept of DSTBC encoding and decoding, different types of mapping and their associated constellation, system model which will be referred to in later chapters. This chapter also discusses the peak-to-average power ratio problem caused by constellation expansion associated with certain type of DSTBC mapping and proposes ways to tackle it.

Since DSTBC is based on Alamouti's space-time block code, it is fruitful to include the background on Alamouti's scheme which is applied to coherent multiple antenna systems in Section 2.2. Section 2.3 explains the details of DSTBC encoding and decoding which also includes two types of mapping to be used throughout in this thesis. Section 2.4 describes a few extensions of DSTBC based on orthogonal design to more than two transmit antennas. Section 2.5 briefly discusses closely related differential modulation schemes and their advantages. Section 2.6 presents a constellation expansion problem inherited in DSTBC. Section 2.7 proposes DSTBC without constellation expansion for two or more transmit antennas based on Alamouti's scheme and orthogonal designs. Section 2.8 proposes a more practical DSTBC scheme without constellation expansion, the scheme which extends naturally from $\pi/4 - QPSK$ in single antenna systems. Section 2.9 provides a summary of this chapter.

2.2 Alamouti's Scheme

Before we explain the operation of DSTBC encoder and decoder, let us discuss the most popular STBC transmission scheme named Alamouti's scheme. The context is taken from [2] but the matrix setting is used here instead of the scalar one in [2] For two transmit antennas, Alamouti proposed an efficient transmission scheme which is in a matrix form [2]

$$\boldsymbol{D} = \begin{bmatrix} s_1 & s_2 \\ -s_2^* & s_1^* \end{bmatrix} \tag{2.1}$$

We refer to this matrix as a *transmission matrix* or a *transmission block*. The symbols s_1 and s_2 are from an M-ary constellation and are transmitted from the first and second antennas, respectively, at the first symbol interval. The symbols $-s_2^*$ and s_1^* are transmitted from the first and second antennas, respectively, at the second symbol interval. One important property of Alamouti's scheme is that the transmission matrix is an orthogonal matrix, i.e., $\boldsymbol{D}\boldsymbol{D}^H = \boldsymbol{D}^H\boldsymbol{D} = \boldsymbol{I}$ where ^{H} is the Hermitian operator and $\boldsymbol{I}$ is a 2-by-2 identity matrix. This property yields a remarkable linear complexity at the receiver.

Assume that the channel gains are fixed during a transmission matrix and there is one receive antenna, the received signals at the first and second symbol intervals, r_1 and r_2, can be written in a vector form as

$$\begin{bmatrix} r_1 \\ r_2 \end{bmatrix} = \begin{bmatrix} s_1 & s_2 \\ -s_2^* & s_1^* \end{bmatrix} \begin{bmatrix} a_1 \\ a_2 \end{bmatrix} + \begin{bmatrix} w_1 \\ w_2 \end{bmatrix} \tag{2.2}$$

where a_1, a_2 are channel gains from the first and second transmit antennas, respectively, w_1, w_2 represent additive white Gaussian noise (AWGN) generated as complex Gaussian random variables with zero mean and variance σ_w^2. To decode the symbols, the received signals in (2.2) can be written as

$$\begin{bmatrix} r_1 & -r_2^* \\ r_2 & r_1^* \end{bmatrix} = \begin{bmatrix} s_1 & s_2 \\ -s_2^* & s_1^* \end{bmatrix} \begin{bmatrix} a_1 & -a_2^* \\ a_2 & a_1^* \end{bmatrix} + \begin{bmatrix} w_1 & -w_2^* \\ w_2 & w_1^* \end{bmatrix} \tag{2.3}$$

Suppose the receiver has perfect channel gain information, coherent detection is possible by first linearly combining the receive signals by multiplying (2.3) by a matrix $\begin{bmatrix} a_1^* & a_2^* \\ -a_2 & a_1 \end{bmatrix}$ which yields

$$\begin{bmatrix} r_1 & -r_2^* \\ r_2 & r_1^* \end{bmatrix} \begin{bmatrix} a_1^* & a_2^* \\ -a_2 & a_1 \end{bmatrix} = \left(|a_1|^2 + |a_2|^2\right) \begin{bmatrix} s_1 & s_2 \\ -s_2^* & s_1^* \end{bmatrix} + \begin{bmatrix} w_1 & -w_2^* \\ w_2 & w_1^* \end{bmatrix} \begin{bmatrix} a_1^* & a_2^* \\ -a_2 & a_1 \end{bmatrix} \quad (2.4)$$

The elements in the first row of each side of (2.4) are written as

$$z_1 = r_1 a_1^* + r_2^* a_2 = \left(|a_1|^2 + |a_2|^2\right) s_1 + w_1 a_1^* + w_2^* a_2 \quad (2.5)$$

$$z_2 = r_1 a_2^* - r_2^* a_1 = \left(|a_1|^2 + |a_2|^2\right) s_2 + w_1 a_2^* - w_2^* a_1 \quad (2.6)$$

With this linear combining, each symbol will have low signal energy only if both transmission paths reflected in channel gains a_1, a_2 are in deep fade. Therefore, the symbol s_1 and s_2 enjoy two levels of diversity. Then, maximum-likelihood decoding is performed by

$$\min_{\hat{s}_i} \left| z_l - \left(|a_1|^2 + |a_2|^2\right) \hat{s}_i \right|^2, i = 1, 2, \ldots, M, l = 1, 2 \quad (2.7)$$

where $\hat{s}_i$ is a trial symbol. This shows the most important property of STBC which is the fact that maximum-likelihood decoding decouples the transmitted symbols. Therefore, decoding complexity does not grow exponentially with number of transmit antennas.

Alamouti's scheme was extended to more than two transmit antennas in [9] where STBC based on orthogonal design was introduced and some important properties were proved. Orthogonal design ensures linear decoding complexity. It is proved that Alamouti's scheme is a unique complex orthogonal design that provides full-rate and full-diversity STBC. For complex orthogonal design with full-diversity, the maximum rate of complex orthogonal design is 3/4 for three and four transmit antennas and the maximum rate is 1/2 for more than four transmit antennas [9]. More recent research reveals STBC with rate higher than 1/2 for five and six transmit antennas [10].

In this thesis, we would often refer to Alamouti's scheme, especially when we compare the performance between DSTBC and coherent detection of STBC.

2.3 DSTBC Encoding and Decoding

For a single transmit antenna system, differential phase-shift keying with differential detection (DPSK) has been a successful transmission scheme when the receiver does not use channel information. For two transmit antennas, there are a few main schemes for differential modulation. In this thesis, DSTBC from [3] is studied because of its simple encoding and decoding. The following material in this section is mostly summarized from [3] but presented with the matrix setting.

2.3.1 DSTBC Encoding

The DSTBC transmission matrix is shown in Alamouti's format as in (2.1). Suppose the previous transmission matrix is $\boldsymbol{D}_{n-1}$, differential encoding is performed by

$$\boldsymbol{D}_n = \boldsymbol{G}_n \boldsymbol{D}_{n-1} \tag{2.8}$$

where $\boldsymbol{D}_n = \begin{bmatrix} s_{2n} & s_{2n+1} \\ -s_{2n+1}^* & s_{2n}^* \end{bmatrix}$ represents a transmission matrix at the n^{th} block interval and $\boldsymbol{G}_n = \begin{bmatrix} g_{2n} & g_{2n+1} \\ -g_{2n+1}^* & g_{2n}^* \end{bmatrix}$ represents a data or information matrix at the n^{th} block interval. The n^{th} block interval contains the signal at symbol interval $2n$ and $2n+1$ for the system with two transmit antennas. The constellation of $\boldsymbol{D}_n$ is not needed to be the same as the constellation of $\boldsymbol{G}_n$ since matrix multiplication does not necessarily preserve the magnitude of the elements. The constellation of $\boldsymbol{D}_n$ is noted as a *transmission constellation* and the constellation of $\boldsymbol{G}_n$ is noted as a *mapping constellation*. The selection of the mapping constellation, i.e., the mapping from data bits to a data matrix, exists in a few ways in the literature. In this thesis, two different methods to choose a data matrix $\boldsymbol{G}_n$ will be discussed.

2.3.1.1 Tarokh&Jafarkhani's Mapping

The mapping originally proposed in [3] referred to Tarokh&Jafarkhani's mapping is done as follows. A vector $\boldsymbol{d}_n = [d_{2n}\ d_{2n+1}]^t$, which represents the n^{th} pair of data symbols, is selected from a unit energy M-ary (2^{n_d}-ary) PSK constellation according to the $2n_d$ data bits using Gray mapping. Then, a data matrix $\boldsymbol{G}_n$ is determined by forming an Alamouti's matrix of a data vector and multiplying it by a unitary matrix as

$$\boldsymbol{G}_n = \begin{bmatrix} g_{2n} & g_{2n+1} \\ -g_{2n+1}^* & g_{2n}^* \end{bmatrix} = \frac{1}{2} \begin{bmatrix} d_{2n} & d_{2n+1} \\ -d_{2n+1}^* & d_{2n}^* \end{bmatrix} \begin{bmatrix} 1 & -1 \\ 1 & 1 \end{bmatrix} \tag{2.9}$$

The factor $\frac{1}{2}$ in (2.9) ensures that the average total transmit power from two transmit antennas is one. It can be proved that this mapping yields all vectors $[g_{2n}\ g_{2n+1}]$ of equal length [3]. Most parts in this thesis will use this type of mapping.

2.3.1.2 Separate Mapping

Instead of mapping by (2.9), it is possible to select data symbols in $\boldsymbol{G}_n$ directly, i.e., the first n_d bits are mapped to g_{2n} and the second n_d bits are mapped to g_{2n+1}, chosen from a unit energy M-ary PSK constellation.

$$\boldsymbol{G}_n = \begin{bmatrix} g_{2n} & g_{2n+1} \\ -g_{2n+1}^* & g_{2n}^* \end{bmatrix} \qquad g_{2n}, g_{2n+1} \in M\text{-ary PSK} \tag{2.10}$$

This has an advantage of the ability to decouple each symbol in the decoding. So the decoding complexity does not grow exponentially with number of transmit antennas. However, this type of mapping generates more symbols in the transmission constellations which results in higher PAPR. In this thesis, this mapping will be used only in Chapter 6 which is more convenient when TCM concatenated with DSTBC is considered.

It can be verified that all the vectors $[g_{2n}\ g_{2n+1}]$ have equal lengths (norms) for both types of mapping. This property will be used in the differential decoding. Also, the error performance is equivalent for both types of mapping.

2.3.2 Differential Decoding

Analogously to DPSK and coherent detection of PSK, differential decoding of DSTBC without CSI has about 3-dB inferior performance compared to coherent detection of STBC. Differential decoding lies on the assumption of fixed channels during two transmission matrices. Let us define the following:

$$\boldsymbol{R}_n = \begin{bmatrix} r_{2n} & -r_{2n+1}^* \\ r_{2n+1} & r_{2n}^* \end{bmatrix}, \boldsymbol{D}_n = \begin{bmatrix} s_{2n} & s_{2n+1} \\ -s_{2n+1}^* & s_{2n}^* \end{bmatrix},$$
$$\boldsymbol{\Lambda} = \begin{bmatrix} a_1 & -a_2^* \\ a_2 & a_1^* \end{bmatrix}, \boldsymbol{W}_n = \begin{bmatrix} w_{2n} & -w_{2n+1}^* \\ w_{2n+1} & w_{2n}^* \end{bmatrix}, \tag{2.11}$$

where $\boldsymbol{R}_n$ is a received signal matrix at the n^{th} block interval, $\boldsymbol{\Lambda}$ is a channel gain matrix where time index has been omitted, $\boldsymbol{W}_n$ is a noise matrix at the n^{th} block interval. With these notations, the received signals at block interval n and $n-1$ can be written as

$$\boldsymbol{R}_n = \boldsymbol{D}_n\boldsymbol{\Lambda} + \boldsymbol{W}_n \quad \text{and} \quad \boldsymbol{R}_{n-1} = \boldsymbol{D}_{n-1}\boldsymbol{\Lambda} + \boldsymbol{W}_{n-1}. \tag{2.12}$$

Differential decoding is done by determining

$$\boldsymbol{R}_n\boldsymbol{R}_{n-1}^H = \boldsymbol{D}_n\boldsymbol{\Lambda}\boldsymbol{\Lambda}^H\boldsymbol{D}_{n-1}^H + \boldsymbol{D}_n\boldsymbol{\Lambda}\boldsymbol{W}_{n-1}^H + \boldsymbol{W}_n\boldsymbol{\Lambda}^H\boldsymbol{D}_{n-1}^H + \boldsymbol{W}_n\boldsymbol{W}_{n-1}^H, \tag{2.13}$$

Since $\boldsymbol{\Lambda}^H\boldsymbol{\Lambda} = \left(|a_1|^2 + |a_2|^2\right)\boldsymbol{I}$, thus substituting (2.8) into (2.13) yields

$$\boldsymbol{R}_n\boldsymbol{R}_{n-1}^H = \left(|a_1|^2 + |a_2|^2\right)\boldsymbol{G}_n + \boldsymbol{D}_n\boldsymbol{\Lambda}\boldsymbol{W}_{n-1}^H + \boldsymbol{W}_n\boldsymbol{\Lambda}^H\boldsymbol{D}_{n-1}^H + \boldsymbol{W}_n\boldsymbol{W}_{n-1}^H. \tag{2.14}$$

Because the last three terms on the right side of (2.14) are noise, and the factor $\left(|a_1|^2 + |a_2|^2\right)$ does not affect the decision if all vectors $[g_{2n}\ g_{2n+1}]$ have equal lengths (norms), differential decoding finds a data matrix $\hat{\boldsymbol{G}}$ whose Euclidean distance to $\boldsymbol{R}_n\boldsymbol{R}_{n-1}^H$ is minimum. Equivalently in a scalar form, let us define

$$z_1 = r_{2n}r_{2n-2}^* + r_{2n+1}^*r_{2n-1} \quad \text{and} \quad z_2 = r_{2n}r_{2n-1}^* - r_{2n+1}^*r_{2n-2}. \tag{2.15}$$

From (2.14) and for both Tarokh&Jafarkhani's mapping and separate mapping, differential decoding finds

$$\underset{\hat{g}_{2n},\hat{g}_{2n+1}}{\arg\min} \left|z_1 - \hat{g}_{2n}\right|^2 + \left|z_2 - \hat{g}_{2n+1}\right|^2. \tag{2.16}$$

Further simplification obtains

$$\arg\max_{\hat{g}_{2n},\hat{g}_{2n+1}} \mathrm{Re}\left(z_1^* \hat{g}_{2n} + z_2^* \hat{g}_{2n+1}\right). \tag{2.17}$$

For separate mapping, since the symbol g_{2n} and g_{2n+1} are independently chosen, they can be decoded separately. For Tarokh&Jafarkhani's mapping, all $[g_{2n}\ \ g_{2n+1}]$ pairs must be tried. Once g_{2n} and g_{2n+1} are chosen, the data bits can be recovered.

Note that for Tarokh&Jafarkhani's mapping, with a few extra computation steps, the symbols in the decoding can be decoupled as well. This is done by substituting (2.9) into (2.17). After a little manipulation, we obtain the decision rule

$$\arg\max_{\hat{d}_{2n},\hat{d}_{2n+1}} \mathrm{Re}\left(\left(z_1^* - z_2^*\right)\hat{d}_{2n} + \left(z_1^* + z_2^*\right)\hat{d}_{2n+1}\right), \tag{2.18}$$

where $\hat{d}_{2n}, \hat{d}_{2n+1}$ can be decoded separately.

2.4 DSTBC for More Than Two Transmit Antennas

Although this thesis concentrates on DSTBC with two transmit antennas, it is worthwhile to briefly discuss DSTBC for more than two transmit antennas. In Section 2.7.2, DSTBC without constellation expansion will also be extended to the case of more than two transmit antennas.

Due to its constraint on the orthogonality of transmission matrix, a small number of DSTBC schemes have been discovered. In [11], full-rate DSTBC with real constellations and half-rate DSTBC with complex constellations for four and three transmit antennas have been proposed.

For four transmit antennas and real constellations, the data matrix is of the form

$$\boldsymbol{G}_n = \begin{bmatrix} g_{4n+1} & g_{4n+2} & g_{4n+3} & g_{4n+4} \\ -g_{4n+2} & g_{4n+1} & -g_{4n+4} & g_{4n+3} \\ -g_{4n+3} & g_{4n+4} & g_{4n+1} & -g_{4n+2} \\ -g_{4n+4} & -g_{4n+3} & g_{4n+2} & g_{4n+1} \end{bmatrix} \tag{2.19}$$

and the transmission matrix is of the form

$$\boldsymbol{D}_n = \begin{bmatrix} s_{4n+1} & s_{4n+2} & s_{4n+3} & s_{4n+4} \\ -s_{4n+2} & s_{4n+1} & -s_{4n+4} & s_{4n+3} \\ -s_{4n+3} & s_{4n+4} & s_{4n+1} & -s_{4n+2} \\ -s_{4n+4} & -s_{4n+3} & s_{4n+2} & s_{4n+1} \end{bmatrix}. \tag{2.20}$$

Each row of $\boldsymbol{D}_n$ represents symbols to be transmitted from the first to the fourth transmit antennas at each symbol interval simultaneously.

For complex constellations, the data matrix as in (2.19) is still used while the obtained transmission matrix as in (2.20) from differential encoding is concatenated with its complex conjugate which yields a rate-1/2 DSTBC as

$$\boldsymbol{D}_n = \begin{bmatrix} s_{4n+1} & s_{4n+2} & s_{4n+3} & s_{4n+4} \\ -s_{4n+2} & s_{4n+1} & -s_{4n+4} & s_{4n+3} \\ -s_{4n+3} & s_{4n+4} & s_{4n+1} & -s_{4n+2} \\ -s_{4n+4} & -s_{4n+3} & s_{4n+2} & s_{4n+1} \\ s^*_{4n+1} & s^*_{4n+2} & s^*_{4n+3} & s^*_{4n+4} \\ -s^*_{4n+2} & s^*_{4n+1} & -s^*_{4n+4} & s^*_{4n+3} \\ -s^*_{4n+3} & s^*_{4n+4} & s^*_{4n+1} & -s^*_{4n+2} \\ -s^*_{4n+4} & -s^*_{4n+3} & s^*_{4n+2} & s^*_{4n+1} \end{bmatrix}. \tag{2.21}$$

Note that this differential encoding which applies (2.19) and (2.20) is a little different from what was presented in [11]. Here, the scheme can be written in terms of differential encoding explicitly as in (2.8). For three transmit antennas, differential encoding is the same as for four transmit antennas except that one column of the transmission matrix is omitted.

Differential decoding for both four and three transmit antennas is simplified from [11]

which is to determine

$$\begin{aligned} z_1 &= r_{4n+1}r^*_{4n-3} + r_{4n+2}r^*_{4n-2} + r_{4n+3}r^*_{4n-1} + r_{4n+4}r^*_{4n} \\ z_2 &= r_{4n+1}r^*_{4n-2} - r_{4n+2}r^*_{4n-3} - r_{4n+3}r^*_{4n} + r_{4n+4}r^*_{4n-1} \\ z_3 &= r_{4n+1}r^*_{4n-1} + r_{4n+2}r^*_{4n} - r_{4n+3}r^*_{4n-3} - r_{4n+4}r^*_{4n-2} \\ z_4 &= r_{4n+1}r^*_{4n} - r_{4n+2}r^*_{4n-1} + r_{4n+3}r^*_{4n-2} - r_{4n+4}r^*_{4n-3}. \end{aligned} \tag{2.22}$$

Thus, further simplification of differential decoding obtains the decision metric

$$\underset{\hat{g}_{4n+1},\hat{g}_{4n+2},\hat{g}_{4n+3},\hat{g}_{4n+4}}{\arg\max} \quad \mathrm{Re}\left(z_1^*\hat{g}_{4n+1} + z_2^*\hat{g}_{4n+2} + z_3^*\hat{g}_{4n+3} + z_4^*\hat{g}_{4n+4}\right) \tag{2.23}$$

2.5 Other Types of Differential Schemes for Multiple Transmit Antennas

As discussed so far, DSTBC refers to specific differential schemes in which the data matrix $\boldsymbol{G}$ acts a 'template' for data symbols to stay as elements of the matrix. In addition, both the data matrix and the transmission matrix are orthogonal matrices, i.e., $\boldsymbol{D}\boldsymbol{D}^H = \boldsymbol{D}^H\boldsymbol{D} = k_1\boldsymbol{I}$ and $\boldsymbol{G}\boldsymbol{G}^H = \boldsymbol{G}^H\boldsymbol{G} = k_2\boldsymbol{I}$, where k_1, k_2 are constants. However, there are other differential schemes for multiple transmit antennas for which the data matrix and the transmission matrix are not necessarily orthogonal. One significant class of such a scheme is referred to as differential space-time modulation (DSTM) and was proposed in [5] and [4]. Both papers consider data matrices to be unitary matrices because they can approach the capacity of unknown multiple-input multiple-output (MIMO) channels [12]. Since the unitary property is less strict than the orthogonal property, many more differential space-time schemes are possible.

Hughes presented an optimal DSTM constructed from a matrix group and proved that optimal DSTM based on groups is equivalent to a cyclic code or a dicyclic code only. For two transmit antennas, data matrices of a cyclic code are generated by a generator matrix

[5]

$$\begin{bmatrix} e^{j2\pi/M_g} & 0 \\ 0 & e^{j2\pi k/M_g} \end{bmatrix} \tag{2.24}$$

and data matrices of a dicyclic code are generated by generator matrices [5]

$$\begin{bmatrix} e^{j2\pi/(M_g/2)} & 0 \\ 0 & e^{-j2\pi k/(M_g/2)} \end{bmatrix}, \begin{bmatrix} 0 & -1 \\ 1 & 0 \end{bmatrix}, \tag{2.25}$$

where M_g is the number of data matrices belong to the group. For more than two transmit antennas, Hughes also classified DSTM based on group construction [13]. It is shown that for square transmission matrices and an odd number of transmit antennas, optimal DSTM is equivalent to a cyclic code in which the data matrices are generated by [13]

$$\begin{bmatrix} e^{j2\pi k_1/M_g} & 0 & \dots & 0 \\ 0 & e^{j2\pi k_2/M_g} & \dots & 0 \\ \vdots & \vdots & \ddots & \vdots \\ 0 & 0 & \dots & e^{j2\pi k_N/M_g} \end{bmatrix}. \tag{2.26}$$

For square transmission matrices and even number of transmit antennas, optimal DSTM is equivalent to either a cyclic code or dicyclic code in which the data matrices are generated by [13]

$$\begin{bmatrix} e^{j2\pi k_1/(M_g/2)} & 0 & \dots & 0 \\ 0 & e^{j2\pi k_2/(M_g/2)} & \dots & 0 \\ \vdots & \vdots & \ddots & \vdots \\ 0 & 0 & \dots & e^{j2\pi k_N/(M_g/2)} \end{bmatrix}, \begin{bmatrix} O & -\boldsymbol{I}_{N/2} \\ \boldsymbol{I}_{N/2} & 0 \end{bmatrix}. \tag{2.27}$$

The main reason for using DSTM from a group is that it simplifies searching for an optimal code, and the transmission matrices are guaranteed to avoid constellation expansion.

The seminal work which classifies DSTM based on unitary group for all possible rates and number of transmit antennas appeared in [14], while a systematic method of nongroup construction is only in its the beginning stages.

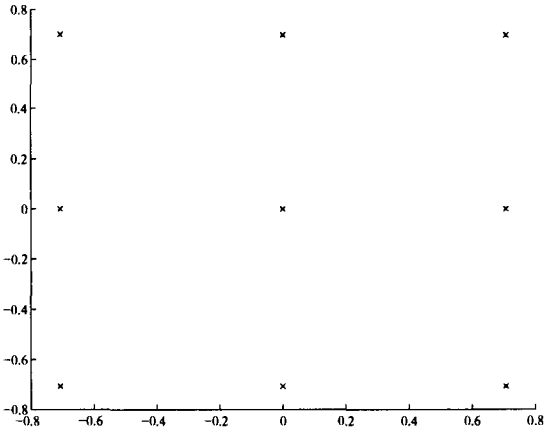

Figure 2.1. *Transmission constellation of DSTBC for two transmit antennas with data vectors in QPSK*

2.6 Constellation Expansion of DSTBC

Unlike DPSK in which the symbol generated by differential encoding by multiplying two PSK symbols results in another PSK symbol, DSTBC encoding by multiplying two PSK symbol matrices may not result in another PSK symbol matrix. First, let us consider DSTBC with Tarokh&Jafarkhani's mapping. If a data vector $\boldsymbol{d}_n = [d_{2n}d_{2n+1}]^t$ is chosen from a BPSK constellation, the transmission matrix will be in BPSK and no constellation expansion occurs. However, when a data vector $\boldsymbol{d}_n$ is chosen from a QPSK constellation, the obtained transmission matrix will be 9-QAM as in Fig. 2.1. For a data vector $\boldsymbol{d}_n$ in 8-PSK constellation, the transmission constellation expands even more. After two transmission block intervals, there are 57 possible symbols generated from differential encoding as shown in Fig. 2.2(a). After three transmission block intervals, there are 185 possible symbols generated from differential encoding as shown in Fig. 2.2(b). For separate mapping, we found that constellation expansion occurs and alternates between odd and even transmission block intervals. Figs. 2.3(a) and (b) show 9-QAM transmission constellation generated from differential encoding with separate mapping of QPSK symbols.

Constellation expansion leads to high PAPR problem which may cause shifting of the

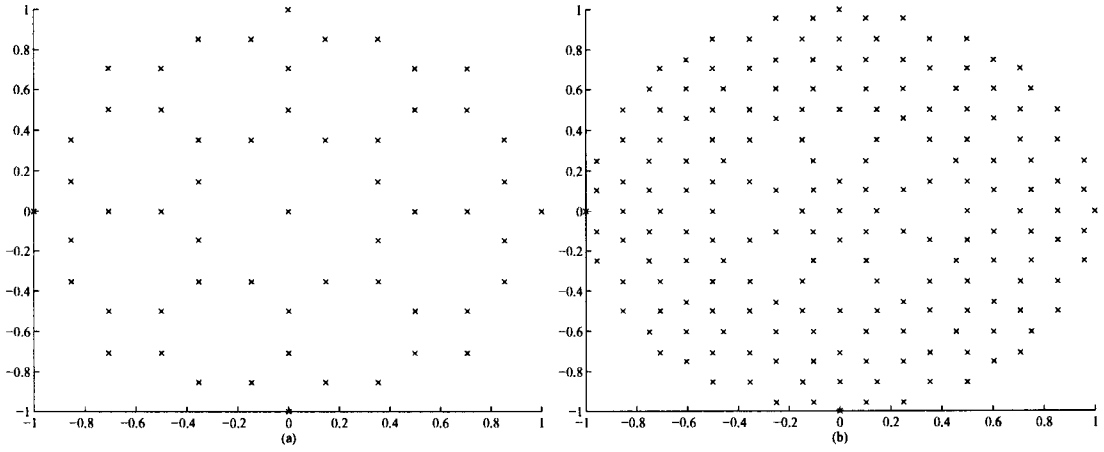

Figure 2.2. *Transmission constellation of DSTBC for two transmit antennas with data vectors in 8-PSK (a) after two transmission block intervals and (b) after three transmission block intervals*

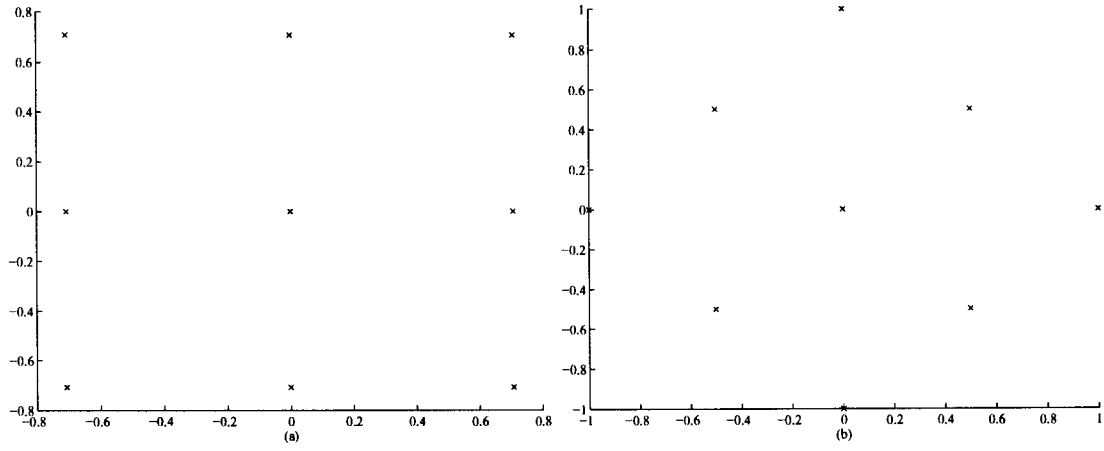

Figure 2.3. *Transmission constellation of DSTBC for two transmit antennas with data vectors in 8-PSK (a) for odd transmission block intervals and (b) for even transmission block intervals*

operation point of power amplifier to a nonlinear region which in turn producs power clipping and/or distortion. This problem was recently mentioned in [15] where trade-offs between diversity and PAPR and design of space-time in peak-power limited system were investigated. Since the transmission constellation is generated by the product of matrices of mapping constellation, it implies that the PAPR of the transmission constellation is greater than or equal to the PAPR of the mapping constellation [15].

2.7 DSTBC without constellation expansion

2.7.1 DSTBC without constellation expansion for two transmit antennas

Constellation expansion occurs from the addition in the matrix multiplication of differential encoding (2.8). For two transmit antennas, this addition can be avoided if the data matrices $\boldsymbol{G}_n$ are diagonal or antidiagonal. Specifically, two conditions are proposed

Condition 1: The data matrices for two transmit antennas are in the form

$$\begin{bmatrix} g_{2n} & 0 \\ 0 & g_{2n}^* \end{bmatrix} \text{ or } \begin{bmatrix} 0 & g_{2n+1} \\ -g_{2n+1}^* & 0 \end{bmatrix}.$$

Condition 2: The elements g_{2n}, g_{2n+1} are one of the M complex roots of unity.

Condition 1 ensures that there is no addition performed in the encoding. Condition 2 ensures that the encoding results only in the symbol rotation along the M-PSK signal constellation. These two conditions preserve the constellation size and shape. For a given constellation, the number of data matrices satisfying the above conditions is $2M$. Therefore, the code rate, which is defined as the number of transmitted symbols per channel use, is $\log_2(2M)/2\log_2 M$. Comparing to DSTBC without these conditions whose code rate is one means that the rate of the code is sacrificed to achieve constellation preservation.

Let us consider the examples of DSTBC without constellation expansion. Table 2.1 shows the mapping from the input bits to $[g_{2n}g_{2n+1}]$ with QPSK and 8-PSK constellation for

Table 2.1. *DSTBC for two transmit antennas with rate (a) 3/4,(b) 2/3*

(a)

input	$[g_{2n}, g_{2n+1}]$
000	$[1, 0]$
001	$[0, -1]$
011	$[0, -j]$
010	$[j, 0]$
110	$[0, 1]$
111	$[-1, 0]$
101	$[-j, 0]$
100	$[0, j]$

(b)

input	$[g_{2n}, g_{2n+1}]$
0000	$[1, 0]$
0001	$\left[\frac{1}{\sqrt{2}} + \frac{1}{\sqrt{2}}j, 0\right]$
0011	$[j, 0]$
0010	$\left[-\frac{1}{\sqrt{2}} + \frac{1}{\sqrt{2}}j, 0\right]$
0110	$[-1, 0]$
0111	$\left[-\frac{1}{\sqrt{2}} - \frac{1}{\sqrt{2}}j, 0\right]$
0101	$[-j, 0]$
0100	$\left[\frac{1}{\sqrt{2}} - \frac{1}{\sqrt{2}}j, 0\right]$
1100	$[0, -1]$
1101	$\left[0, -\frac{1}{\sqrt{2}} - \frac{1}{\sqrt{2}}j\right]$
1111	$[0, -j]$
1110	$\left[0, \frac{1}{\sqrt{2}} - \frac{1}{\sqrt{2}}j\right]$
1010	$[0, 1]$
1011	$\left[0, \frac{1}{\sqrt{2}} + \frac{1}{\sqrt{2}}j\right]$
1001	$[0, j]$
1000	$\left[0, -\frac{1}{\sqrt{2}} + \frac{1}{\sqrt{2}}j\right]$

DSTBC with two transmit antennas. The obtained codes have rate 3/4 and 2/3, respectively.

Decoding of DSTBC without signal constellation expansion is very simple. Due to Condition 1. of the mapping, decoding in (2.17) reduces to either

$$\max_{g_{2n}} \mathrm{Re}(R1^* g_{2n}) \text{ or } \max_{B} \mathrm{Re}(R2^* g_{2n+1}) \tag{2.29}$$

where g_{2n} and g_{2n+1} are two of the M roots of unity. The decoder chooses g_{2n} or g_{2n+1} as a decision component whichever yields a higher metric value. The other component is zero. Then, the decoder converts the decision vector back to the data bits. With this

decoding scheme, the number of comparisons required is the same as in (2.17) but there is no addition.

Note that the given mapping is chosen such that only one bit is different between two closest vectors $[g_{2n}\ g_{2n+1}]$'s (i.e., Gray mapping) with respect to their Euclidean distance. This choice of mapping follows naturally from distance property between mapping vectors which will be explained in Section 2.7.3.

2.7.2 DSTBC without Constellation Expansion for Four and Three Transmit Antennas

The constraints can be applied to an arbitrary number of transmit antennas, however, high rate loss will occur. Even in the case of a real constellation, the mapping constellation BPSK is expanded to 5-PAM in the transmission constellation. We suggest a mapping vector as in Table 2.2 to obtain a rate 3/4 DSTBC for four antennas. Rate 1/2 and rate 1/4 can also be constructed by further discarding some mapping vectors. The constellation is preserved to be BPSK. For other real constellations, the maximum rate of DSTBC without constellation expansion is $\log_2(4M)/4\log_2 M$. For complex constellations, the maximum rate of DSTBC for four antennas is 1/2 [11]. If we apply the constraints to avoid constellation expansion, the maximum rate will be $\log_2(4M)/8\log_2 M$.

For the case of three transmit antennas, a transmission matrix is obtained by deleting one column from the transmission matrix for four transmit antennas [11] while its maximum rate is still $\log_2(4M)/8\log_2 M$.

2.7.3 Connections Between DSTBC without Constellation Expansion and DSTM

As mentioned in [5], DSTBC for two transmit antennas with binary elements is a group code. We observe that DSTBC without signal constellation expansion is a group code as well. For example, the code in Table 2.1(a) corresponds to a dicyclic group code with

Table 2.2. *Rate 3/4 DSTBC for four and three transmit antennas*

input	$[g_{4n+1}\ g_{4n+2}\ g_{4n+3}\ g_{4n+4}]$
000	[1 0 0 0]
001	[0 0 0 1]
010	[0 1 0 0]
011	[0 0 1 0]
100	[0 0 −1 0]
101	[0 −1 0 0]
110	[0 0 0 −1]
111	[−1 0 0 0]

an initial matrix $\boldsymbol{D}_0 = \begin{bmatrix} 1 & 1 \\ -1 & 1 \end{bmatrix}$ and generator matrices $\left\{ \begin{bmatrix} j & 0 \\ 0 & -j \end{bmatrix}, \begin{bmatrix} 0 & -1 \\ 1 & 0 \end{bmatrix} \right\}$ which is actually a quarternion code in [5]. In general, since the data matrix $\boldsymbol{G}_n$ is of the form $\begin{bmatrix} g_{2n} & 0 \\ 0 & g_{2n}^* \end{bmatrix}$ or $\begin{bmatrix} 0 & g_{2n+1} \\ -g_{2n+1}^* & 0 \end{bmatrix}$, the generator matrix of the code is $\left\{ \begin{bmatrix} e^{j2\pi k/M} & 0 \\ 0 & e^{-j2\pi k/M} \end{bmatrix} \right\}$ for a cyclic code or $\left\{ \begin{bmatrix} e^{j2\pi k/M} & 0 \\ 0 & e^{-j2\pi k/M} \end{bmatrix}, \begin{bmatrix} 0 & 1 \\ -1 & 0 \end{bmatrix} \right\}$ for a dicyclic code. Consequently, decoding method in [5], or a reduced complexity version in [16] can be applied as well.

For four transmit antennas, the code in Table 2.2 corresponds to a dicyclic code with an initial matrix

$$\boldsymbol{D}_0 = \begin{bmatrix} 1 & 1 & 1 & 1 \\ -1 & 1 & -1 & 1 \\ -1 & 1 & 1 & -1 \\ 1 & 1 & -1 & 1 \end{bmatrix}$$

associated with the generator matrices

$$\begin{bmatrix} 0 & 0 & 0 & -1 \\ 0 & 0 & 1 & 0 \\ 0 & -1 & 0 & 0 \\ 1 & 0 & 0 & 0 \end{bmatrix}, \begin{bmatrix} 0 & 0 & 1 & 0 \\ 0 & 0 & 0 & 1 \\ -1 & 0 & 0 & 0 \\ 0 & -1 & 0 & 0 \end{bmatrix}$$

This code is equivalent to an optimal dicyclic group code in [13] ($R = 0.75$, Table III) but the symbols are in BPSK instead of QPSK. This code is one example of a group code that has the same performance as the optimal code in [13] but lives in a smaller constellation. It is still an interesting open problem to find such codes for other constellations and other numbers of transmit antennas.

Next, let us consider distance property of the code. The performance of DSTBC or full-rank DSTM for $\mathcal{N}$ transmit antennas, which can be written as $\boldsymbol{S}_n = \boldsymbol{G}_n \boldsymbol{D}_{n-1}$, is determined by *coding advantage* or *product distance* defined as [5]

$$\begin{aligned} \Lambda_P(\boldsymbol{D}_n, \tilde{\boldsymbol{D}}_n) &= \left| \left(\boldsymbol{D}_n - \tilde{\boldsymbol{D}}_n\right) \left(\boldsymbol{D}_n - \tilde{\boldsymbol{D}}_n\right)^H \right|^{\frac{1}{\mathcal{N}}} \\ &= \mathcal{N} \cdot \left| \left(\boldsymbol{G}_n - \tilde{\boldsymbol{G}}_n\right) \left(\boldsymbol{G}_n - \tilde{\boldsymbol{G}}_n\right)^H \right|^{\frac{1}{\mathcal{N}}} = 2\Lambda_P(\boldsymbol{G}_n, \tilde{\boldsymbol{G}}_n) \end{aligned}$$

where $|.|$ is the determinant of the matrix. Now, for DSTBC in which the data matrix is in a specific form $\begin{bmatrix} g_{2n} & g_{2n+1} \\ -g_{2n+1}^* & g_{2n}^* \end{bmatrix}$, the product distance between two codewords is

$$\Lambda_P(\boldsymbol{D}_n, \tilde{\boldsymbol{D}}_n) = 2 \cdot$$

$$\left| \begin{bmatrix} (g_{2n} - \tilde{g}_{2n}) & -(g_{2n+1} - \tilde{g}_{2n+1})^* \\ (g_{2n+1} - \tilde{g}_{2n+1}) & (g_{2n} - \tilde{g}_{2n})^* \end{bmatrix} \begin{bmatrix} (g_{2n} - \tilde{g}_{2n}) & -(g_{2n+1} - \tilde{g}_{2n+1})^* \\ (g_{2n+1} - \tilde{g}_{2n+1}) & (g_{2n} - \tilde{g}_{2n})^* \end{bmatrix}^H \right|^{\frac{1}{2}}$$

$$= 2 \cdot \left(|g_{2n} - \tilde{g}_{2n}|^2 + |g_{2n+1} - \tilde{g}_{2n+1}|^2 \right) = 2 \cdot \Lambda_E(\boldsymbol{G}_n, \tilde{\boldsymbol{G}}_n)^2$$

where $\Lambda_E(\boldsymbol{G}_n, \tilde{\boldsymbol{G}}_n)$ is defined as *Euclidean distance* between mapping vectors staying in the first row of $\boldsymbol{G}_n$ and $\tilde{\boldsymbol{G}}_n$. For general cases, if the data matrix is in a specific form

Table 2.3. *Properties of differential space-time block codes*

N	$\mathcal{C}$	$\mathcal{T}$	rate	$\hat{\Lambda}_E$
2	BPSK	BPSK	1/2	2
2	BPSK†	BPSK	1	1.414
2	QPSK	QPSK	3/4	1.414
2	QPSK†	9-QAM	1	1
2	8-PSK	8-PSK	2/3	0.7654
2	8-PSK†	57-APSK	1	0.7357
3,4	BPSK‡	5-PAM	1	1
3,4	BPSK	BPSK	3/4	1.414

Note: $\mathcal{C}$ is the mapping constellation

$\mathcal{T}$ is the transmission constellation

$\hat{\Lambda}_E$ is the minimum Euclidean distance between mapping vectors

† DSTBC from [3] ‡ DSTBC from [11]

such that $\boldsymbol{G}_n\boldsymbol{G}_n^H = \boldsymbol{G}_n^H\boldsymbol{G}_n = (|g_{2n}|^2 + |g_{2n+1}|^2 + \ldots + |g_{2n+\mathcal{N}}|^2)\,\boldsymbol{I}$, the product distance can be written as $\Lambda_P(\boldsymbol{D}_n, \tilde{\boldsymbol{D}}_n) = \mathcal{N}\Lambda_E(\boldsymbol{G}_n, \tilde{\boldsymbol{G}}_n)^2$. This means that the computation of product distance, which involves finding the determinant of the matrix, can be reduced to the computation of Euclidean distance between vectors only. This result is useful for DSTBC design with orthogonal data matrices, especially for a higher number of transmit antennas where the computation of the determinant is complicated. In addition, to have good bit error performance, it is natural to assign Gray mapping associated with mapping vectors with respect to the Euclidean distance between them.

2.7.4 Simulation Results

Table 2.3 lists different DSTBC schemes along with their properties. Rate 1/2 BPSK for two transmit antennas is included with the mapping vector [1 0] and [-1 0]. Note that DSTBC from [3] and [11] has minimum Euclidean distance equal to the minimum distance

between two closest symbols in the mapping constellation. To make a fair comparison between various DSTBC with different rates, we plot the bit error rate (BER) vs average energy per bit to noise power spectral density (E_b/N_0) which can be computed as $\frac{E_b}{N_0} = \frac{\text{SNR}}{\log_2 M \cdot \text{rate}}$, SNR is the signal to noise ratio defined in [3]. Fig. 2.4 shows the simulation results of DSTBC with and without constellation expansion for two transmit antennas. It is interesting to see that rate-1/2 BPSK, rate-1 BPSK, rate-3/4 QPSK and rate-1 9-QAM achieve the same performance. (This seems to be an analogy of BPSK and QPSK having the same performance in AWGN channels. Here DSTBC have more dimensions to place the symbols and so more possible rates) Among the codes, the rate-3/4 QPSK might be the most favorable scheme because it transmits 1.5 bps/Hz on average and does not expand the constellation. Rate-2/3 8-PSK and rate-1 57-APSK have higher transmission rates but they have inferior performance.

Fig. 2.5 shows the performance of DSTBC for four and three transmit antennas. In both cases, DSTBC with rate-3/4 BPSK has 1-dB gain to rate-1 5-PAM while the former transmits 0.75 bps/Hz and the latter transmits 1 bps/Hz. Due to the fact that DSTBC transmission matrix has the same format as that of STBC, all DSTBC schemes provide full spatial diversity. This can be seen from the slopes of the BER performances which are the same as original schemes from [3] and [11].

2.8 $\pi/4$–DQPSK–STBC

Differential detection avoids carrier recovery and yields fast synchronization. For mobile applications, the transmitted signal may have to be nonlinearly amplified [17] which is more power efficient than to be amplified with a linear amplifier. However, a nonlinear amplifier requires the modulation scheme to have small signal envelope fluctuations otherwise spectral sidelobes will occur. $\pi/4$–DQPSK has been a well-known scheme in such a scenario for single antenna systems. Its signal envelope avoids the zero-crossing point which causes nonlinearity in the nonlinear power amplification. Quantitatively, with a transmit

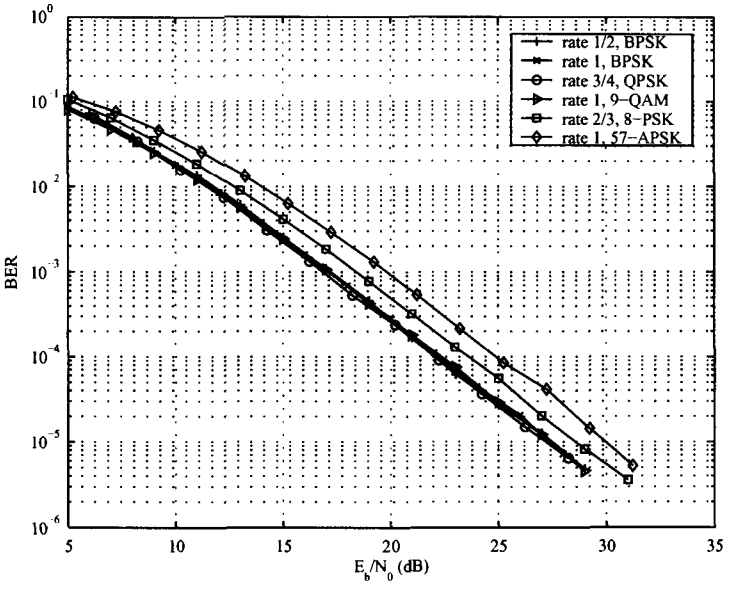

Figure 2.4. *Performance of DSTBC with two transmit antennas under quasi-static Rayleigh fading channel*

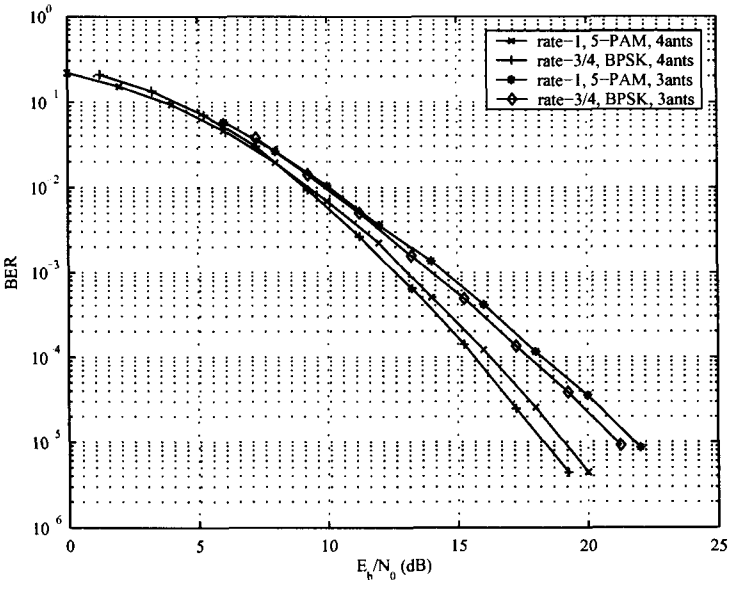

Figure 2.5. *Performance of DSTBC with four and three transmit antennas under quasi-static Rayleigh fading channel*

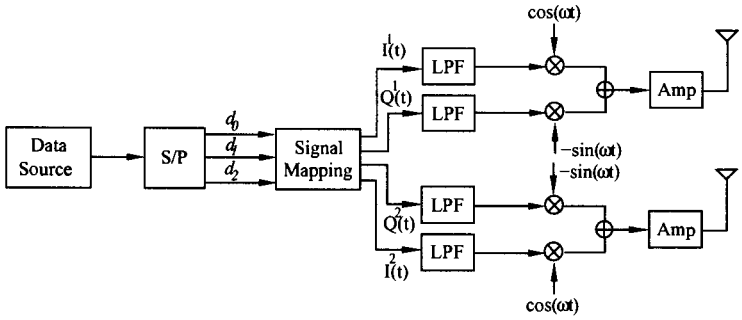

Figure 2.6. *$\pi/4$–DQPSK–STBC Transmitter Model*

filter with roll-off factor at 0.35, $\pi/4$–DQPSK has about 1.5 dB PAPR better than PSK modulation. This section introduces a specific $\pi/4$– shifted differential QPSK space-time block codes ($\pi/4$–DQPSK–STBC) which has peak-to-average power ratio improvement while sustains the same performance of the equivalent code.

2.8.1 $\pi/4$–DQPSK–STBC Transmitter Model

The main purpose of using $\pi/4$–DQPSK–STBC is to achieve full spatial diversity and small signal envelope fluctuations as well as low complexity transmitter and receiver. Similar to $\pi/4$–QPSK in single antenna systems, differential encoding and decoding of $\pi/4$–DQPSK–STBC is preferable to direct symbol mapping and coherent detection in terms of complexity [17]. The transmitter model of $\pi/4$–DQPSK–STBC is shown in Fig. 2.6. Three input data bits, $[d_0 d_1 d_2]$, enter signal mapping at each block transmission interval. One block interval occupies two symbol intervals. Therefore, the transmission rate of $\pi/4$–DQPSK–STBC is 1.5 bps/Hz. As an initial transmission block, the transmitter transmits a symbol block in the form of Alamouti's scheme [2]. The symbols $1/\sqrt{2}$ and $1/2 + j/2$ are transmitted from the first and second antennas, respectively, at the first symbol interval. Then, the symbols $-1/2 + j/2$ and $1/\sqrt{2}$ are transmitted from the first and second antennas, respectively, at the second symbol interval. Hence, the total transmit power is one.

Let $I^i(t)$ and $Q^i(t)$ denote the unfiltered baseband pulses in the in-phase and quadrature-

phase channel for transmit antenna i^{th}, respectively. The complex baseband symbol I_k^i and Q_k^m, which are the amplitudes of $I^i(t)$ and $Q^i(t)$ during symbol duration $kT \leq t < (k+1)T$, can be determined by the following rule:

(1) If $d_0 = 0$,

$$I_k^i = I_{k-2}^i cos(\phi_k) - Q_{k-2}^i sin(\phi_k)$$
$$Q_k^i = Q_{k-2}^i cos(\phi_k) + I_{k-2}^i sin(\phi_k)$$

(2) If $b_0 = 1$,

$$I_k^i = I_{k-1}^i cos(\phi_k) - Q_{k-1}^i sin(\phi_k)$$
$$Q_k^i = Q_{k-1}^i cos(\phi_k) + I_{k-1}^i sin(\phi_k)$$

for $i = 1, 2$, and at symbol interval $k+1$,

$$\begin{aligned} I_{k+1}^1 &= -I_k^2, Q_{k+1}^1 = Q_k^2 \\ I_{k+1}^2 &= I_k^1, Q_{k+1}^2 = -Q_k^1 \end{aligned} \tag{2.34}$$

The mapping from data bits to ϕ_k depends on $[d_0 d_1 d_2]$ which is shown in Table 2.4. With this mapping, it ensures that symbols transmitted from each antenna are from the QPSK constellation and the $\pi/4$-shifted QPSK constellation alternately. Note that (2.34) corresponds to the Alamouti's transmission scheme [2].

2.8.2 Property of $\pi/4$–DQPSK–STBC

We can readily show that $\pi/4$–DQPSK–STBC is a subset of DSTBC described in [3] with a reduced number of mapping vectors. It is also a group code. In fact, $\pi/4$–DQPSK–STBC is equivalent to a quarternion code in [5]. Suppose the set of generator matrices of the quarternion code is $\mathcal{G}$, the set of generator matrices of $\pi/4$–DQPSK–STBC $\mathcal{G}'$ is obtained by unitary transformation $\mathcal{G}' = U\mathcal{G}U^H$ where $U = \begin{bmatrix} e^{-j\pi/8} & 0 \\ 0 & e^{j\pi/8} \end{bmatrix}$. We obtain the generator matrices of $\pi/4$–DQPSK–STBC as $\left\{ \begin{bmatrix} j & 0 \\ 0 & -j \end{bmatrix}, \begin{bmatrix} 0 & -e^{-j\pi/4} \\ e^{j\pi/4} & 0 \end{bmatrix} \right\}$. Therefore,

Table 2.4. *Mapping for $\pi/4$–DQPSK–STBC*

$[b_0 b_1 b_2]$	ϕ_k
000	0
001	$-\pi/2$
010	$\pi/2$
011	π
100	$\pi/4$
101	$-\pi/4$
110	$3\pi/4$
111	$-3\pi/4$

the code achieves full diversity and the same symbol error performance as the quarternion code. The optimal receivers in [3] or [5] can be applied, however, in the following, the sub-optimal differential receiver is presented which performs very close to the optimal receiver but has less complexity.

2.8.3 $\pi/4$–DQPSK–STBC Receiver Model

The suboptimal differential receiver is similar to the receiver proposed in [16] at the beginning. Nevertheless, further simplification which exploits the structure of $\pi/4$–DQPSK–STBC can be done. We assume that one receive antenna is available. First, the receiver computes

$$\begin{aligned} z_1 &= r_{2n} r^*_{2n-2} + r^*_{2n+1} r_{2n-1} \\ z_2 &= r_{2n} r^*_{2n-1} - r^*_{2n+1} r_{2n-2} \end{aligned} \tag{2.35}$$

where r_k is the received signal at symbol interval k^{th}. The decision rule for the output bits, $[\hat{d}_0 \hat{d}_1 \hat{d}_2]$, is as follows:

1. If $|z_1| > |z_2|$, then $\hat{d}_0 = 0$. Then, the receiver determines $z_1 e^{j\pi/4}$.
   If $\mathrm{Re}[z_1 e^{j\pi/4}] > 0$, then $\hat{d}_1 = 0$, otherwise $\hat{d}_1 = 1$.

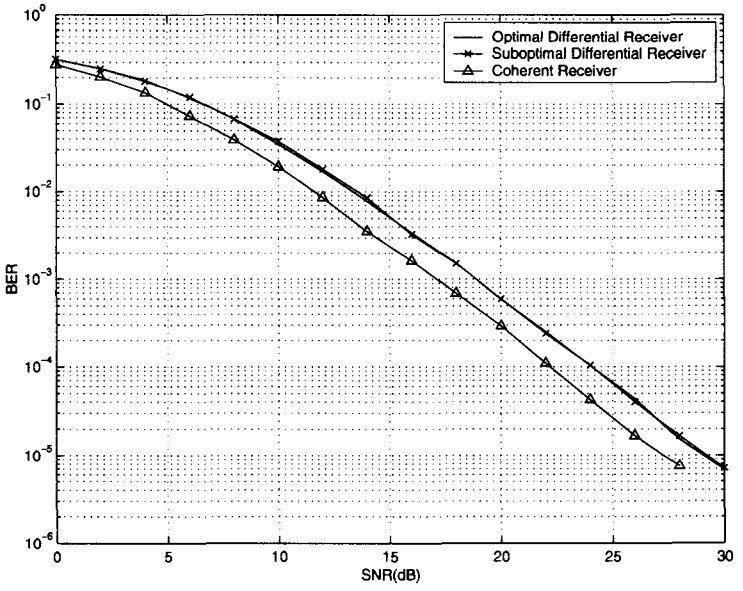

Figure 2.7. *Performance of $\pi/4$–DQPSK–STBC optimal, suboptimal differential receivers and coherent receiver, two transmit antennas and one receive antenna*

If $\text{Im}[z_1 e^{j\pi/4}] > 0$, then $\hat{d}_2 = 0$, otherwise $\hat{d}_2 = 1$.

2. If $|z_1| < |z_2|$, then $\hat{d}_0 = 1$.

   If $\text{Re}[z_2] > 0$, then $\hat{d}_1 = 0$, otherwise $\hat{d}_1 = 1$.

   If $\text{Im}[z_2] > 0$, then $\hat{d}_2 = 0$, otherwise $\hat{d}_2 = 1$.

With this suboptimal receiver, only three comparisons are needed to decode three input bits.

2.8.4 Simulation Results

Fig. 2.7 shows the performance of optimal and suboptimal differential receivers for $\pi/4$–DQPSK–STBC. The optimal differential receiver follows the approach in [3] or [5] in which seven comparisons are needed to decode three input bits. We can see that there is no visible difference of the performance between optimal and suboptimal differential receiver while both have about a 2-dB degradation as compared to a coherent receiver.

2.9 Summary

Basic concepts of DSTBC including encoding and decoding have been described in this chapter. Connections with other types of DSTBC and extension to more than two transmit antennas have been discussed. DSTBC without constellation expansion has been proposed for two, three and four transmit antennas accompanied with their bit-to-symbol mappings. DSTBC without constellation expansion offers tradeoff between data rate and BER performance while retaining the PSK symbol constellation in the transmission. A novel modulation scheme named $\pi/4 - DQPSK - STBC$ has been introduced along with its suboptimal decoding receiver. This modulation provides similar performance to a quarternion code with rate 1.5 bits/second while retaining the advantage of $\pi/4$-shifted signals.

Chapter 3

Block-Typed Receivers for DSTBC

3.1 Introduction

While conventional differential detection normally uses only two consecutive received blocks to detect DSTBC, performance improvements can be achieved by considering more than two received blocks. The purpose of this chapter is to discuss one category of DSTBC receiver so-called block-typed receiver which means that the receiver considers several received blocks at the same time and tries to make an optimal decision for several symbols simultaneously. After obtaining the detected symbols from these several blocks, the next several received blocks are treated independently from the previously detected symbols. This scheme is usually referred to as multiple symbol differential detection (MSDD).

Section 3.2 discusses MSDD for DSTBC. The decision metric is derived heuristically from the differential decoding equation which considers not only two consecutive received blocks but also next further blocks. Section 3.3 proposes two reduced complexity versions which are multiple differential feedback detection (MDFD) and reduced search detection (RSD). Section 3.4 provides simulation results and discussion. A summary of this chapter is given in Section 3.5.

3.2 Multiple Symbol Differential Detection of DSTBC

Multiple symbol differential detection (MSDD) has been known to fill the gap between differential detection of DPSK and coherent detection [18]. The basic idea is to extend the observation length and make a joint decision from more than two received symbols. For the case of DSTBC, MSDD extends the observation length and makes a joint decision from more than two received signal blocks. In [6], MSDD is applied to DSTBC and a small improvement is shown. However, only a specific case of three-block observation length with BPSK constellation was considered in the simulation. An extension of MSDD of DSTBC is derived in [19] where a general observation length is considered and the results include BPSK and QPSK constellations.

In the following, a heuristic approach to derive MSDD of DSTBC for a quasi-static fading channel is shown. The obtained metric corresponds to the one derived from maximum-likelihood approach in [19].

First let us consider the observation length of three blocks. Suppose the receiver has received matrices $\boldsymbol{R}_n, \boldsymbol{R}_{n-1}, \boldsymbol{R}_{n-2}$ and the channels are fixed during these intervals. Complementarily to the relation $\boldsymbol{R}_n\boldsymbol{R}_{n-1}^H$, the receiver determines

$$\boldsymbol{R}_n\boldsymbol{R}_{n-2}^H = \boldsymbol{D}_n\boldsymbol{\Lambda}\boldsymbol{\Lambda}^H\boldsymbol{D}_{n-2}^H + \boldsymbol{D}_n\boldsymbol{\Lambda}\boldsymbol{W}_{n-2}^H + \boldsymbol{W}_n\boldsymbol{\Lambda}^H\boldsymbol{D}_{n-2}^H + \boldsymbol{W}_n\boldsymbol{W}_{n-2}^H. \tag{3.1}$$

Using $\boldsymbol{\Lambda}^H\boldsymbol{\Lambda} = (|a_1|^2 + |a_2|^2)\,\boldsymbol{I}$ and $\boldsymbol{D}_n = \boldsymbol{G}_n\boldsymbol{G}_{n-1}\boldsymbol{D}_{n-2}$, (3.1) becomes

$$\boldsymbol{R}_n\boldsymbol{R}_{n-2}^H = \left(|a_1|^2 + |a_2|^2\right)\boldsymbol{G}_n\boldsymbol{G}_{n-1} + \boldsymbol{D}_n\boldsymbol{\Lambda}\boldsymbol{W}_{n-2}^H + \boldsymbol{W}_n\boldsymbol{\Lambda}^H\boldsymbol{D}_{n-2}^H + \boldsymbol{W}_n\boldsymbol{W}_{n-2}^H. \tag{3.2}$$

It is seen that the combined symbol $\boldsymbol{G}_n\boldsymbol{G}_{n-1}$ has two-level diversity and is affected by noise terms. Let us define the following

$$\begin{aligned}
z_{1,n|n-1} &= r_{2n}r_{2n-2}^* + r_{2n+1}^*r_{2n-1} \quad \text{and} \quad z_{2,n|n-1} = r_{2n}r_{2n-1}^* - r_{2n+1}^*r_{2n-2},\\
z_{1,n-1|n-2} &= r_{2n-2}r_{2n-4}^* + r_{2n-1}^*r_{2n-3} \quad \text{and} \quad z_{2,n-1|n-2} = r_{2n-2}r_{2n-3}^* - r_{2n-1}^*r_{2n-4},\\
z_{1,n|n-2} &= r_{2n}r_{2n-4}^* + r_{2n+1}^*r_{2n-3} \quad \text{and} \quad z_{2,n|n-2} = r_{2n}r_{2n-3}^* - r_{2n+1}^*r_{2n-4}.
\end{aligned} \tag{3.3}$$

We obtain the metric for MSDD with observation length of three as

$$\begin{aligned}\underset{\hat{g}_{2n-2},\hat{g}_{2n-1},\hat{g}_{2n},\hat{g}_{2n+1}}{\arg\min} & \left|z_{1,n|n-1}-\hat{g}_{2n}\right|^2+\left|z_{2,n|n-1}-\hat{g}_{2n+1}\right|^2+\left|z_{1,n-1|n-2}-\hat{g}_{2n-2}\right|^2 \\ + & \left|z_{2,n-1|n-2}-\hat{g}_{2n-1}\right|^2+\left|z_{1,n|n-2}-\hat{\chi}_{1,n|n-2}\right|^2+\left|z_{2,n-1|n-2}-\hat{\chi}_{2,n|n-2}\right|^2 \end{aligned} \quad (3.4)$$

where $\hat{\chi}_{1,n|n-2}=\hat{g}_{2n}\hat{g}_{2n-2}-\hat{g}_{2n+1}\hat{g}^*_{2n-1}$ and $\hat{\chi}_{2,n|n-2}=\hat{g}_{2n}\hat{g}_{2n-1}+\hat{g}_{2n+1}\hat{g}^*_{2n-2}$ represent combined symbols for the n^{th} and $(n-2)^{th}$ received blocks. Further simplification obtains

$$\begin{aligned}\underset{\hat{g}_{2n-2},\hat{g}_{2n-1},\hat{g}_{2n},\hat{g}_{2n+1}}{\arg\max} & \operatorname{Re}\Big(z^*_{1,n|n-1}\hat{g}_{2n}+z^*_{2,n|n-1}\hat{g}_{2n+1}+z^*_{1,n-1|n-2}\hat{g}_{2n-2}+z^*_{2,n-1|n-2}\hat{g}_{2n-1} \\ & +z^*_{1,n|n-2}\hat{\chi}_{1,n|n-2}+z^*_{2,n|n-2}\hat{\chi}_{2,n|n-2}\Big). \end{aligned} \quad (3.5)$$

In general, the product of $\boldsymbol{R}_{n-i}\boldsymbol{R}^H_{n-j}, i<j, i=0,1,\ldots,L-1$ can be written as

$$\boldsymbol{R}_{n-i}\boldsymbol{R}^H_{n-j}=\left(|a_1|^2+|a_2|^2\right)\boldsymbol{G}_{n-i}\boldsymbol{G}_{n-j+1}+\boldsymbol{D}_{n-i}\boldsymbol{\Lambda}\boldsymbol{W}^H_{n-j}+\boldsymbol{W}_{n-i}\boldsymbol{\Lambda}^H\boldsymbol{D}^H_{n-j}+\boldsymbol{W}_{n-i}\boldsymbol{W}^H_{n-j}. \quad (3.6)$$

The MSDD metric for observation length L becomes

$$\underset{\hat{g}_{2n-2(L-2)},\hat{g}_{2n-2(L-2)+1},\cdots,\hat{g}_{2n},\hat{g}_{2n+1}}{\arg\max} \operatorname{Re}\left(\sum_{i=0}^{L-1}\sum_{j=i+1}^{L} z^*_{1,n-i|n-j}\hat{\chi}_{1,n-i|n-j}+z^*_{2,n-i|n-j}\hat{\chi}_{2,n-i|n-j}\right) \quad (3.7)$$

where

$$\begin{aligned} z_{1,n-i|n-j} &= r_{2(n-i)}r^*_{2(n-j)}+r^*_{2(n-i)+1}r_{2(n-j)+1} \\ z_{2,n-i|n-j} &= r_{2(n-i)}r^*_{2(n-j)+1}-r^*_{2(n-i)+1}r_{2(n-j)} \end{aligned} \quad (3.8)$$

and the combined symbols can be computed recursively as

$$\begin{aligned} \hat{\chi}_{1,n-i|n-j} &= \hat{\chi}_{1,n-i|n-j+1}\hat{g}_{2(n-j+1)}-\hat{\chi}_{2,n-i|n-j+1}\hat{g}^*_{2(n-j+1)+1} \\ \hat{\chi}_{2,n-i|n-j} &= \hat{\chi}_{1,n-i|n-j+1}\hat{g}_{2(n-j+1)+1}+\hat{\chi}_{2,n-i|n-j+1}\hat{g}^*_{2(n-j+1)} \end{aligned} \quad (3.9)$$

where

$$\hat{\chi}_{1,n-i|n-i-1}=\hat{g}_{2(n-i)},\quad \hat{\chi}_{2,n-i|n-i-1}=\hat{g}_{2(n-i)+1}. \quad (3.10)$$

When the observation length is reduced to two, (3.7) becomes a differential detection metric (2.17). Similarly to MSDD of DPSK sequence, the receiver complexity grows exponentially with the observation length and the order of signal constellation [18]. The number of received block pairs $\boldsymbol{R}_{n-i}\boldsymbol{R}_{n-j}^{H}$ considered in the summation in (3.7) is $\binom{L}{2}$ and the number of symbols to be compared in the joint decision is $M^{2(L-1)}$, which is relatively large. The value two in the exponent is due to the block nature of space-time block code with two transmit antennas. If the number of transmit antennas is more than two, the decoder is even more complex. Hence, it is natural to consider reduced complexity schemes that have been applied successfully with DPSK to the case of DSTBC. Note that the MSDD metric in (3.7) corresponds to the optimal MSDD metric derived in [19] using the maximum likelihood criterion.

3.3 Reduced Complexity MSDD of DSTBC

3.3.1 Multiple Differential Feedback Detection

The computational complexity of the MSDD metric (3.7) can be reduced dramatically by using decision feedback. Multiple differential feedback detection (MDFD) assumes that all previous symbols have been detected correctly [20]. For DSTBC, all previous detected symbol blocks are substituted in the MSDD metric (3.7). Specifically, the trial symbols $\left\{\hat{g}_{2n-2(L-2)}, \hat{g}_{2n-2(L-2)+1}, \cdots, \hat{g}_{2n-2}, \hat{g}_{2n-1}\right\}$ are replaced by the ones previously detected. No joint decision between previous symbol blocks and present block is performed. The number of trial symbol blocks to be compared is equal to that of conventional differential detection, which is M^2. For example, for $L = 3$, the previously detected symbols $\tilde{g}_{2n-2}, \tilde{g}_{2n-1}$ replace the trial symbols $\hat{g}_{2n-2}, \hat{g}_{2n-1}$ (including those presenting in the combined symbols $\hat{\chi}_{1,n|n-2}, \hat{\chi}_{2,n|n-2}$) to determine (3.5).

MDFD is known to improve the performance over differential detection (DD) [20] but a performance degradation is observed due to error propagation. The same phenomenon is

observed in MDFD for DSTBC.

3.3.2 Reduced Search Detection

This approach tries to reduce the number of trial symbols in the MSDD decision metric. It is intuitive that the detection of $\tilde{g}_{2n}, \tilde{g}_{2n+1}$ from the received $[r_{2n-2}r_{2n-1}], [r_{2n}r_{2n+1}]$ is more reliable than using other received blocks which are further away. Therefore, reduced search detection (RSD) performs all comparisons for each adjacent received block pair using conventional differential detection metric and keeps q best symbols to be tentative decisions. Then, RSD determines decoded symbols from MSDD metric (3.7) by comparing only combinations of symbols from those tentative symbols. RSD performs joint decisions between several symbol blocks but the number of comparisons is reduced. For $q = 2$, the number of comparisons in the MSDD metric reduces to that of DSTBC with BPSK. The number of comparisons of RSD is $(L-1)M^2 + q^{2(L-1)}$ $(M > 2)$ which is much less than $M^{2(L-1)}$ in the optimal MSDD.

3.4 Simulation Results and Discussion

The simulation performances of DSTBC with MSDD and the above two reduced complexity MSDD schemes are studied. For DSTBC, Tarokh's mapping (2.9) is applied. The system consists of two transmit antennas and one receive antenna. The channel is a quasi-static Rayleigh fading channel. SNR is defined as the ratio of total transmit energy from two antennas, which is normalized to be one, and noise power spectral density N_0.

3.4.1 Performance of MSDD

Fig. 3.1 shows the performance of the optimal MSDD of DSTBC using BPSK. When $L = 3$, MSDD has about 0.5 dB gain over conventional differential detection (DD) $(L = 2)$ at BER 10^{-3}. Further gain can be improved by increasing the observation length L. The

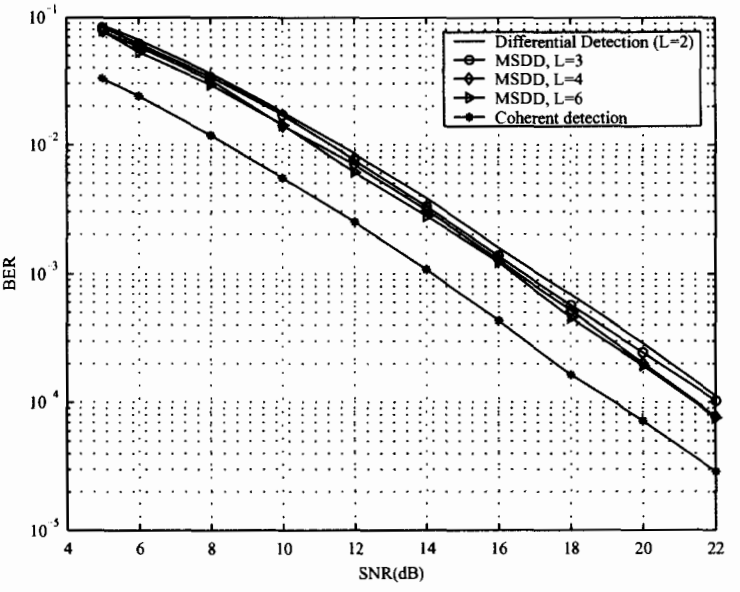

Figure 3.1. *Performance of MSDD of DSTBC with BPSK under quasi-static Rayleigh fading channel*

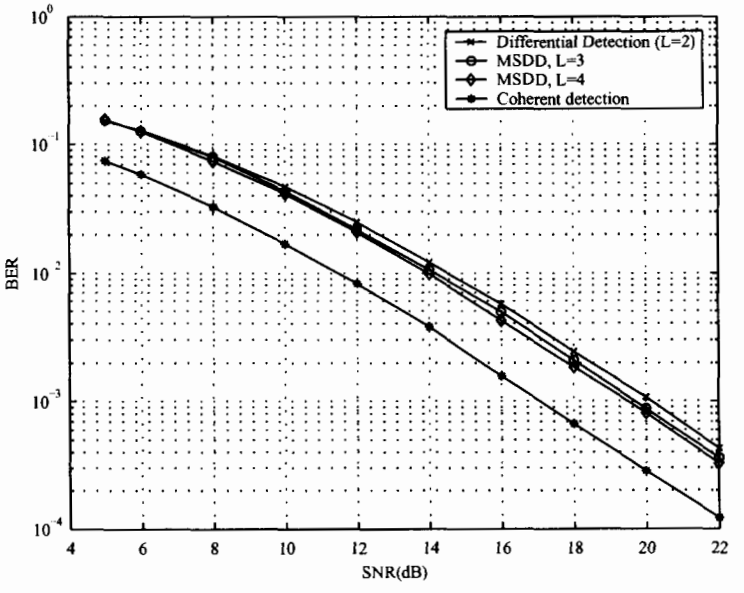

Figure 3.2. *Performance of MSDD of DSTBC with QPSK under quasi-static Rayleigh fading channel*

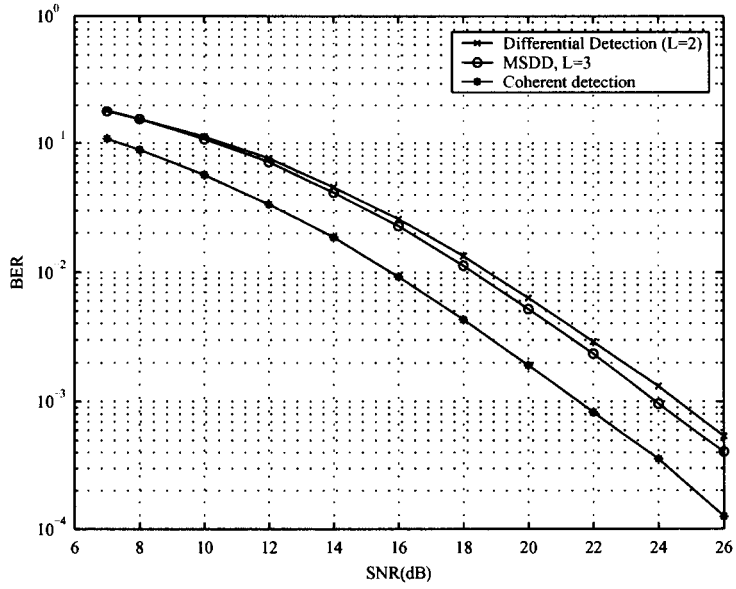

Figure 3.3. *Performance of MSDD of DSTBC with 8PSK under quasi-static Rayleigh fading channel*

largest gain is achieved when L is increased from two to three. With $L = 6$, the gain is about 0.8 dB at BER 10^{-3}. The improvement when L is greater than 6 is difficult to see. Fig. 3.2 and Fig. 3.3 show the performance of optimal MSDD of DSTBC using QPSK and 8-PSK, respectively. MSDD of QPSK with L greater than 4 and MSDD of 8-PSK with L greater than 3 are prohibitively complicated. For QPSK, maximum gain of MSDD is 0.7 dB over DD with $L = 4$ at BER 10^{-3}. And for 8-PSK, MSDD with $L = 3$ yields about 0.7 dB over DD at BER 10^{-3}.

3.4.2 Performance of MDFD

Fig. 3.4 compares the performance of MDFD and MSDD of DSTBC with BPSK. The performance degradation of MDFD compared to MSDD is extremely small for any values of L. With MDFD, the observation length can be made as large as $L = 21$ as in Fig. 3.5 and performance gain of 1 dB compared to conventional differential detection

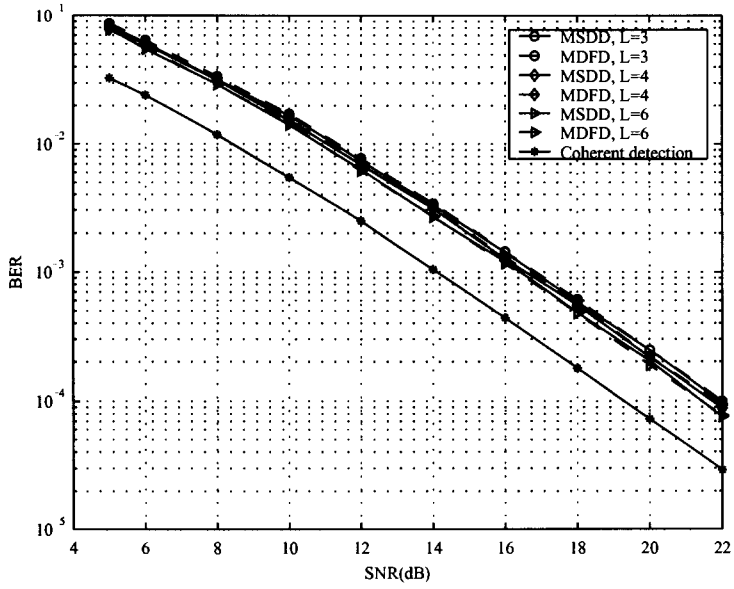

Figure 3.4. *Performance of MSDD vs MDFD of DSTBC with BPSK under quasi-static Rayleigh fading channel*

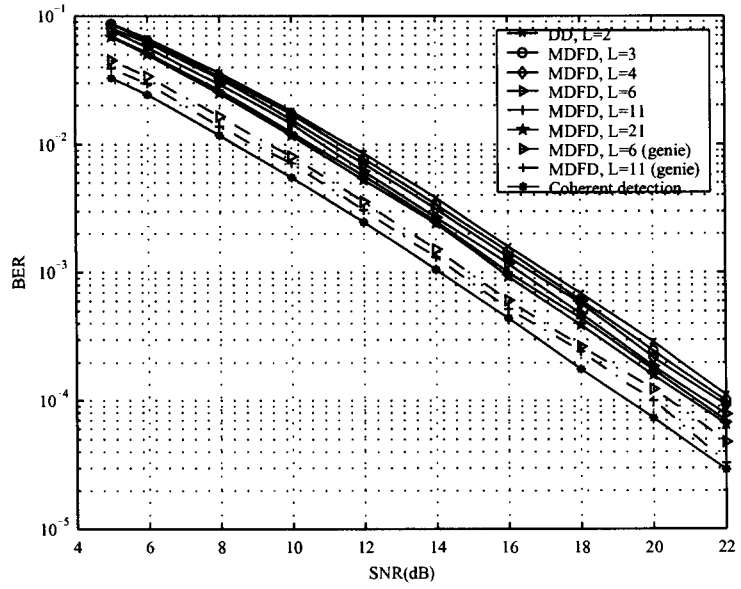

Figure 3.5. *Performance of MDFD with BPSK under quasi-static Rayleigh fading channel*

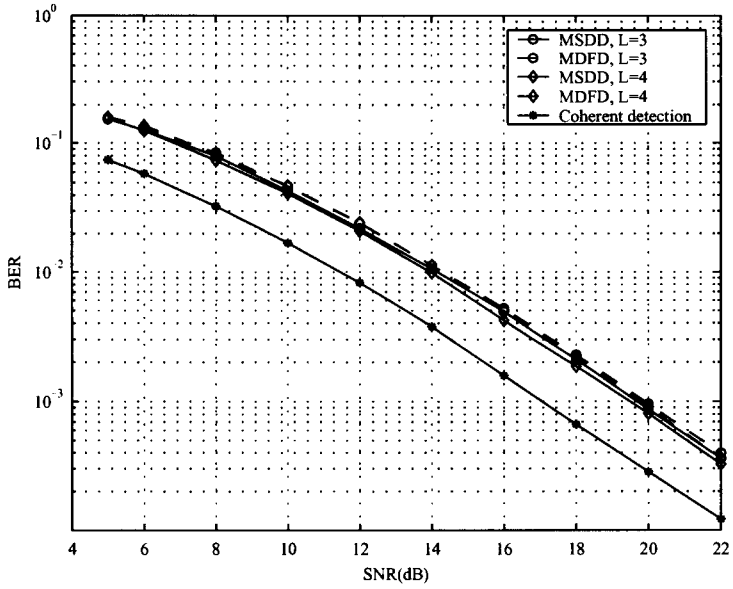

Figure 3.6. *Performance of MSDD vs MDFD of DSTBC with QPSK under quasi-static Rayleigh fading channel*

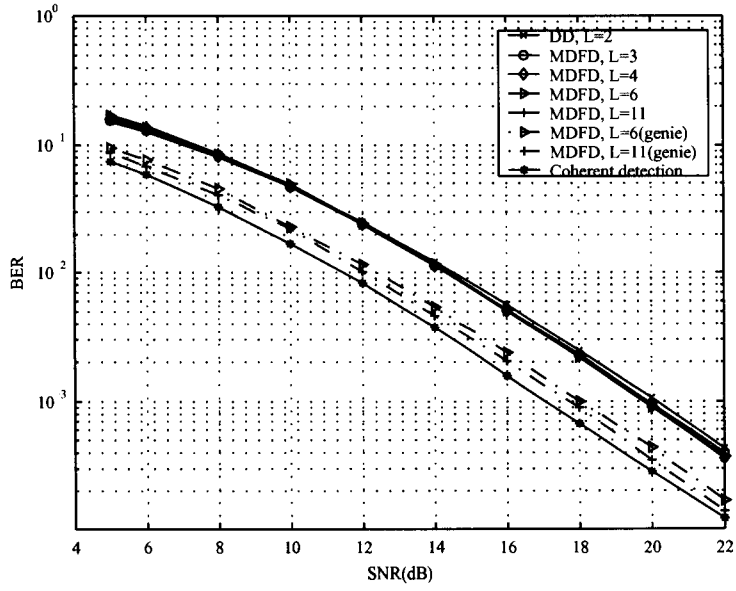

Figure 3.7. *Performance of MDFD with QPSK under quasi-static Rayleigh fading channel*

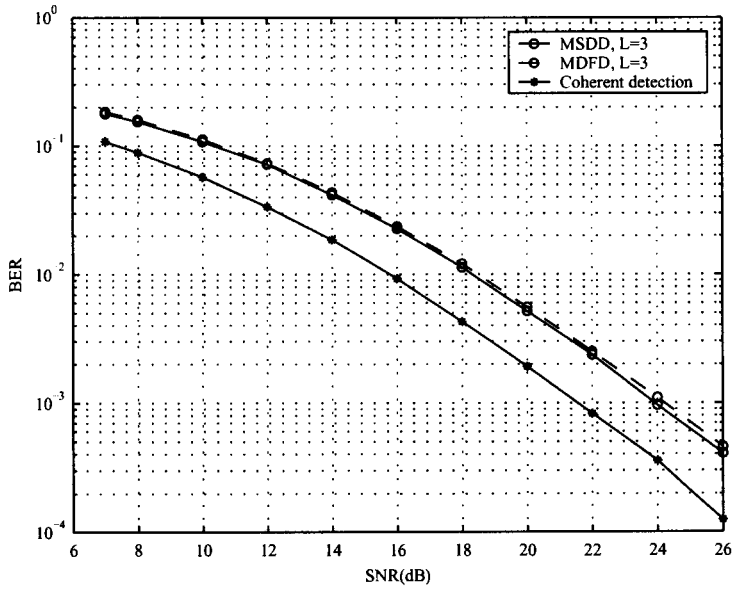

Figure 3.8. *Performance of MSDD vs MDFD of DSTBC with 8-PSK under quasi-static Rayleigh fading channel*

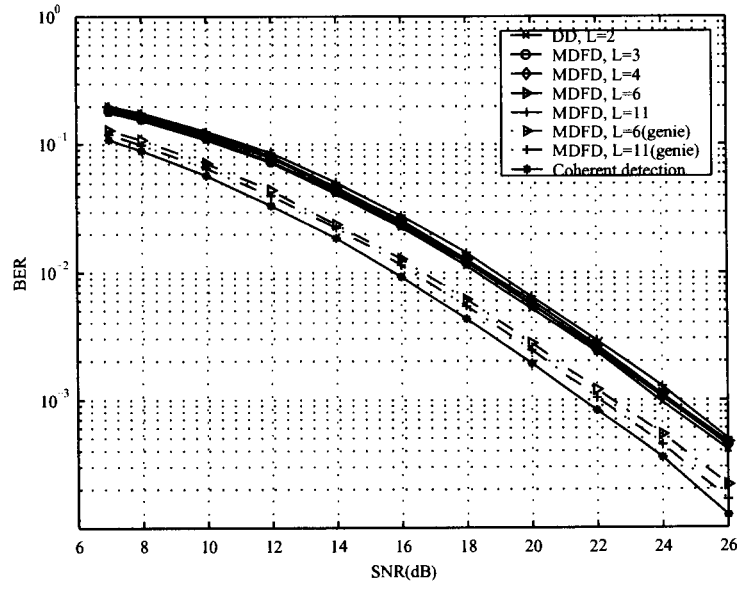

Figure 3.9. *Performance of MDFD with 8-PSK under quasi-static Rayleigh fading channel*

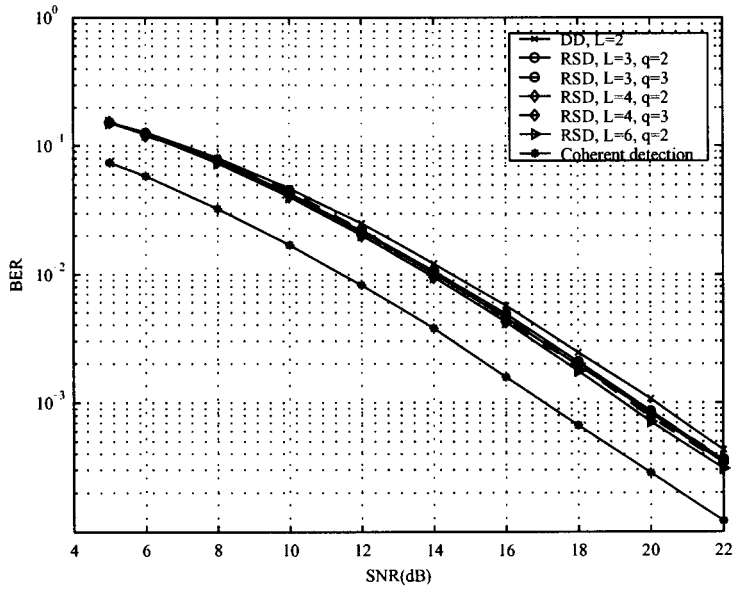

Figure 3.10. *Performance of RSD of DSTBC with QPSK under quasi-static Rayleigh fading channel*

is achieved. MDFD suffers from error propagation compared to genie decision feedback (correct decision feedback symbols). For genie decision feedback, MDFD can approach the performance of coherent detection with large L.

Fig. 3.6 and 3.8 compare the performance of MDFD and MSDD of DSTBC with QPSK and 8-PSK, respectively. MSDD of QPSK with L greater than 4 and MSDD of 8-PSK with L greater than 3 are prohibitively complicated. For QPSK, maximum gain over DD of MSDD is 0.7 dB with $L = 4$ at BER 10^{-3}. For 8-PSK, MSDD with $L = 3$ yields about 0.7 dB over DD at BER 10^{-3}. As in Fig. 3.7 and 3.9, MDFD provides 0.4 dB maximum gain regardless of L for both QPSK and 8-PSK DSTBC. In fact, increasing observation length L, MDFD results in performance degradation due to error propagation of incorrect feedback. This can be seen clearly in the case of 8-PSK whose performance with $L = 11$ and $L = 6$ are worse than that obtained with $L = 3$. With genie decision feedback, the performance of QPSK and 8-PSK can approach to that of coherent detection similar to the BPSK case.

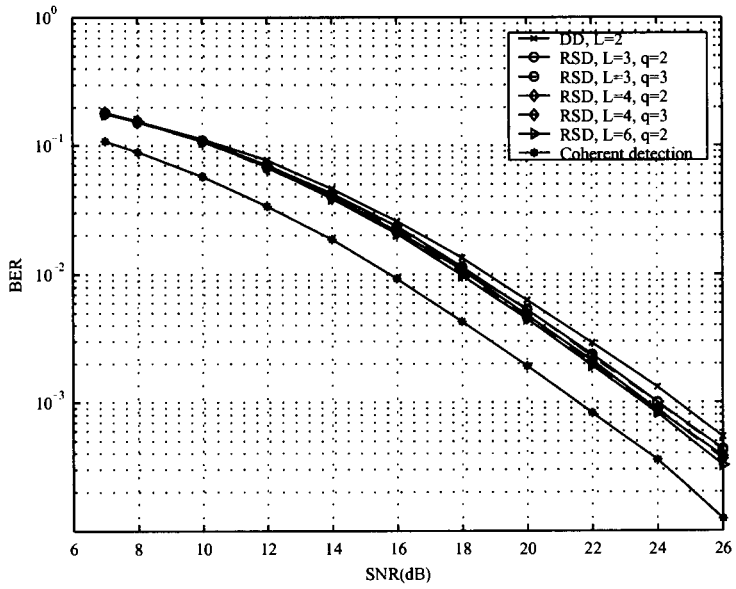

Figure 3.11. *Performance of RSD of DSTBC with 8-PSK under quasi-static Rayleigh fading channel*

3.4.3 Performance of RSD

Fig. 3.10 and 3.11 present the performance of reduced search detection of DSTBC with QPSK and 8-PSK, respectively. The effects of $q = 2, 3$ are also shown. It can be seen that increasing from $q = 2$ (solid line) to $q = 3$ does not improve the performance much in both QPSK and 8-PSK cases. About 1 dB gain can be achieved with $L = 6, q = 2$ for both QPSK and 8-PSK cases.

For QPSK, comparing Fig. 3.2 and 3.10 indicates the performance gain of RSD with $L = 6, q = 2$ over MSDD with $L = 4$ at lower complexity. The former requires $(6 - 1)4^2 + 2^{2(6-1)} = 1104$ comparisons while the latter requires $4^{2(4-1)} = 4096$ comparisons. Similarly, for 8-PSK, RSD with $L = 6, q = 2$ outperforms MSDD with $L = 4$ at lower complexity. The former requires $(6 - 1)8^2 + 2^{2(6-1)} = 1344$ comparisons while the latter requires $8^{2(3-1)} = 4096$ comparisons. Therefore, the performance gain achieved by RSD comes even at the reduction of complexity.

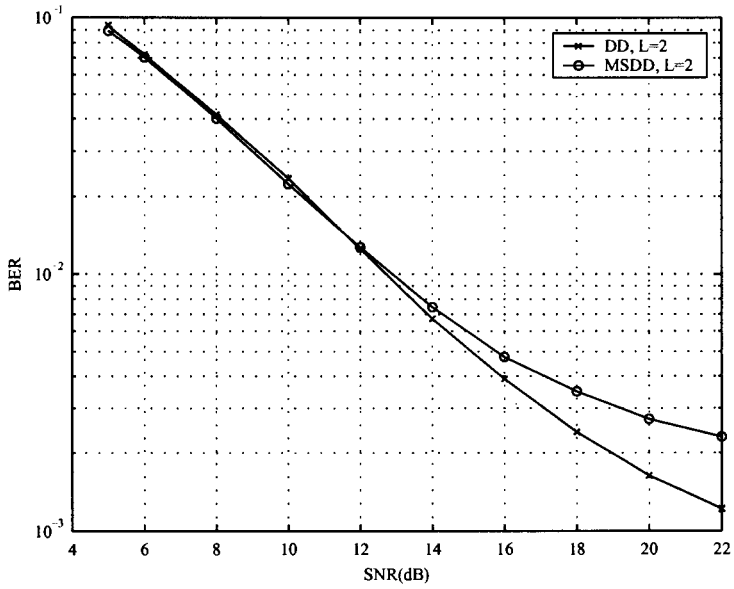

Figure 3.12. *Performance of MSDD with BPSK when the channel is time varying,* $f_dT = 0.02$

3.5 Performance of MSDD in Time-Varying Channels

MSDD and reduced complexity MSDD schemes presented so far work based on the assumption of fixed channel gains during a transmission frame. Therefore, they are applicable only to a fixed or very slowly varying channel. When the channel is time-varying, all the above MSDD and reduced complexity MSDD schemes seem to fail. Fig. 3.12 shows the performance of MSDD compared with DD of DSTBC with BSPK when the fading rate $f_dT = 0.02$. It is clear that MSDD with $L = 3$ has inferior performance to DD. This reflects the assumption of fixed channel gains during the observation length, which has more effect on MSDD.

The plots also indicate the trend of error floor at high SNR. In the next chapter, trellis-typed receivers will be derived. They are more appropriate to apply with time-varying channels.

3.6 Summary

This chapter presents the block-typed receiver for DSTBC. A heuristic MSDD metric has been derived which corresponds to the optimal metric from ML-criterion. The performance of MSDD of DSTBC with BPSK, QPSK and 8-PSK have been presented. Since MSDD with larger observation lengths seems to be an impossible solution, two reduced complexity schemes are proposed. MDFD performs well with BPSK and can improve the performance of MSDD over DD at the same number of comparisons of MSDD. However, MDFD suffers from performance degradation when applied with QPSK and 8-PSK due to error propagation. In this case, RSD is applied instead and it achieves an additional gain over MSDD by extending the length of observation with lower number of comparisons compared to MSDD. To conclude, the reduced complexity schemes for MSDD enable an increase in observation length to gain better performance over conventional DD.

Chapter 4

Trellis-Typed Receivers for DSTBC

4.1 Introduction

When the channel is time-varying, block-typed receivers perform poorly due to their assumption of fixed channel gains during the observation length. To circumvent this problem, an optimal receiver for time-varying channels has to be derived.

Several developments of ML receivers for PSK and DPSK in time varying channels for single antenna systems can be found in [21], [22], [23]. The main purpose of using an ML receiver is to mitigate an irreducible error floor which exists when DD is applied. This type of receiver is generally composed of two main components. The first component is a linear predictor which outputs predicted channel gains. The second component is a trellis-typed Viterbi receiver whose branch metric is the Euclidean distance between channel gain values obtained from received symbols and those obtained from the linear predictor. Usually, the Viterbi algorithm incorporating per-survivor processing yields low complexity receivers. These receivers have good performance and can reduce the error floor significantly.

In MIMO systems, there is some research focusing on improved receivers for DSTBC or DSTM in time varying channels. In [24], optimal receiver of DSTM applying MSDD and suboptimal receiver applying MDFD have been derived for flat Rayleigh fading channels. The suboptimal receiver provides large performance gains over conventional DD while the complexity increases moderately. Another suboptimal receiver of DSTM was derived in [25] where the prediction coefficients are designed without any knowledge of

the channel and noise statistics. It performs close to the optimal receiver when the maximum normalized (by signaling interval) Doppler frequency is low (~ 0.01). Both studies considered a DSTM signal with diagonal structure because it yields a simple decision rule. For DSTBC, an approximate ML receiver was derived in [7]. The receiver outperforms the conventional DD significantly. It reduces the error floor at least an order of magnitude.

In this chapter, we concentrate on Tarokh's DSTBC [3] for BPSK constellation. The receiver proposed in [7] is modified to compensate for the assumption of fixed channel coefficients during one transmission block. A multistage receiver is proposed for DSTBC. In the first stage, the same receiver as in [7] is applied. After the first stage, the receiver computes channel estimates from the tentative decision. These channel estimates will be exploited in later stages with modified detectors to subtract the so-called *intrablock interference* (IBI). The idea of iterative channel estimation and symbol detection has been applied elsewhere, for example, with multistage decision-directed receiver in DS-CDMA system [26]. However, this situation is different from all previous cases in terms of considering this special interference cancellation.

This chapter focuses on the approximate ML receiver for DSTBC derived in [7] with BPSK constellation. First, we further explore the structure of a linear predictor embedded in the receiver, study the performance of the receiver under mismatched SNR and fading rate conditions, and analyze the BER performance of the receiver by a union bound on the bit error probability. Second, a modified receiver, named *multistage receiver*, is proposed to mitigate IBI by exploiting channel estimates obtained from the detection at the first stage. A modified receiver yields further reduction of the error floor left from an approximate ML receiver. This chapter is organized as follows. Section 4.2 describes system model. Section 4.3 briefly summarizes conventional differential receiver and approximate ML receiver. Section 4.4 discusses the structure of the linear predictor and its properties. Section 4.5 studies the receiver with mismatched SNR and fading rate values by means of simulation. Section 4.6 evaluates the upper bound on the BER of the approximate ML receiver. Section 4.7 proposes a multistage receiver and its operation. Section 4.8 presents simulation results

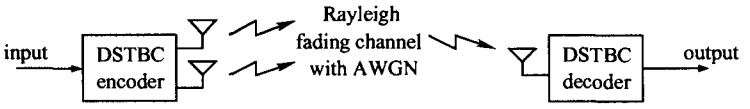

Figure 4.1. *System model*

and discussion on multistage receiver. Section 4.9 discusses the multistage receiver with an outer convolutional code. Section 4.10 derives the soft-output from an approximate ML receiver to be used in the convolutional code decoder and presents its performance. A summary of this chapter is given in Section 4.11.

4.2 System Model

The system model shown in Fig. 4.1 and notations follow from [7] with Tarokh&Jafarkhani's mapping DSTBC mapping in (2.9). The system consists of two transmit antennas and one receive antenna. The extension to more than two transmit antennas can be done by applying DSTBC from [11] and extension to more than one receive antenna is straightforward.

With BPSK constellation, differential encoding in this manner preserves the constellation. The system achieves 1 bit/sec/Hz transmission rate and enjoys two orders of diversity. For higher modulation schemes, the approach in [7] and in this paper can still be applied. However, the complexity of the receiver will be higher due to constellation expansion.

In contrast to Chapter 2 and 3, the channel considered is a time-varying, frequency-flat Rayleigh fading channel with Doppler power spectrum according to Jakes model. The channels corresponding to different transmit antennas are assumed to be independent and identically distributed. Let $a_i[n]$ denote the fading process corresponding to the i^{th} transmit antenna where $i = 1, 2$. Then, $a_1[n]$ and $a_2[n]$ are zero mean complex Gaussian random variables, each with unit variance and autocorrelation $R_{a_i}[m] = R_a[m] = J_0(2\pi f_d T m)$ where $J_0(\cdot)$ is the zeroth-order Bessel function of the first kind, $f_d T$ is the normalized fading rate or normalized maximum Doppler frequency.

The receiver in [7] assumes constant channel gains within a transmission block, i.e.,

during the $(2n)^{th}$ and $(2n+1)^{th}$ signaling intervals. With this assumption, the received signal vector $\boldsymbol{r}_n = [r_{2n}\ r_{2n+1}]^t$ can be written as [7]

$$\boldsymbol{r}_n = \boldsymbol{D}_n \boldsymbol{a}_n + \boldsymbol{w}_n \tag{4.1}$$

where $\boldsymbol{a}_n = [a_1[2n]\ a_2[2n]]^t$ is a channel gain vector and $\boldsymbol{w}_n = [w_{2n}\ w_{2n+1}]^t$ is a noise vector. The elements w_{2n} and w_{2n+1} are zero mean complex Gaussian random variables, each with variance $1/(2\text{SNR}) = \sigma_w^2/2$ per dimension.

4.3 Conventional Receiver and Approximate ML Receiver

Differential detection of DSTBC assumes fixed channel gains during two consecutive transmission blocks. It is known that differential detector is optimal for a quasi-static channel [7]. From Section 2.3.2, the receiver computes a vector $\boldsymbol{z}_n = [z_n^1\ z_n^2]^t$, with $z_n^1 = r[2n]r^*[2n-2] + r^*[2n+1]r[2n-1]$ and $z_n^2 = r[2n]r^*[2n-1] - r^*[2n+1]r[2n-2]$. The decision rule of this receiver is

$$\hat{\boldsymbol{d}}_n = \arg\min_{\boldsymbol{d}_n} \|\boldsymbol{z}_n - \boldsymbol{g}_n\|^2. \tag{4.2}$$

where $\boldsymbol{g}_n = [g_{2n}\ g_{2n+1}]$ and $\|.\|^2$ is a square Euclidean norm of a vector. This receiver will be noted as a *conventional receiver* (CR) [7].

An approximate ML receiver is derived in [7]. It is *approximate* in the sense that it was derived based on the assumption of fixed channel gains during a transmission block while actual fading channels change continuously. The receiver applies the Viterbi algorithm on a trellis representation of all possible transmitted sequences. The detected sequence, $\hat{\boldsymbol{D}}_0, \hat{\boldsymbol{D}}_1, \ldots, \hat{\boldsymbol{D}}_{N-1}$, is the one which maximizes the log-likelihood function

$$l(\boldsymbol{r}|\boldsymbol{s}) = -\sum_{n=0}^{N-1} \left\| \boldsymbol{D}_n^H \boldsymbol{r}_n - \hat{\boldsymbol{a}}_n \right\|^2 \tag{4.3}$$

where $\hat{\boldsymbol{a}}_n = \sum_{k=1}^{Q} b_k^Q \boldsymbol{D}_{n-k}^H \boldsymbol{r}_{n-k}$ represents the Q^{th} order prediction of $\boldsymbol{a}_n$. $\{b_1^Q b_2^Q \ldots b_Q^Q\}$ is a set of linear prediction coefficients of the process $\boldsymbol{y}_n = \boldsymbol{D}_n^H \boldsymbol{r}_n = \boldsymbol{a}_n + \boldsymbol{w}_n$ [7]. Later,

we will omit the superscript Q in b_k^Q as it is clear that a Q^{th} order linear predictor is being used. The prediction coefficients can be determined from Cholesky decomposition of the matrix $\boldsymbol{M}^{-1} = \boldsymbol{B}^H \Xi \boldsymbol{B}$ where

$$\boldsymbol{M} = \begin{bmatrix} R_a[0] + \sigma_w^2 & R_a[-2] & \dots & R_a[-2Q] \\ R_a[2] & R_a[0] + \sigma_w^2 & \dots & R_a[-2(Q-1)] \\ \vdots & \vdots & \ddots & \vdots \\ R_a[2Q] & R_a[2(Q-1)] & \dots & R_a[0] + \sigma_w^2 \end{bmatrix} \tag{4.4}$$

and

$$\boldsymbol{B} = \begin{bmatrix} -b_0^0 & 0 & 0 & \dots & 0 \\ -b_1^1 & -b_0^1 & 0 & \dots & 0 \\ -b_2^2 & -b_1^2 & -b_0^2 & \dots & 0 \\ \vdots & \vdots & \vdots & \ddots & \vdots \\ -b_Q^Q & -b_{Q-1}^Q & -b_{Q-2}^Q & \dots & -b_0^Q \end{bmatrix}, \tag{4.5}$$

Ξ is a diagonal matrix containing inverse mean square values of prediction error as diagonal elements. After the receiver obtains the detected sequence $\{\hat{\boldsymbol{D}}_0, \hat{\boldsymbol{D}}_1, \dots, \hat{\boldsymbol{D}}_{N-1}\}$, it can determine the data sequence $\{\hat{\boldsymbol{G}}_1, \hat{\boldsymbol{G}}_2, \dots \hat{\boldsymbol{G}}_{N-1}\}$. From (4.3), the detection problem can be stated as to find the data sequence such that it minimizes the square error between the channel gains computed from the received signals and those from the predicted values.

The trellis structure of DSTBC can be defined as follows. Each trellis interval corresponds to a transmission matrix $\boldsymbol{D}_n$. For BPSK, the trellis consists of 2^{2Q} states with 2^2 branches emerging from each state and terminating at each state. Each state represents a Q-couple transmitted vector $\boldsymbol{\Gamma}_n = [\boldsymbol{s}_n \ \boldsymbol{s}_{n-1} \ \dots \ \boldsymbol{s}_{n-Q+1}]$. The branch metric associated with each transition can be defined as [7]

$$\Lambda(\boldsymbol{\Gamma}_{n-1}, \boldsymbol{d}_n) = \left\| \boldsymbol{D}_n^H \boldsymbol{r}_n - \sum_{k=1}^{Q} b_k^Q \boldsymbol{D}_{n-k}^H \boldsymbol{r}_{n-k} \right\|^2. \tag{4.6}$$

Exploiting per-survivor processing technique, the number of states can be reduced to 2^{2P} with $P < Q$. Now, the trial symbols and the symbols used in the prediction associated with each branch metric $\Lambda(\boldsymbol{\Gamma}_{n-1}, \boldsymbol{d}_n)$ are determined those associated with the transition

and those along the survivor path terminating at the state Γ_{n-1}. The detection algorithm described above is referred to as a *Viterbi receiver* (VR).

4.4 The Structure of a Linear Predictor

A linear predictor is a crucial component for the metric computation in the Viterbi receiver. It is a linear FIR filter whose output is a predicted value of the input sequence, which in this case is a sequence of channel gains. The linear predictor for DSTBC can be considered as a *two-step* linear predictor, which forms the prediction of the value $\hat{a}[n]$ by a weighted linear combination of the past input values $a[n-2], a[n-4], \ldots, a[n-2Q]$. The prediction coefficients of this predictor are equivalent to that of a linear predictor for single antenna system with a double maximum Doppler frequency. Since each channel is independent and identically distributed, the prediction coefficients are the same for each channel.

Fig. 4.2 shows the prediction coefficients of a linear predictor of order two to four and their associated mean square prediction errors at $f_d T = 0.05$. There are similarities between the properties of the prediction coefficients for DSTBC and those for single antenna systems [23]. For all orders, when SNR reaches a certain level, the prediction coefficients become constant, i.e., independent of the noise variance. It is also found that as the fading rate becomes higher, the prediction coefficients become constant at lower SNR values. This is because as the fading rate increases, the channel process $\boldsymbol{a}_n$ becomes less correlated (its spectrum is closer to noise power spectrum) and it behaves like a noise process itself. Fig. 4.2(e) shows the mean square prediction errors with different prediction orders. It can be used as a rough guideline to choose an appropriate prediction order. As the prediction order increases, the mean square prediction error reduces at SNR below 20 dB. The most significant improvement occurs when the prediction order increases from two to three. At SNR greater than 20 dB, it seems that the linear predictor with order greater than five cannot significantly reduce the mean square prediction error. We choose the order of linear predictor to be five in the remaining of this chapter.

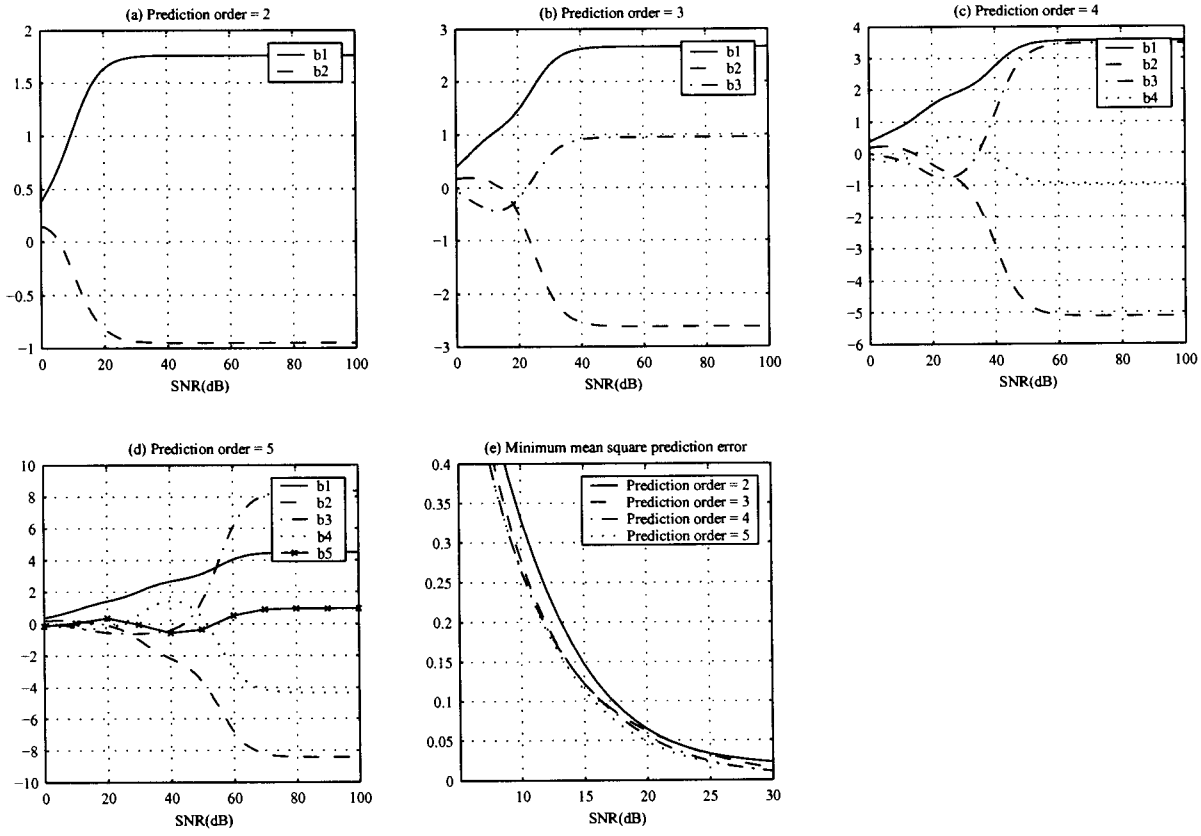

Figure 4.2. *Prediction coefficients and their associated mean square prediction errors, at* $f_dT = 0.05$

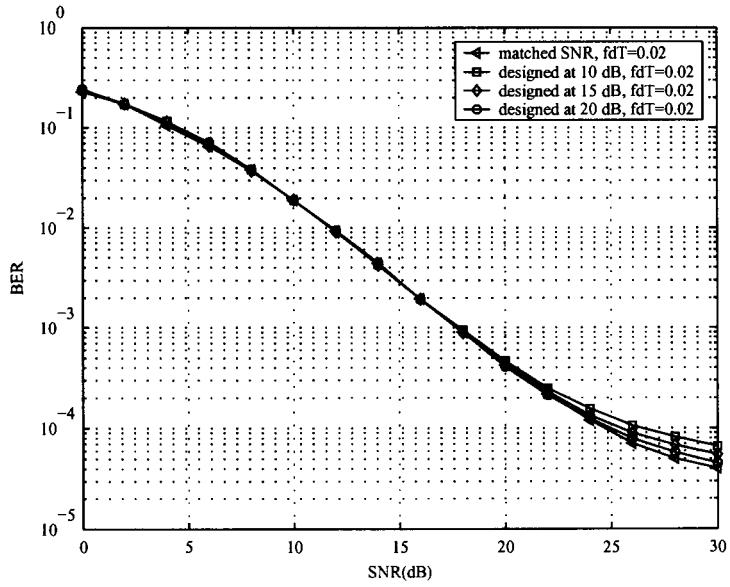

Figure 4.3. *Mismatched SNR effect to the bit error rate when the designed SNRs are 10, 15 and 20 dB at* $f_dT = 0.02$

4.5 Viterbi Receiver with Mismatched SNR and Fading Rate

Although there might be some discussions on mismatched SNR or fading rate in other contexts, this section discusses the effect of mismatched SNR or fading rate on the performance of Viterbi receiver with DSTBC. A particular difference lies on the effect of the so-called *intrablock interference* (defined in Section 4.7) to the performance especially at high SNR. It should be noted that although the received signal has varying *instantaneous* SNR, the linear predictor uses fixed *average* SNR value as a design parameter. To gain better performance, it is possible to apply an adaptive linear predictor design (e.g., [27], [28]) at the price of higher complexity.

Fig. 4.3 and 4.4 show the performances of Viterbi receiver using fixed designed SNR. At $f_dT = 0.02$, a mismatched SNR value has little effect at SNR below 20 dB. There exists only a small performance gap between mismatched cases and matched SNR at SNR higher

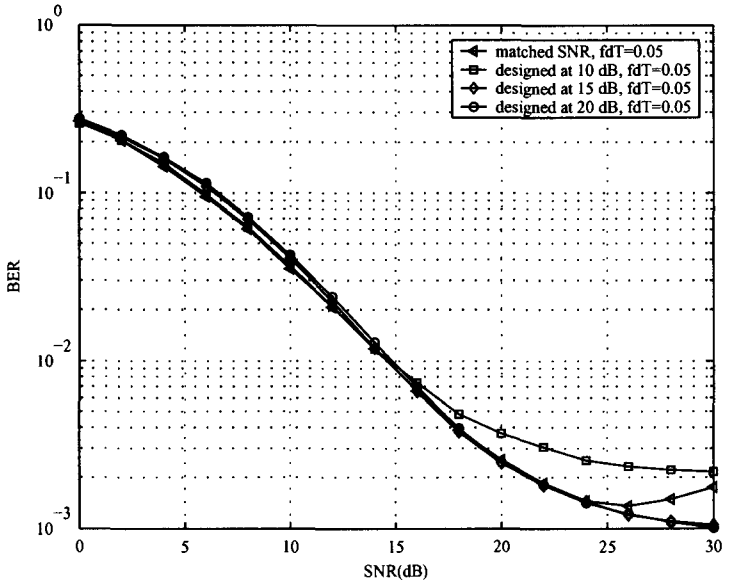

Figure 4.4. *Mismatched SNR effect to the bit error rate when the designed SNRs are 10, 15 and 20 dB at* $f_dT = 0.05$

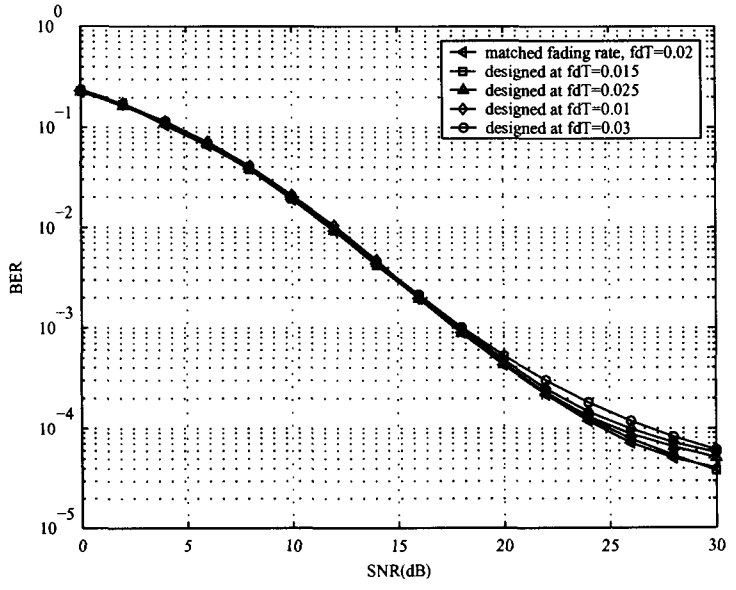

Figure 4.5. *Mismatched fading rate effect to the bit error rate at* $f_dT = 0.02$

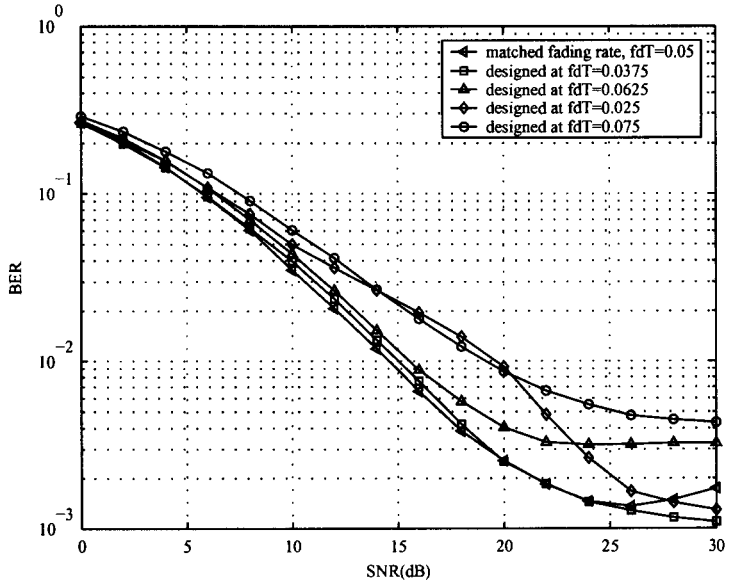

Figure 4.6. *Mismatched fading rate effect to the bit error rate at* $f_dT = 0.05$

than 20 dB. At $f_dT = 0.05$, the effect of mismatched SNR is more pronounced. At SNR higher than 15 dB, there is a large performance gap between the mismatched designed SNR of 10 dB and the matched SNR case. However, with the designed SNR equal to 15 and 20 dB, the receiver still performs quite well compared to the matched SNR case.

It should be noted that for the linear predictor designed with matched SNR, the bit error rate increases with SNR for SNR higher than 25 dB. The reason for this behavior can be given as follows. At high SNR and high fading rate, the intrablock interference is relatively large compared to the amount of noise. Consequently, the linear predictor designed with matched SNR is not truly optimal at high SNR. We have performed simulations where the channel gains are kept constant during a transmission block and found that the above behavior did not occur. This verifies the given reason.

This behavior also depends on the order of the linear predictor. Different orders yield different SNR values at which the BER starts to increase with SNR. However, it is not clear at what SNR combined with what fading rate this will occur. From the results shown in Fig. 4.4, it can be seen that using a fixed lower SNR value for the design of linear predictor

than the matched high SNR value avoids this behavior. In later sections, when the receiver operates at SNR higher than 20 dB, we use a fixed designed SNR value of 20 dB.

A similar observation is found with mismatched fading rate effect. The fading rate mismatch has more a pronounced effect at $f_dT = 0.05$ in Fig.4.6 than at $f_dT = 0.02$ in Fig.4.5. At $f_dT = 0.02$, only a small discrepancy between the performance with mismatched fading rate and that with matched fading rate occurs at SNR higher than 20 dB. Even with the mismatched design of $f_dT = 0.01$ or 0.03 ($\pm 50\%$ mismatch), the receiver still works quite well compared to a matched fading rate. However, at $f_dT = 0.05$, the fading rate mismatch causes a large performance degradation. Interestingly, with a mismatched fading rate higher than the matched value, the performance has more degradation than that with the designed fading rate lower than the matched value. For example, with the design of $f_dT = 0.0375$ (25% mismatch, lower than the actual value), the receiver still works quite well compared to the design with matched fading rate. However, with the design of $f_dT = 0.0625$ (25% mismatch, higher than the matched value), the degradation is more distinct at SNR higher than 18 dB. In addition, at high SNR, the effect of intrablock-interference seems to induce slower fading than the actual fading rate so that the linear predictors designed for lower fading rates (designed for $f_dT = 0.025, f_dT = 0.0375$) perform fairly well.

4.6 Viterbi Receiver Analysis

Since the receiver is trellis-based, we can apply a standard union bound approach to derive the upper bound on the bit error probability. The analysis ideally assumes a known fading rate and SNR and therefore prediction coefficients.

First, the branch metric (4.6) associated with the transmitted block $\boldsymbol{D}_n$ is rewritten as

$$\begin{aligned}\Lambda(\boldsymbol{D}_n) &= \left\| \boldsymbol{D}_n^H \boldsymbol{r}_n - \sum_{k=1}^{Q} b_k \boldsymbol{D}_{n-k}^H \boldsymbol{r}_{n-k} \right\|^2 \\ &= \left\| \sum_{k=0}^{Q} \tilde{b}_k \boldsymbol{D}_{n-k}^H \boldsymbol{r}_{n-k} \right\|^2 \\ &= \sum_{k=0}^{Q} \sum_{k'=0}^{Q} \tilde{b}_k \tilde{b}_{k'}^* \boldsymbol{r}_{n-k'}^H \boldsymbol{D}_{n-k'} \boldsymbol{D}_{n-k}^H \boldsymbol{r}_{n-k}\end{aligned} \tag{4.7}$$

where $\tilde{b}_0 = 1, \tilde{b}_k = -b_k$. The error event of length L is defined as the event of the error sequence diverging from the transmitted sequence at the n^{th} epoch (block interval) and remerging to the transmitted sequence at the $(n + L - 1)^{th}$ epoch on the trellis. Since the branch metric (4.7) is a function of the symbol block associated with the branch as well as the symbol blocks in the prediction, the PEP depends on the symbols on the error event paths as well as $Q \times 2$ symbols prior to the error event. Without loss of generality, suppose the error event starts from epoch zero, i.e., the error event of length L starts from $\boldsymbol{D}_0$ to $\boldsymbol{D}_{L-1}$. Therefore, we define $\boldsymbol{\mathcal{D}}_L = \{\boldsymbol{D}_{-Q}, \boldsymbol{D}_{-Q+1}, \ldots, \boldsymbol{D}_0, \boldsymbol{D}_1, \ldots, \boldsymbol{D}_{L-1}\}$ and $\tilde{\boldsymbol{\mathcal{D}}}_L = \{\boldsymbol{D}_{-Q}, \boldsymbol{D}_{-Q+1}, \ldots, \tilde{\boldsymbol{D}}_0, \tilde{\boldsymbol{D}}_1, \ldots, \tilde{\boldsymbol{D}}_{L-1}\}$.

Let $P(\boldsymbol{\mathcal{D}}_L \rightarrow \tilde{\boldsymbol{\mathcal{D}}}_L)$ denote the pairwise error probability (PEP) of the error event of length L associated with the sequences $\boldsymbol{\mathcal{D}}_L$ and $\tilde{\boldsymbol{\mathcal{D}}}_L$. Similar to [22], an upper bound on the BER can be obtained from the union bound of the number of error bits averaged over transmitted sequences and corresponding error sequences from all error events which is written as

$$P_b < \sum_{L, \boldsymbol{\mathcal{D}}_L, \tilde{\boldsymbol{\mathcal{D}}}_L} \frac{P(\boldsymbol{\mathcal{D}}_L) P(\boldsymbol{\mathcal{D}}_L \rightarrow \tilde{\boldsymbol{\mathcal{D}}}_L) e(\boldsymbol{\mathcal{D}}_L \rightarrow \tilde{\boldsymbol{\mathcal{D}}}_L)}{2\log_2 M} \tag{4.8}$$

where $P(\boldsymbol{\mathcal{D}}_L)$ is the probability of transmitted sequence $\boldsymbol{\mathcal{D}}_L$, $e(\boldsymbol{\mathcal{D}}_L \rightarrow \tilde{\boldsymbol{\mathcal{D}}}_L)$ is the number of error bits arising from this error event and $2\log_2 M$ is the number of information bits per

trellis interval. The PEP of error event of length L is expressed as

$$P(\mathcal{D}_L \to \tilde{\mathcal{D}}_L) = P\left(\sum_{n=0}^{L-1}\Lambda(\boldsymbol{D}_n) > \sum_{n=0}^{L-1}\Lambda(\tilde{\boldsymbol{D}}_n)\right)$$
$$= P\left(\sum_{n=0}^{L-1}\sum_{k=0}^{Q}\sum_{k'=0}^{Q} \boldsymbol{r}_{n-k'}^H \left(\tilde{b}_k\tilde{b}_{k'}^*(\boldsymbol{D}_{n-k'}\boldsymbol{D}_{n-k}^H - \tilde{\boldsymbol{D}}_{n-k'}\tilde{\boldsymbol{D}}_{n-k}^H)\right)\boldsymbol{r}_{n-k} > 0\right). \tag{4.9}$$

The left hand side inside the bracket in the probability in (4.9) can be written as a Gaussian quadratic form, $z = \vec{r}^H \boldsymbol{Y}\vec{r}$, where $\vec{r} = \left[\boldsymbol{r}_{-Q}^t, \boldsymbol{r}_{-Q+1}^t, \ldots, \boldsymbol{r}_0^t, \ldots, \boldsymbol{r}_{L-1}^t\right]^t$ is a $2(L+Q)\times 1$ complex vector and $\boldsymbol{Y}$ is a $2(L+Q)\times 2(L+Q)$ Hermitian symmetric matrix. The matrix $\boldsymbol{Y}$ is composed of an array of 2×2 block matrices $\boldsymbol{y}_{ij}$, $i,j = -Q, -Q+1, \ldots, 0, \ldots, L-1$ where

$$\boldsymbol{y}_{ij} = \begin{cases} \boldsymbol{0}_{2\times 2} & ;|i-j| > Q, \\ \sum_{m=u}^{v} \tilde{b}_{m-j}\tilde{b}_{m-i}^* \left(\boldsymbol{D}_i\boldsymbol{D}_j^H - \tilde{\boldsymbol{D}}_i\tilde{\boldsymbol{D}}_j^H\right) & ;\text{otherwise}, \end{cases} \tag{4.10}$$

$\boldsymbol{0}_{2\times 2}$ is a 2×2 zero matrix and the indices of the summation u, v are expressed as

$$u = \begin{cases} 0 & ;i \le 0 \text{ and } j \le 0, \\ \max(i,j) & ;\text{otherwise} \end{cases}$$
$$v = \begin{cases} L-1 & ;i \ge L-Q-1 \text{ and } j \ge L-Q-1, \\ \min(i+Q, j+Q) & ;\text{otherwise}. \end{cases} \tag{4.11}$$

The characteristic function of a Gaussian quadratic form z is given as [29]

$$\Phi_z(\xi) = \frac{1}{\det[I - j2\xi\boldsymbol{R}_r\boldsymbol{Y}]}$$
$$= \prod_{\forall\, \text{eig}_i(\boldsymbol{R}_r\boldsymbol{Y})\neq 0} (1 - j2\xi\text{eig}_i(\boldsymbol{R}_r\boldsymbol{Y}))^{-1} \tag{4.12}$$

where $\boldsymbol{R}_r = E[\vec{r}\vec{r}^H]$, det[.] is a determinant of a matrix and $\text{eig}_i(\boldsymbol{R}_r\boldsymbol{Y})$ is the i^{th} eigenvalue of the matrix $\boldsymbol{R}_r\boldsymbol{Y}$. The PEP in (4.9) can be evaluated by integration of the probability density function of z from zero to infinity. Therefore, this is similar to the result in [22]

(See Appendix A),

$$\begin{aligned} P(\boldsymbol{\mathcal{D}}_L \to \tilde{\boldsymbol{\mathcal{D}}}_L) &= \int_0^\infty \frac{1}{2\pi} \int_{-\infty}^{\infty} \Phi_z(\xi) \exp(-j\xi\kappa) d\xi d\kappa \\ &= \frac{1}{2} + \frac{1}{2\pi} \int_{-\infty}^{\infty} \frac{\Phi_z(\xi)}{j\xi} d\xi. \end{aligned} \tag{4.13}$$

To evaluate the integral in (4.13), we can apply the residue theorem which transforms an indefinite integral of a rational function to a summation of residues [30]. The residue theorem yields different forms of results according to the nature of eigenvalues of the matrix $\boldsymbol{R}_r \boldsymbol{Y}$.

Since $\boldsymbol{R}_r$ is positive semidefinite and $\boldsymbol{Y}$ is Hermitian, it can be shown that all eigenvalues of $\boldsymbol{R}_r \boldsymbol{Y}$ are real. Let $\mathcal{P}$ denote a set of nonzero eigenvalues of $\boldsymbol{R}_r \boldsymbol{Y}$. For a length L error event, it is observed that there are $4 \times (L-1)$ nonzero eigenvalues. Among these nonzero eigenvalues, half of them are positive and the other half are negative. Furthermore, these nonzero eigenvalues fall into one of the following two cases.

Case 1: All nonzero eigenvalues are distinct. In this case, the poles of (4.12) are simple. By applying the residue theorem, the PEP can be expressed as (See Appendix A)

$$P(\boldsymbol{\mathcal{D}}_L \to \tilde{\boldsymbol{\mathcal{D}}}_L) = 1 - \sum_{p_i \in \mathcal{P}, p_i < 0} \prod_{p_j \in \mathcal{P}, j \neq i} \frac{1}{1 - p_j/p_i} \tag{4.14}$$

Case 2: There are $2 \times (L-1)$ distinct nonzero eigenvalues, each with multiplicity two. In this case, let $\tilde{\mathcal{P}}$ denote a set of *distinct* nonzero eigenvalues of $\boldsymbol{R}_r \boldsymbol{Y}$. Then, the PEP can be expressed as (See Appendix A)

$$P(\boldsymbol{\mathcal{D}}_L \to \tilde{\boldsymbol{\mathcal{D}}}_L) = 1 - \sum_{p_i \in \tilde{\mathcal{P}}, p_i < 0} \left(\prod_{p_j \in \tilde{\mathcal{P}}, p_j \neq p_i} \frac{1}{\left(1 - \frac{p_j}{p_i}\right)^2} + \frac{2}{\prod_{p_j \neq p_i} \left(1 - \frac{p_j}{p_i}\right)^2} \cdot \sum_{p_j \neq p_i} \frac{1}{\left(1 - \frac{p_i}{p_j}\right)} \right) \tag{4.15}$$

The union bound of bit error probability (4.7) is a function of all lengths of error events, which is an infinite sum, and therefore it must be truncated. The union bound is still reliable if the bound includes a finite number of dominant error events under certain conditions. When fading is moderately fast and SNR is high, short length error events are dominant

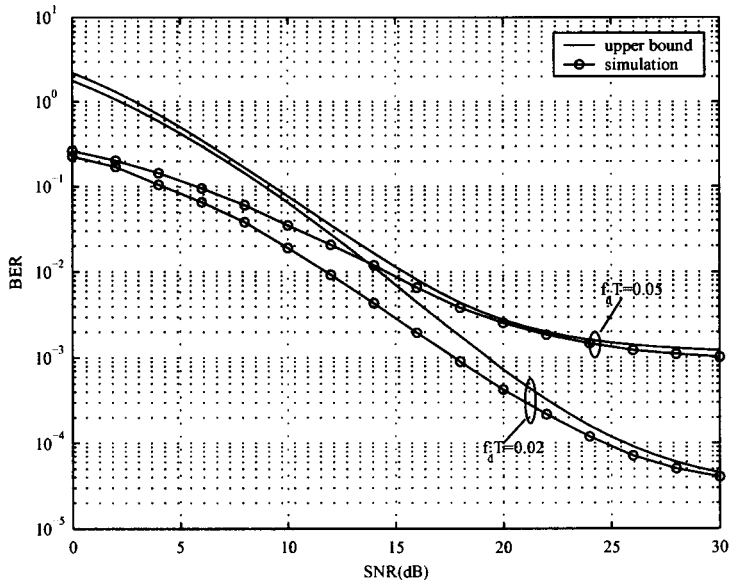

Figure 4.7. *Upper bound on the bit error probability versus simulation results of Viterbi receiver*

[22]. In this case, the union bound of bit error probability can be evaluated by including only short length error events.

Fig. 4.7 shows the simulation performance of a Viterbi receiver for DSTBC and the union bound on bit error probability when $f_dT = 0.02, 0.05$. The bounds include length-two and length-three error events. Including error events with longer lengths does not affect the bound at SNR higher than 16 dB when $f_dT = 0.05$ and at SNR higher than 20 dB when $f_dT = 0.02$. The bound is rather loose when the fading rate is lower or the SNR is lower, which is natural for a union upper bound.

4.7 Multistage Receiver

Since the Viterbi receiver was derived based on the assumption of fixed channel gains during a transmission block while the actual channels vary continuously, the main idea of the new receiver is to try to eliminate the effect of the actual channel gains varying within

a transmission block.

With the actual channel, the elements of the received vector $\boldsymbol{r}_n$ can be written as

$$\begin{aligned} r_{2n} &= s_{2n}a_1[2n] + s_{2n+1}a_2[2n] + w_{2n}, \\ r_{2n+1} &= -s^*_{2n+1}a_1[2n+1] + s^*_{2n}a_2[2n+1] + w_{2n+1}. \end{aligned} \tag{4.16}$$

Each received sample in (4.16) is affected from channel gains in its own symbol interval. Next, let us represent the channel gains at odd symbol intervals relative to the channel gains at prior symbol intervals by defining $\Delta a_1 = a_1[2n+1] - a_1[2n]$ and $\Delta a_2 = a_2[2n+1] - a_2[2n]$. Now, r_{2n+1} in (4.16) can be written in terms of the channel gains in the previous interval as,

$$r_{2n+1} = -s^*_{2n+1}(a_1[2n] + \Delta a_1) + s^*_{2n}(a_2[2n] + \Delta a_2) + w_{2n+1}. \tag{4.17}$$

Suppose the Viterbi algorithm is working on the branch in which the transmitted block $\boldsymbol{D}_n$ is associated, determining $\boldsymbol{D}_n^H \boldsymbol{r}_n$ with r_{2n} from (4.16) and r_{2n+1} from (4.17) yields the noise corrupted channel gains

$$\begin{aligned} \grave{a}_1[2n] &= s^*_{2n}r_{2n} - s_{2n+1}r_{2n+1} \\ &= a_1[2n] + I1_n + s^*_{2n}w_{2n} - s_{2n+1}w_{2n+1} \\ \grave{a}_2[2n] &= s^*_{2n+1}r_{2n} + s_{2n}r_{2n+1} \\ &= a_2[2n] + I2_n + s^*_{2n+1}w_{2n} + s_{2n}w_{2n+1}, \end{aligned} \tag{4.18}$$

where $I1_n = 0.5\Delta a_1 - \Delta a_2 s^*_{2n}s_{2n+1}$, $I2_n = 0.5\Delta a_2 - \Delta a_1 s_{2n}s^*_{2n+1}$. The values $I1_n, I2_n$ represent *intrablock interference* (IBI). This means that even when the Viterbi algorithm is working on the branch in which the correct transmission block is associated, the computed channel gains are affected by IBI. Therefore, even there is no noise, one can expect an irreducible error floor caused by IBI with the Viterbi receiver. The amount of IBI depends on how rapidly the channel varies. At higher fading rates, the average power of IBI is higher. If the channel is fixed during one transmission block, $I1_n, I2_n$ are zero and the Viterbi receiver becomes an optimal maximum-likelihood receiver.

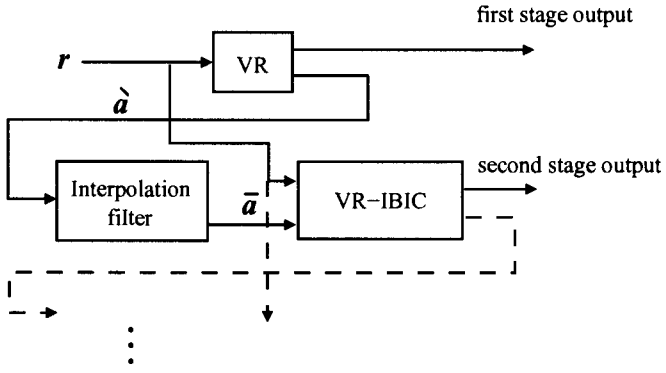

Figure 4.8. *Multistage receiver for DSTBC*

From the above discussion, if the channel gains are available at the receiver, the branch metric can be modified to mitigate the effect of IBI. Hence, the new receiver is proposed to operate in more than one stage. The first stage has no channel gain information while the later stages obtain channel gain information from the prior stages.

Fig. 4.8 shows the components of the proposed *multistage receiver* (MR). The first stage is composed of only a Viterbi receiver (VR). Each later stage is composed of an interpolation filter and a modified Viterbi receiver named *Viterbi receiver with intrablock interference cancellation* (VR-IBIC). The operation of the multistage receiver is explained as follows:

First stage: The Viterbi receiver functions as usual. In addition, channel estimates computed from the detected sequence are computed. Suppose the receiver obtains the detected sequence $\{\hat{\boldsymbol{D}}_0, \hat{\boldsymbol{D}}_1, \ldots, \hat{\boldsymbol{D}}_{N-1}\}$. Then, it computes 'rough' channel estimates $\grave{\boldsymbol{a}}_n = [\grave{a}_1[2n]\ \grave{a}_2[2n]]^t$ from

$$\grave{\boldsymbol{a}}_n = \hat{\boldsymbol{D}}_n^H \boldsymbol{r}_n, \qquad n = 0, 1, \ldots, N-1, \tag{4.19}$$

and sends them to the next stage receiver.

Second stage and later stages: The obtained rough channel estimates are computed only at even intervals and are affected by IBI which appears like noise. To reduce the effect of IBI and to obtain channel estimates at odd intervals, a low pass interpolation

filter is exploited before the channel estimates enter the VR-IBIC. This is done by padding a zero between each rough channel estimate. Then, the inputs of the interpolation filter are $[\grave{a}_1[0], 0, \grave{a}_1[2], \ldots, 0, \grave{a}_1[2N-2]]$ and $[\grave{a}_2[0], 0, \grave{a}_2[2], \ldots, 0, \grave{a}_2[2N-2]]$. The output sampling rate of the interpolation filter is the same as the symbol rate. The filter outputs the 'refined' channel estimates $\bar{\boldsymbol{a}}_n = [\bar{a}_1[n]\ \bar{a}_2[n]]^t, n = 0, 1, \ldots, 2N-2$, to be employed at the VR-IBIC.

Now, VR-IBIC computes the IBI from $\bar{I1}_n = 0.5\Delta\bar{a}_1 - \Delta\bar{a}_2\hat{s}^*_{2n}\hat{s}_{2n+1}$ and $\bar{I2}_n = 0.5\Delta\bar{a}_2 - \Delta\bar{a}_1\hat{s}_{2n}\hat{s}^*_{2n+1}$ where $\Delta\bar{a}_1 = \bar{a}_1[2n+1] - \bar{a}_1[2n], \Delta\bar{a}_2 = \bar{a}_2[2n+1] - \bar{a}_2[2n]$ and $\hat{s}_{2n}, \hat{s}_{2n+1}$ are the symbols associated with the branch in which Viterbi algorithm is working on. To remove the IBI, the branch metric (4.6) is modified to

$$\Lambda_{IC}(\boldsymbol{\Gamma}_n, \boldsymbol{d}_n) = \left\| \boldsymbol{D}_n^H \boldsymbol{r}_n - \bar{\boldsymbol{I}}_n - \sum_{k=1}^{Q} b_k \left(\boldsymbol{D}_{n-k}^H \boldsymbol{r}_{n-k} - \bar{\boldsymbol{I}}_{n-k} \right) \right\|^2 \tag{4.20}$$

where $\bar{\boldsymbol{I}}_n = [\bar{I1}_n\ \bar{I2}_n]^t$. In this manner, the IBI is removed from both the channel gains computed from the current received signals and from the prediction. So, the sequence of channel gains becomes more suitable for a two-step linear predictor which has been derived without considering IBI.

If the later stage is to be continued, the rough channel estimates have to be computed again by (4.19) and are transferred to the later stage receiver.

We can approximate the additional complexity of MR compared to VR for each trellis interval as follows. Suppose DSTBC uses an M-ary constellation. Let N_s be number of stages and N_{tap} be the number of taps of the interpolation filter. To obtain $\Delta\bar{a}_1$ or $\Delta\bar{a}_1$, each requires $N_{tap}/2$ multiplications, $N_{tap}/2 - 1$ additions and 1 subtraction. To obtain $\bar{I1}$ or $\bar{I2}$, each requires 3 multiplications and 1 subtraction for each combination of transmitted symbols in a block. For each branch metric, it requires additional $2(Q+1)$ subtractions. In summary, MR requires an additional $(N_{tap}+6M^2)(N_s-1)$ multiplications and $(N_{tap} + M^2 + 2(Q+1)M^{2P})(N_s - 1)$ additions/subtractions for each trellis interval compared to VR.

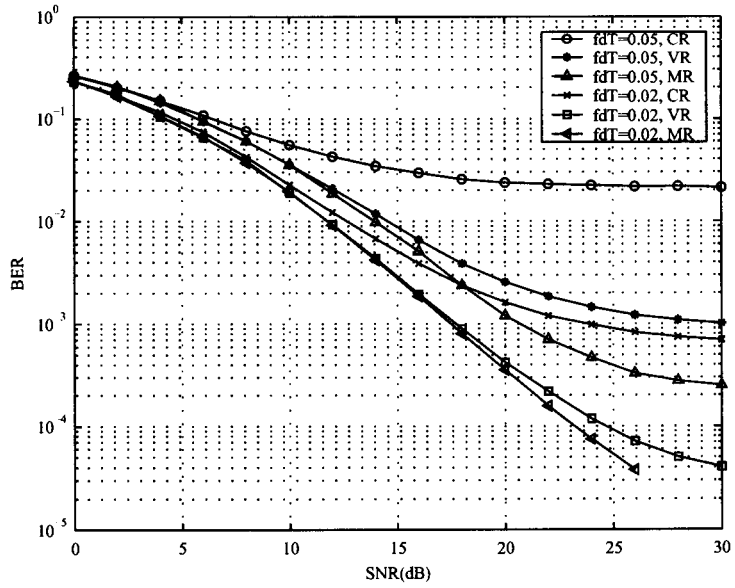

Figure 4.9. *Performance of DSTBC with BPSK, at* $f_dT = 0.02$ *and* $f_dT = 0.05$ *with CR, VR, and MR with two stages*

4.8 Results and Discussion

This section compares simulation results between CR, VR and MR. For MR, the interpolation filter is a raised-cosine filter with roll-off factor $\alpha = 0.2$. The cutoff frequency of the interpolation filter is chosen to be some small amount higher than f_dT to avoid cutting high amplitude spectrum at the edge of the fading spectral band. The cutoff frequency for $f_dT = 0.02$ is 0.0275 and for $f_dT = 0.05$ is 0.075. The number of filter taps is 100 and 80 for $f_dT = 0.02$ and $f_dT = 0.05$, respectively. They are chosen to have enough taps such that the filter retains a raised-cosine power spectrum. The number of stages is two.

In Fig. 4.9, the BER performances of DSTBC are compared when the receivers are MR, CR, and VR. We can see that although VR reduces the error floor associated with CR significantly, some considerable amount of error floor due to IBI still exists, especially at $f_dT = 0.05$. At this fading rate, MR outperforms VR for SNR greater than 12 dB as the channel estimates from the first stage become more reliable. Nevertheless, at $f_dT = 0.02$,

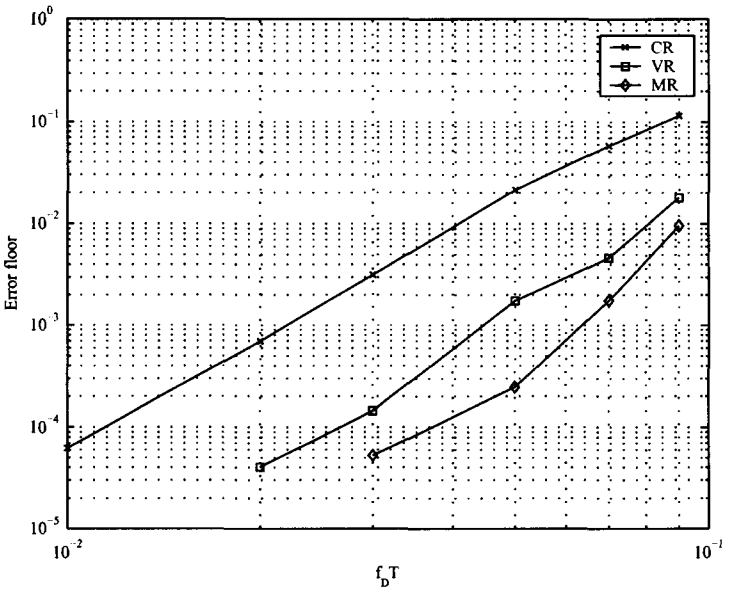

Figure 4.10. *Error floor of DSTBC with CR, VR, and MR with two stages evaluated at SNR = 30 dB*

MR outperforms VR for SNR greater than 16 dB. The improvement of MR at $f_dT = 0.02$ is not as much as at $f_dT = 0.05$ because, on average, the amount of IBI is smaller at $f_dT = 0.02$. We conclude that MR can further reduce the error floor left from VR with only a two-stage receiver. When the number of stages is greater than two, however, MR provides virtually no improvement.

Fig. 4.10 compares the error floor of CR, VR and MR evaluated at SNR = 30 dB. It is seen that MR significantly reduces the error floor from VR and CR. MR can achieve about a half-order of magnitude error floor improvement over VR.

4.9 Multistage Receiver with an Outer Convolutional Code

It is interesting to see whether MR would perform well in a coded system. A convolutional code concatenated with DSTBC is studied without an interleaver according to the system in Fig. 4.11. Fig. 4.12 shows the BER performance of CR, VR, and MR in a coded system

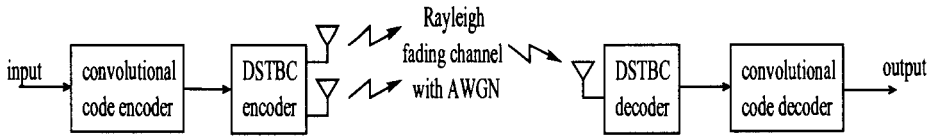

Figure 4.11. *convolutional coded - DSTBC system model*

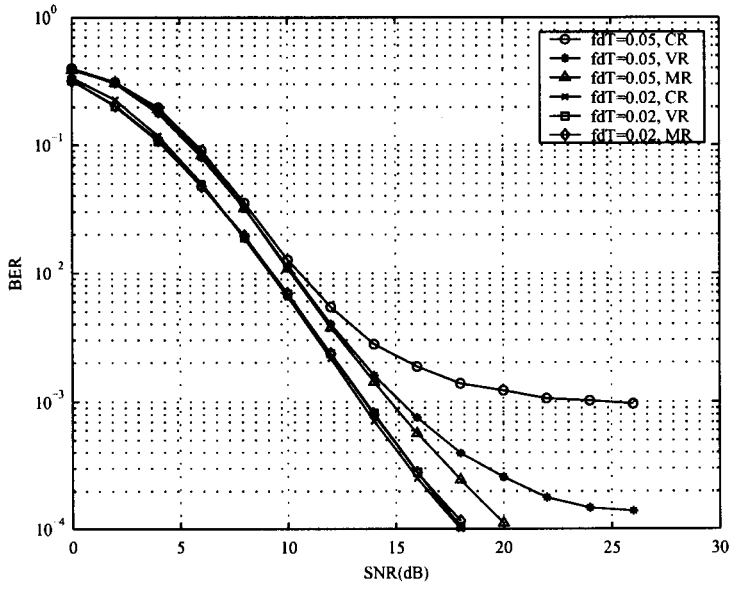

Figure 4.12. *Performance of convolutional coded - DSTBC with BPSK, at* $f_dT = 0.02, 0.05$ *with CR, VR, and MR with two stages*

without an interleaver. A rate 1/2, convolutional code with constraint length = 5, proposed in EDGE system is chosen [31]. The generator matrix is $\left[1 + D^3 + D^4 \quad 1 + D + D^3 + D^4\right]$. The overall transmission rate is 0.5 bps/Hz. It can be seen that the convolutional code improves the BER performance of CR and VR significantly. At $f_dT = 0.05$, MR outperforms VR at SNR higher than 12 dB with two stages. However, at $f_dT = 0.02$, there is virtually no improvement using MR or VR within this SNR region. One reason for this is that, at this fading rate, the amount of IBI is small such that the error bits caused by IBI can be corrected by the powerful convolutional code decoder. Another reason is that the operating SNR is not high enough for the error floor to appear.

One might ask if we can use the output sequence from the convolutional code decoder and recode it back to a DSTBC sequence, which should be more reliable, and then use that sequence to compute channel estimates for the second stage. However, it is found from our simulations (not shown) that using the output sequence from the convolutional code decoder does not have visible gain over typical MR within this SNR region and this increases complexity.

4.10 Soft-Output Multistage Receiver

It is well-known that using soft-output decision improves the performance of concatenated codes over hard-output decision. To improve the performance of convolutional coded-DSTBC system, soft-output from the DSTBC receiver has to be derived. In the context of concatenated codes, there are two main types of soft-output algorthms. One is maximum a posteriori probability (MAP) and the other is soft-output Viterbi algorithm (SOVA) [32]. MAP algorithm is the optimal soft-output algorithm but has very high complexity while SOVA has lower complexity but inferior performance [33]. Next, we will derive a soft output from DSTBC Viterbi receiver by a modification of SOVA algorithm.

SOVA finds the state sequence, and thus data sequence that maximizes the conditional probability [32]

$$p\left(\boldsymbol{\Gamma}_{0,1,\ldots,N-1}|\boldsymbol{r}_{0,1,\ldots,N-1}\right)=\frac{p\left(\boldsymbol{\Gamma}_{0,1,\ldots,N-1},\boldsymbol{r}_{0,1,\ldots,N-1}\right)}{p\left(\boldsymbol{r}_{0,1,\ldots,N-1}\right)}. \tag{4.21}$$

Since the denominator is the same for all hypothesis sequences, we can only maximize the nominator. Viterbi algorithm works on the code trellis and at the n^{th} epoch it chooses the survivor path whose metric maximizes $p\left(\boldsymbol{\Gamma}_{\tilde{n}\leq n},\boldsymbol{r}_{\tilde{n}\leq n}\right)$. The probability $p\left(\boldsymbol{\Gamma}_{\tilde{n}\leq n},\boldsymbol{r}_{\tilde{n}\leq n}\right)$ can be written as

$$p\left(\boldsymbol{\Gamma}_{\tilde{n}\leq n},\boldsymbol{r}_{\tilde{n}\leq n}\right)=\prod_{\tilde{n}\leq n}p\left(\boldsymbol{\Gamma}_{\tilde{n}},\boldsymbol{r}_{\tilde{n}}\right)=\prod_{\tilde{n}\leq n}p\left(\boldsymbol{r}_{\tilde{n}}|\boldsymbol{G}_{\tilde{n}}\right)P\left(\boldsymbol{G}_{\tilde{n}}\right)=\prod_{\tilde{n}\leq n}p\left(\boldsymbol{r}_{\tilde{n}}|\boldsymbol{D}_{\tilde{n}}\right)P\left(\boldsymbol{D}_{\tilde{n}}\right), \tag{4.22}$$

where $P(\boldsymbol{G}_{\tilde{n}})$ and $P(\boldsymbol{D}_{\tilde{n}})$ are a priori probabilities of data block $\boldsymbol{G}_{\tilde{n}}$ and transmission block $\boldsymbol{D}_{\tilde{n}}$, respectively.

Suppose the receiver assumes that the channel estimates obtained from the linear predictor is perfect, the conditional probability $p(\boldsymbol{r}_n|\boldsymbol{D}_n, \boldsymbol{a}_n)$ is Gaussian and can be written as

$$p(\boldsymbol{r}_n|\boldsymbol{D}_n, \boldsymbol{a}_n) = K_1 \cdot e^{-\|\boldsymbol{r}_n - \boldsymbol{D}_n\boldsymbol{a}_n\|^2/K_2}, \tag{4.23}$$

where K_1, K_2 are constant irrelevant of decision. Replacing $p(\boldsymbol{r}_{\tilde{n}}|\boldsymbol{D}_{\tilde{n}})$ in (4.22) with $p(\boldsymbol{r}_n|\boldsymbol{D}_n, \boldsymbol{a}_n)$ and taking logarithm, we obtain the maximum likelihood metric for Viterbi algorithm as $-\sum_{n=0}^{N-1} \|\boldsymbol{r}_n - \boldsymbol{D}_n\boldsymbol{a}_n\|^2 + \log P(\boldsymbol{D}_n)$ and the branch metric is

$$\|\boldsymbol{r}_n - \boldsymbol{D}_n\boldsymbol{a}_n\|^2 + \log P(\boldsymbol{D}_n). \tag{4.24}$$

The second term in (4.24) represents a priori information. In the context of iterative decoding, this term is exploited by the extrinsic information from the previous iteration. Since we are not focusing on iterative decoding, the second term is dropped from SOVA. Therefore, the first term in (4.24) is equivalent to the branch metric in (4.6) for VR. For VR-IBIC, the branch metric for SOVA is equivalent to (4.20).

Let $\Upsilon_i^j(n)$ be the *minimum* additive path metric among the transitions corresponding to the coded bit zero ($j = 0$) or coded bit one ($j = 1$) transmitted from the i^{th} antenna at the n^{th} epoch. Now, to find a soft output for a coded bit zero, $\Omega_i^0(n)$, SOVA computes

$$\Omega_i^0(n) = \frac{e^{\Upsilon_i^0(n)}}{e^{\Upsilon_i^0(n)} + e^{\Upsilon_i^1(n)}} \tag{4.25}$$

and a soft output for a coded bit one is $\Omega_i^1(n) = 1 - \Omega_i^0(n)$. This soft output represents the reliability (probability) of coded bit to be zero or one transmitted from the i^{th} antenna at the n^{th} epoch. The convolutional code decoder then applies these soft outputs instead of hard output bits in the convolutional code decoding.

Fig. 4.13 clearly shows the superior performance of soft-output algorithms of VR and MR with two stages. Soft-output VR and MR has 3 dB and 5 dB gain over hard-output VR and MR at $f_dT = 0.02$ and $f_dT = 0.05$, respectively. The soft-output VR and MR at

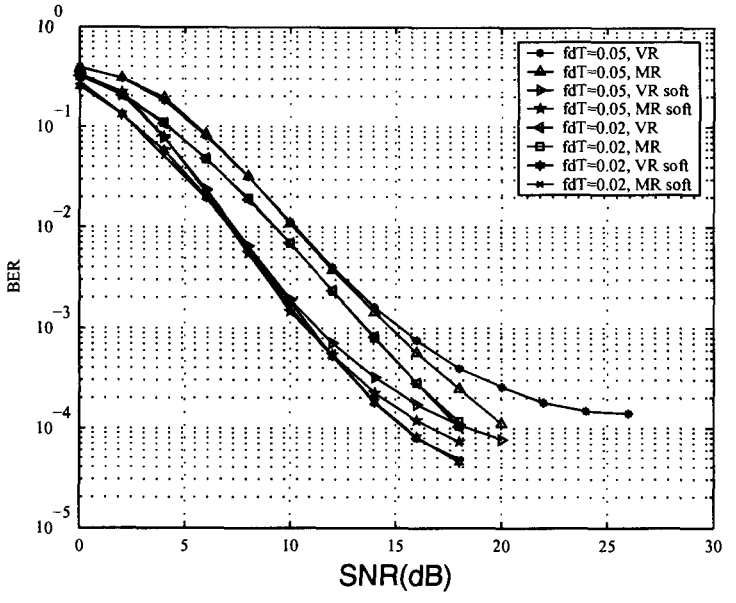

Figure 4.13. *Performance of convolutional coded - DSTBC with BPSK, at* $f_dT = 0.02, 0.05$ *with hard- and soft-output VR, and MR with two stages*

$f_dT = 0.05$ even outperform hard-output VR and MR at $f_dT = 0.02$. At $f_dT = 0.05$, soft-output MR still outperforms soft-output VR when SNR is greater than 10 dB, although this gain is smaller than the gain achieved in hard-output MR at higher SNR. At $f_dT = 0.02$, soft-output MR does not have visible gain compared to soft-output VR which is similar to the hard-output case. Note that the simulation results shown does not perform recoding of output bits from the convolutional code decoder. Similarly to the hard-output case, recoding does not yield a visible gain.

4.11 Summary

An approximate ML receiver for Tarokh's differential space-time block codes is investigated in this section. The effects of SNR and fading rate mismatch are studied. It is shown that the mismatched cases are more sensitive when the fading rate is high. An upper bound on the bit error probability is derived and shown to be tight when the fading rate and

SNR are high. In order to improve the performance of an approximate ML receiver, the multistage receiver is proposed. It accounts for the intrablock interference caused by time-varying characteristics of the channel within a transmission block. With some additional complexity, a multistage receiver provides further improvement over an approximate ML receiver. With a two-stage receiver the error floor is reduced by about a half order of magnitude compared to an approximate ML receiver. The performance of an approximate ML receiver and multistage receiver in the convolutional coded-DSTBC system is also evaluated. Multistage receiver still has a significant gain over an approximate ML receiver at high fading rate. In addition, soft-output Viterbi algorithm for DSTBC decoder is derived. The soft-output receivers show significant gain over hard-output receivers.

Chapter 5

Trellis-Typed Receivers for DSTBC on Spatial Correlated Channels

5.1 Introduction

When the transmit antenna spacing is not enough to ensure uncorrelated transmission paths, the correlation between transmission paths, i.e. spatial correlation, reduces diversity level and therefore BER performance. Suppose the receiver has some information about this spatial correlation, it might be able to incorporate this information in the detection algorithm to improve the performance. The idea of including spatial correlation at the receiver has been discussed in [22] in the context of receive diversity. It is shown that exploiting spatial correlation at the receiver does not substantially improve the bit error rate (BER) compared to the receiver without it. The question is whether the performance can be improved by including spatial correlation information for the transmit diversity scheme.

This chapter presents the performance of Viterbi receiver derived in Chapter 4 under the condition that both time correlation and spatial correlation between transmit antennas exists. An extension of Viterbi receiver which takes the correlation property into account is derived. The linear predictor embedded in the Viterbi receiver is now in a matrix form which can incorporate the information from the other transmission path to improve the quality of channel prediction. Section 5.2 describes the system model. Section 5.3 summarizes the Viterbi receiver with a scalar linear predictor derived from the simple Yule-Walker

equation. Section 5.4 introduces the Viterbi receiver with a matrix linear predictor derived from the multichannel Yule-Walker equation. Section 5.5 discusses the general structure of the matrix linear predictor. Section 5.6 shows an analysis of the performance of the new Viterbi receiver by an upper bound of the frame error rate. Section 5.7 shows the simulation results of DSTBC under spatial correlation and comparisons of these two types of Viterbi receivers. Section 5.8 provides a summary of this chapter.

5.2 System Model

A similar system to that presented in Chapter 4 is studied except that channel has a spatial correlation between two transmission paths from two transmit antennas. Spatial correlation between the two paths can be represented by a simple covariance matrix [34],[35]

$$E\left[\begin{bmatrix} a_1^*[n] \\ a_2^*[n] \end{bmatrix}\begin{bmatrix} a_1[n] & a_2[n] \end{bmatrix}\right] = \begin{bmatrix} 1 & \rho \\ \rho & 1 \end{bmatrix}, \tag{5.1}$$

where ρ represents cross-correlation between two paths. As in [7] and in Chapter 4, the receiver is derived based on the assumption of constant channel gains within a transmission matrix.

5.3 Viterbi Receiver with a Scalar Linear Predictor

The branch metric for the Viterbi receiver (VR) in Chapter 4 is repeated here for convenience,

$$\Lambda(\boldsymbol{\Gamma}_n, \boldsymbol{d}_n) = \left\| \boldsymbol{D}_n^H \boldsymbol{r}_n - \sum_{k=1}^{Q} b_k \boldsymbol{D}_{n-k}^H \boldsymbol{r}_{n-k} \right\|^2 . \tag{5.2}$$

where b_k is the k^{th} linear prediction coefficient of the *two-step* linear predictor of order Q. We can determine coefficients $[b_1 b_2 \ldots b_Q]$ from Cholesky decomposition of the matrix $\boldsymbol{M}^{-1} = \boldsymbol{B}^H \Xi \boldsymbol{B}$ where $\boldsymbol{M}, \boldsymbol{B}$ are defined in (4.4) and (4.5) [7] or equivalently, from

solving *Yule-Walker* equation [36] for a two-step linear predictor

$$\begin{bmatrix} R_a[0]+\sigma_w^2 & R_a[-2] & \dots & R_a[-2Q] \\ R_a[2] & R_a[0]+\sigma_w^2 & \dots & R_a[-2(Q-1)] \\ \vdots & \vdots & \ddots & \vdots \\ R_a[2Q] & R_a[2(Q-1)] & \dots & R_a[0]+\sigma_w^2 \end{bmatrix} \begin{bmatrix} c_0 \\ c_1 \\ c_2 \\ \vdots \\ c_Q \end{bmatrix} = \begin{bmatrix} \sigma_e^2 \\ 0 \\ 0 \\ \vdots \\ 0 \end{bmatrix} \tag{5.3}$$

and $\begin{bmatrix} b_1 & b_2 & \dots & b_Q \end{bmatrix} = -\begin{bmatrix} c_1 & c_2 & \dots & c_Q \end{bmatrix}$ where σ_e^2 is the square prediction error which can be assumed as a constant. The coefficients of the linear predictor are scalar due to the assumption of independent channel paths. We refer to this receiver as a *scalar predictor receiver (SPR).*

5.4 Viterbi Receiver with a Matrix Linear Predictor

When two transmission channels are correlated in a spatial domain, the behavior of one channel affects the other. It is natural to exploit spatial correlation information at the receiver. The prediction coefficient in this case will be in a matrix form. Let $\boldsymbol{R}_{a_1a_2}[m]$ denote cross correlation of channel gains $a_1[n]$ and $a_2[n+m]$, which is expressed as

$$\begin{aligned} \boldsymbol{R}_{a_1a_2}[m] &= E\left[\begin{bmatrix} a_1^*[n] \\ a_2^*[n] \end{bmatrix}\begin{bmatrix} a_1[n+m]a_2[n+m] \end{bmatrix}\right] \\ &= \begin{bmatrix} R_a[m] & \rho R_a[m] \\ \rho R_a[m] & R_a[m] \end{bmatrix} \end{aligned} \tag{5.4}$$

The matrix prediction coefficients $\boldsymbol{B}_k$ are computed from *multichannel Yule-Walker* equation [36] for the two-step linear predictor

$$\begin{bmatrix} \boldsymbol{R}_{a_1a_2}[0]+\sigma_w^2\boldsymbol{I} & \boldsymbol{R}_{a_1a_2}[-2] & \cdots & \boldsymbol{R}_{a_1a_2}[-2(Q-1)] \\ \boldsymbol{R}_{a_1a_2}[2] & \boldsymbol{R}_{a_1a_2}[0]+\sigma_w^2\boldsymbol{I} & \cdots & \boldsymbol{R}_{a_1a_2}[-2(Q-2)] \\ \vdots & \vdots & \vdots & \vdots \\ \boldsymbol{R}_{a_1a_2}[2(Q-1)] & \boldsymbol{R}_{a_1a_2}[2(Q-2)] & \cdots & \boldsymbol{R}_{a_1a_2}[0]+\sigma_w^2\boldsymbol{I} \end{bmatrix} \begin{bmatrix} \boldsymbol{C}_1^t \\ \boldsymbol{C}_2^t \\ \vdots \\ \boldsymbol{C}_Q^t \end{bmatrix} = \begin{bmatrix} \boldsymbol{R}_{a_1a_2}[2] \\ \boldsymbol{R}_{a_1a_2}[4] \\ \ddots \\ \boldsymbol{R}_{a_1a_2}[2(Q-1)] \end{bmatrix} \tag{5.5}$$

and

$$\begin{bmatrix} \boldsymbol{B}_1 & \boldsymbol{B}_2 & \cdots & \boldsymbol{B}_Q \end{bmatrix} = -\begin{bmatrix} \boldsymbol{C}_1 & \boldsymbol{C}_2 & \cdots & \boldsymbol{C}_Q \end{bmatrix} \tag{5.6}$$

The multichannel Yule-Walker equation can be solved efficiently by Levinson-Wiggins-Robinson algorithm [36]. The branch metric for Viterbi algorithm is modified to be

$$\Lambda(\boldsymbol{\Gamma}_n, \boldsymbol{d}_n) = \left\| \boldsymbol{D}_n^H \boldsymbol{r}_n - \sum_{k=1}^{Q} \boldsymbol{B}_k \boldsymbol{D}_{n-k}^H \boldsymbol{r}_{n-k} \right\|^2, \tag{5.7}$$

With this metric, the receiver takes spatial correlation into account. The receiver will be called a *matrix predictor receiver (MPR)*. MPR can be considered as a generalized version of SPR. When channels become spatially uncorrelated ($\rho = 0$), each matrix coefficient $\begin{bmatrix} \boldsymbol{B}_1 \boldsymbol{B}_2 \ldots \boldsymbol{B}_Q \end{bmatrix}$ becomes a diagonal matrix and the coefficients reduce to the scalar version.

5.5 The Structure of a Matrix Linear Predictor

A matrix linear predictor can be interpreted as a multichannel FIR filter which outputs a predicted vector of the input sequence of vectors of channel gains. The matrix linear predictor for DSTBC can be considered as a *two-step* multichannel linear predictor. For two transmit antenna case, the matrix linear predictor forms a prediction vector $[\hat{a}_1[k]\ \hat{a}_2[k]]^t$ by a weighted matrix linear combination of the past input vector $[a_1[k-2]\ a_2[k-2]]^t, [a_1[k-4]\ a_2[k-4]]^t, \ldots, [a_1[k-2Q]\ a_2[k-2Q]]^t$. Suppose the q^{th} matrix coefficient of the linear predictor of order Q is written as $\begin{bmatrix} b_{1q} & b_{2q} \\ b_{3q} & b_{4q} \end{bmatrix}$. Since the channels from the first and

the second antennas are identically distributed and the SNRs of both channels are equal, we obtain $b_{1q} = b_{4q}, b_{2q} = b_{3q}$, i.e., the coefficient matrix is symmetric and has the same diagonal values. This symmetric property is also true for any number of transmit antennas if their channels are identically distributed and the diagonal values are the same if all channels experience the same SNR.

Fig. 5.1 shows the matrix coefficients of the predictor when $f_dT = 0.02, \rho = 0.5$ of different orders and their mean square prediction errors. We can see that when SNR is very high all the coefficients will become constant (independent of SNR). The SNR at which the coefficients become constant is higher for the predictor of higher order. These are the same properties as a scalar linear predictor. One important remark for matrix linear predictor is that when SNR is very high, all the coefficients b_{2q} converge to zero. This means that when SNR is very high, the prediction of one channel is independent of another channel even if they are correlated, i.e., using the information from the other channel is not helpful when SNR is very high. The SNR at which the coefficients b_{2q} converge to zero is higher for the predictor of higher order. The mean square prediction errors in Fig. 5.1(d) indicate that as Q is higher, the mean square prediction error is lower and as SNR is higher, the mean square prediction errors of different Q reach almost the same value. This property is also similar to a scalar linear predictor.

Fig. 5.2 shows the matrix coefficients of the predictor when $f_dT = 0.02, Q = 2$ with different ρ. We can see that when ρ is higher, the amplitudes of the coefficients b_{21}, b_{22} are higher in the region of SNR lower than 40 dB. This means that with a higher spatial correlation, the linear predictor exploits more information from another transmission channel in the lower SNR region. At very high SNR, the coefficients b_{21}, b_{22} become zero which means that there is no need to use information from another transmission channel since the prediction from its own channel is good already. However, since SNR greater than 40 dB is not practical, the MPR should have more advantage than the SPR in the SNR region of interest.

5.6 Performance Analysis

From the metric in (5.2) or (5.7), we can derive a pairwise error probability (PEP) given a transmitted sequence $\boldsymbol{\mathcal{D}}_L$ and a corresponding error sequence $\tilde{\boldsymbol{\mathcal{D}}}_L$ of length L. Following the approach in [22] and Chapter 4, the PEP is given as

$$P(\boldsymbol{\mathcal{D}}_L \to \tilde{\boldsymbol{\mathcal{D}}}_L) = \frac{1}{2} + \frac{1}{2\pi}\int_{-\infty}^{\infty} \frac{\Phi_{\boldsymbol{z}}(\xi)}{j\xi} d\xi, \tag{5.8}$$

where $\Phi(\xi)$ is a characteristic function of a Gaussian quadratic form $\vec{\boldsymbol{r}}^H \boldsymbol{Y} \vec{\boldsymbol{r}}$ and $\boldsymbol{z} = \vec{\boldsymbol{r}} = \left[\boldsymbol{r}_{-Q}^t, \boldsymbol{r}_{-Q+1}^t, \ldots, \boldsymbol{r}_0^t, \ldots, \boldsymbol{r}_{L-1}^t\right]^t$ is a $2(L+Q) \times 1$ complex vector and $\boldsymbol{Y}$ is a $2(L+Q) \times 2(L+Q)$ Hermitian symmetric matrix. The matrix $\boldsymbol{Y}$ consists of an array of 2×2 block matrices $\boldsymbol{y}_{ij}$, $i, j = -Q, -Q+1, \ldots, L-1$ where

$$\boldsymbol{y}_{ij} = \begin{cases} \boldsymbol{0}_{2\times 2} & ; |i-j| > Q, \\ \sum_{m=u}^{v} \left(\boldsymbol{D}_i \tilde{\boldsymbol{B}}_{m-i}^H \tilde{\boldsymbol{B}}_{m-j} \boldsymbol{D}_j^H - \tilde{\boldsymbol{D}}_i \tilde{\boldsymbol{B}}_{m-i}^H \tilde{\boldsymbol{B}}_{m-j} \tilde{\boldsymbol{D}}_j^H \right) & ;\text{otherwise}, \end{cases} \tag{5.9}$$

where $\tilde{\boldsymbol{B}}_i = -\boldsymbol{B}_i$. The elements $\boldsymbol{y}_{ij}$ are different from that of the no spatial correlation case in Chapter 4. Since the product $\boldsymbol{D}_i \tilde{\boldsymbol{B}}_{m-i}^H \tilde{\boldsymbol{B}}_{m-j} \boldsymbol{D}_j^H$ is not commutative, we cannot separate the term inside the summation into a product of the symbol matrices and the prediction coefficient matrices. The indices of the summation u, v are expressed as

$$u = \begin{cases} 0 & ; i \le 0 \text{ and } j \le 0, \\ \max(i,j) & ;\text{otherwise} \end{cases}$$
$$v = \begin{cases} L-1 & ; i \ge L-Q-1 \text{ and } j \ge L-Q-1, \\ \min(i+Q, j+Q) & ;\text{otherwise.} \end{cases} \tag{5.10}$$

The integral in (5.8) can be evaluated using the residue theorem as in Chapter 4 for VR analysis. Unlike the independent transmission paths case, all the nonzero eigenvalues of $\boldsymbol{R}_{\boldsymbol{r}}\boldsymbol{Y}$ are distinct (first-order). Therefore, the pairwise error probability is in only the following form.

$$P(\boldsymbol{\mathcal{D}}_L \to \tilde{\boldsymbol{\mathcal{D}}}_L) = 1 - \sum_{p_i \in \mathcal{P}, p_i < 0} \prod_{p_j \in \mathcal{P}, j \ne i} \frac{1}{1 - p_j/p_i} \tag{5.11}$$

Finally, the upper bound on the BER or FER is determined from a standard union bound. For BER, the same expression as in (4.8) can be used. For FER, the upper bound on FER can be approximated as [37]

$$P_f < \frac{N}{\log_2 M \times \text{no. of states}} \sum_{L,\boldsymbol{\mathcal{D}}_L,\tilde{\boldsymbol{\mathcal{D}}}_L} P(\boldsymbol{\mathcal{D}}_L \rightarrow \tilde{\boldsymbol{\mathcal{D}}}_L), \tag{5.12}$$

where N is the frame length (total symbol interval). It is complicated to include all possible sequence pairs. Nevertheless, the bound is fairly accurate by including only short length sequence pairs which are dominant especially at high SNR.

5.7 Simulation Results and Discussion

We perform simulation to compare the performances of DSTBC with SPR and MPR at different cross-correlation ρ values. The frame length is 260 symbol intervals. The number of states is four, corresponding to a combination of two BPSK symbols. The optimal order of the linear predictor is not clear but it should be chosen such that the output of the predictor properly represents the channels which are modeled as two correlated autoregressive (AR) processes. The order of the linear predictor is five.

Fig. 5.3 shows the effect of spatial correlation and the improvement of using MPR over SPR at SNR = 20 dB when $f_dT = 0.005, 0.01, 0.02$. We can see that the degradation from spatial correlation is not a linear function of ρ. The degradation becomes more severe at higher spatial correlations ($\rho > 0.5$). At $\rho < 0.3$, the performance is very close to the $\rho = 0.0$ case and MPR has no visible gain over SPR. However, as the spatial correlation increases, MPR seems to have better performance over SPR. At $f_dT = 0.005, 0.01$, MPR achieves higher gain over SPR than at $f_dT = 0.02$. Fig. 5.4 shows FER performance when $\rho = 0.0, 0.2, 0.5, 0.8$ and corresponding upper bounds of MPR when $f_dT = 0.01$. The upper bounds include only length two error sequences while including longer sequences does not affect the bounds at high SNR. They seem to be fairly tight and follow the simulation performance. MPR has about 0.4 and 0.6 dB gain over SPR when $\rho = 0.5$ and 0.8, respec-

tively. Note that this gain is not visible in terms of BER which is essentially the same as in the case of receive diversity [22]. At higher fading rates, it is possible for SPR to perform better than MPR. This is because the assumption of fixed channel gains within a block is less valid at high fading rates. The receiver becomes less optimal and it is found that MPR is more sensitive to this effect.

5.8 Summary

The receiver for DSTBC with a matrix linear predictor is proposed and compared to the receiver with a scalar linear predictor. When there is spatial correlation between antennas, it is found that a small gain can be achieved using matrix linear predictor, especially at slow fading. Although this study shows an example of DSTBC with BPSK and two transmit antennas, the receiver can be easily extended to the case of higher modulation schemes and more than two transmit antennas DSTBC (e.g.,[11]).

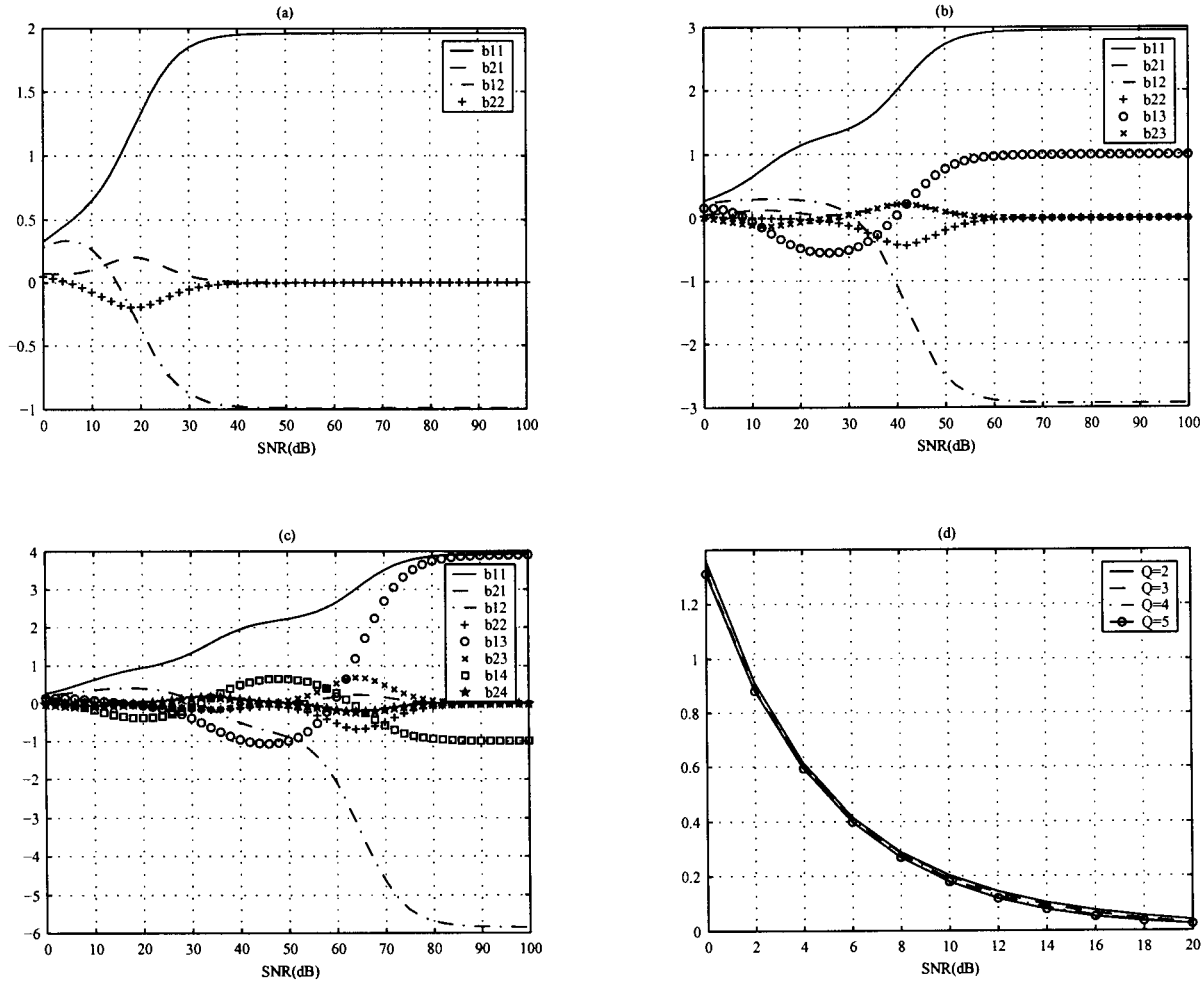

Figure 5.1. *matrix linear prediction coefficients,* $f_d T = 0.02, \rho = 0.5$, *when (a)* $Q = 2$, *(b)* $Q = 3$, *(c)* $Q = 4$ *and (d) the mean square prediction errors when* $Q = 2, 3, 4, 5$.

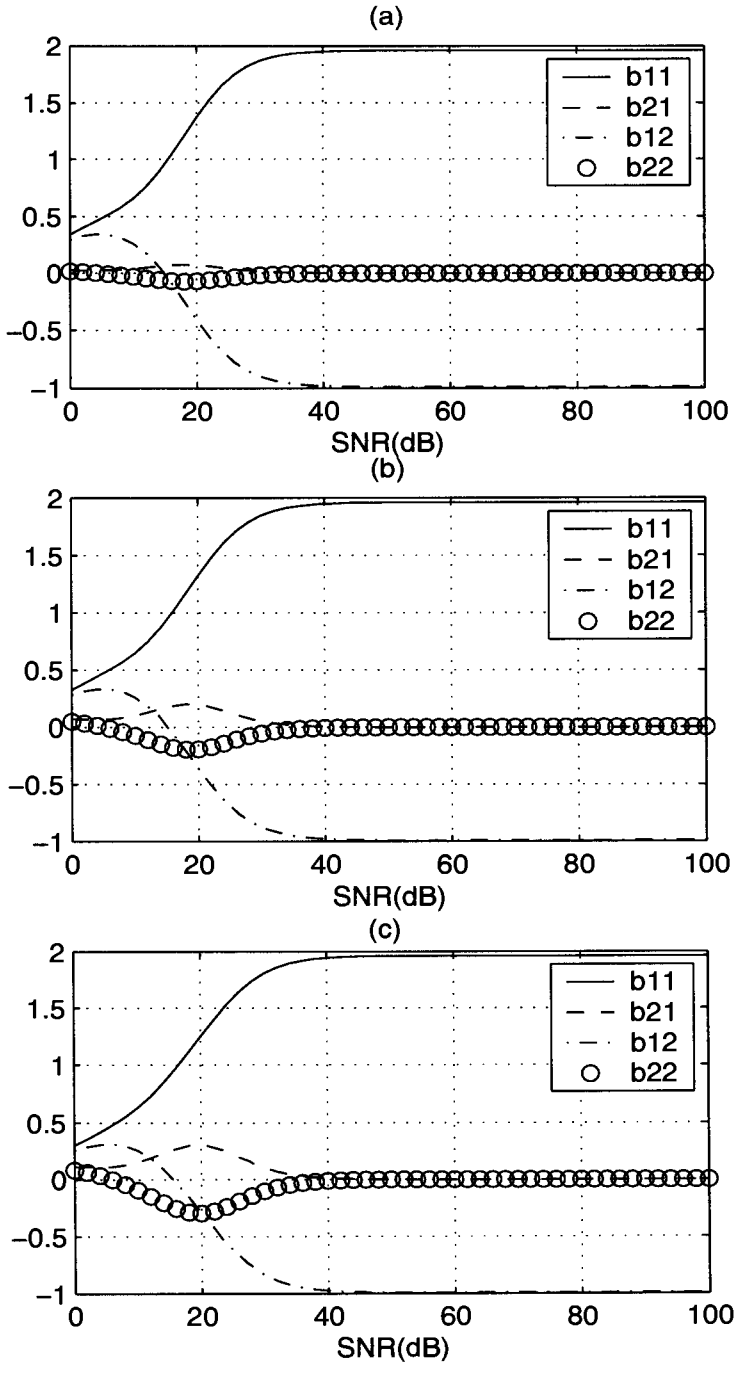

Figure 5.2. *matrix linear prediction coefficients,* $f_d T = 0.02, Q = 2$, *when (a)* $\rho = 0.2$, *(b)* $\rho = 0.5$, *(c)* $\rho = 0.7$

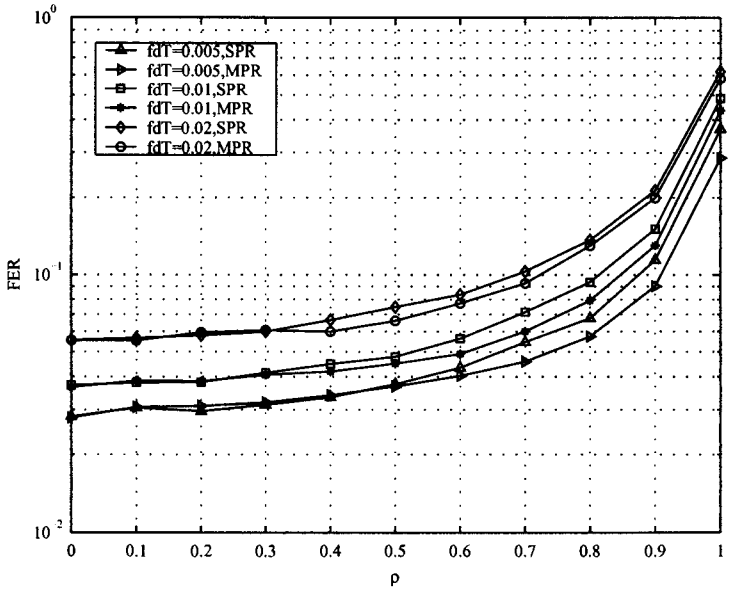

Figure 5.3. *FER simulation performance of DSTBC with BPSK for different spatial correlation values, at SNR=20 dB, with SPR and MPR receivers*

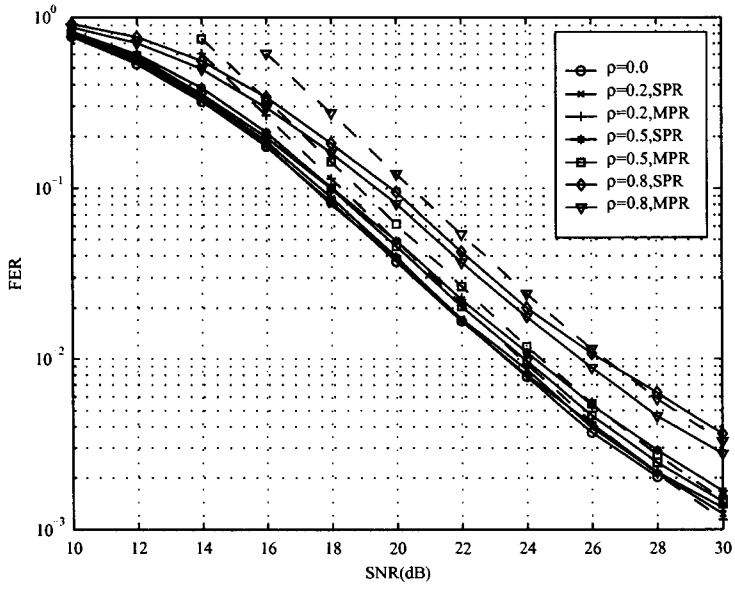

Figure 5.4. *FER simulation performance (solid line) of DSTBC with BPSK, at* $f_dT = 0.01$, $\rho = 0.0, 0.2, 0.5, 0.8$, *with SPR and MPR receivers, and corresponding upper bounds of MPR (dash lines)*

Chapter 6

Trellis-Coded Modulation Concatenated with DSTBC

6.1 Introduction

DSTBC alone does not provide coding gains. To achieve higher coding gains, concatenated code with DSTBC is a viable option. Trellis-coded modulation (TCM) is well-known to achieve a good coding gain without bandwidth expansion or a significant increase in complexity.

If the channel is quasi-static and perfectly known, it is shown in [38] that TCM schemes designed for AWGN channels are still optimal to employ with STBC. For perfectly two-symbol interleaved and perfectly known channels, new design criteria and some example codes are given in [8],[39]. It is concluded in [8],[39] that the design criteria of TCM are the effective code length over span two symbol intervals and the product-sum distance over a span of two symbol intervals.

In this chapter, TCM employed with DSTBC is considered. This system has advantages in that it achieves full spatial diversity and provides coding gain without CSI. Both no interleaver and perfect interleaver cases are discussed. Section 6.2 describes the system model. Section 6.3 derives an upper bound on the pairwise error probability and the design criteria of TCM concatenated with DSTBC with and without perfect interleaving. Although the design criteria are the same as the coherent detection case in [8],[39], TCM schemes

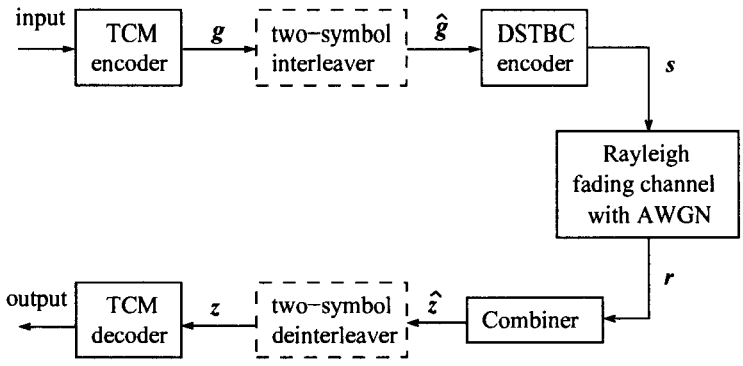

Figure 6.1. *Concatenated TCM-DSTBC System model*

in [8],[39] were designed by hand and no systematic code search was presented. Then, Section 6.4 extends the concept of quasiregular codes [40] with the new design criteria to perform a systematic way of code search. Section 6.5 presents several new rate-2/3 8-PSK TCM schemes and compares them with the existing codes from [41], [42]. Section 6.6 provides a summary of this chapter.

6.2 System Model

The system model is shown in Fig. 6.1. As in previous chapters, DSTBC for two transmit antennas and one receive antenna is assumed, but for convenience in the TCM design, separate mapping as in (2.10) is used. A rate-2/3 TCM encoder with 8-PSK output symbols is assumed. An optional two-symbol interleaver permutes symbol vectors $[g_{2k}\ g_{2k+1}]$ from the output of the TCM encoder. The DSTBC encoder receives interleaved symbol vectors $[\hat{g}_{2k}\,\hat{g}_{2k+1}]$ and performs differential encoding according to (2.8). The channel is frequency-flat Rayleigh fading without spatial correlation between transmit antennas and it is assumed to be static during two consecutive transmission blocks. At the receiver, the combiner

computes a vector $\boldsymbol{z} = [z_{2k}\ z_{2k+1}]$ similar to (2.15)

$$\begin{aligned} z_{2k} &= r_{2k}r^*_{2k-2} + r^*_{2k+1}r_{2k-1} \\ &= (|a_1|^2 + |a_2|^2)\hat{g}_{2k} + [s_{2k}\ s_{2k+1}]\boldsymbol{\Lambda}(a_1\ a_2)N^H_{2k-2} \\ &\quad + N_{2k}\boldsymbol{\Lambda}^H(a_1\ a_2)[s_{2k}\ s_{2k+1}]^H + N_{2k}N^H_{2k-2}, \\ z_{2k+1} &= r_{2k}r^*_{2k-1} - r^*_{2k+1}r_{2k-2} \\ &= (|a_1|^2 + |a_2|^2)\hat{g}_{2k+1} + [s_{2k}\ s_{2k+1}]\boldsymbol{\Lambda}(a_1\ a_2)N^H_{2k-1} \\ &\quad + N_{2k}\boldsymbol{\Lambda}^H(a_1\ a_2)[-s^*_{2k+1}\ s^*_{2k}]^H + N_{2k}N^H_{2k-1} \end{aligned} \tag{6.1}$$

where $\boldsymbol{\Lambda}(a_1\ a_2) = \begin{bmatrix} a_1 & a_2^* \\ a_2 & a_1^* \end{bmatrix}$ and $N_{2k-2} = [n_{2k-2}\ n^*_{2k-1}], N_{2k-1} = [n_{2k-1}\ -n^*_{2k}], N_{2k} = [n_{2k}n^*_{2k+1}]$. The TCM decoder receives the sequence z_{2k}, z_{2k+1} and finds the maximum likelihood coded sequence which minimizes $\mu(\boldsymbol{z}, \hat{\boldsymbol{g}}) = \sum_{k=0}^{N-1} |z_{2k} - \hat{g}_{2k}|^2 + |z_{2k+1} - \hat{g}_{2k+1}|^2$, where $\hat{\boldsymbol{g}}$ is a possible coded sequence on the trellis and N is the block length, assumed to be even.

6.3 Upper Bound on the Pairwise Error Probability

The pairwise error probability (PEP) in this case is the probability that the TCM decoder chooses a maximum likelihood sequence $\tilde{\boldsymbol{g}}$ instead of the transmitted sequence $\boldsymbol{g}$. Applying Chernoff bound to PEP, we obtain

$$P(\boldsymbol{g} \to \tilde{\boldsymbol{g}}|\boldsymbol{a}_1, \boldsymbol{a}_2) \le \prod_{k\in\eta} \mathrm{E}\left[\exp(2\lambda \mathrm{Re}\,(z_{2k}(g_{2k} - \tilde{g}_{2k})^* + z_{2k+1}(g_{2k+1} - \tilde{g}_{2k+1})^*)\right], \tag{6.2}$$

where η is the set of k for which $(g_{2k} \neq \tilde{g}_{2k}$ or $g_{2k+1} \neq g_{2k+1})$ and λ is a Chernoff parameter to be optimized. At high SNR, we can neglect the product terms of noise in (6.1). Substituting (6.1) in (6.2), expanding all noise terms into real and imaginary parts, performing integration and rearranging terms, result in

$$\begin{aligned} P\ \ (\boldsymbol{g} \to \tilde{\boldsymbol{g}}|\boldsymbol{a}_1, \boldsymbol{a}_2) &\le \textstyle\prod_{k\in\eta} \exp\left[\lambda(|a_1|^2 + |a_2|^2)\cdot\ (|g_{2k} - \tilde{g}_{2k}|^2 + |g_{2k+1} - \tilde{g}_{2k+1}|^2)\right] \\ &\quad \cdot\exp\left[4\sigma^2\lambda^2(|a_1|^2 + |a_2|^2)\cdot\ (|g_{2k} - \tilde{g}_{2k}|^2 + |g_{2k+1} - \tilde{g}_{2k+1}|^2)\right], \end{aligned} \tag{6.3}$$

where $|s_{2k}|^2 + |s_{2k+1}|^2 = |s_{2k}|^2 + |s_{2k+1}|^2 = 1$ and $\mathrm{Re}(\tilde{g}_{2k}(g_{2k} - \tilde{g}_{2k})^* + \tilde{g}_{2k+1}(g_{2k+1} - \tilde{g}_{2k+1})^*) = \frac{1}{2}\left(|g_{2k} - \tilde{g}_{2k}|^2 + |g_{2k+1} - \tilde{g}_{2k+1}|^2\right)$ have been used.

Minimizing (6.3) by $\frac{\partial P}{\partial \lambda} = 0$, we obtain $\lambda = -1/8\sigma^2$ and $\sigma^2 = \frac{N_0}{2(E_s/2)}$, where E_s is the total average symbol energy from two transmit antennas. Substituting λ into (6.3) results in

$$P(\boldsymbol{g} \rightarrow \tilde{\boldsymbol{g}}|\boldsymbol{a}_1, \boldsymbol{a}_2) \leq \prod_{k\in\eta} \exp\left[-\frac{E_s}{16N_0}(|\alpha_1|^2 + |\alpha_2|^2)\cdot\ (|g_{2k} - \tilde{g}_{2k}|^2 + |g_{2k+1} - \tilde{g}_{2k+1}|^2)\right]. \tag{6.4}$$

Following the approach in [8],[39], we derive the pairwise error probability for without and with perfect interleaving in a Rayleigh fading channel as follows.

6.3.1 Without Interleaving

We consider a Rayleigh fading channel, where it remains constant over a frame length. Averaging (6.4) with high SNR approximation, we obtain

$$P(\boldsymbol{g} \rightarrow \tilde{\boldsymbol{g}}) \leq \left(\frac{E_s}{16N_0} d_u^2(\boldsymbol{v}, \boldsymbol{r})\right)^{-2}, \tag{6.5}$$

where $d_u^2(\boldsymbol{v}, \boldsymbol{r}) = \sum_{k\in\eta}(|g_{2k} - \tilde{g}_{2k}|^2 + |g_{2k+1} - \tilde{g}_{2k+1}|^2)$. Therefore, the design criterion for TCM is to maximize $d_u^2(\boldsymbol{g}, \tilde{\boldsymbol{g}})$, which is actually *free distance*. Then, optimal TCMs designed for AWGN channel are also optimal to apply with DSTBC in a quasi-static fading channel. The exponent -2 indicates spatial diversity achieved by DSTBC.

6.3.2 Perfect Interleaving

Because DSTBC applies Alamouti's scheme as well, in the following, a perfect two-symbol interleaving is exploited as in [8],[39]. This also applies to a channel which is approximately constant during two consecutive blocks (to allow differential decoding) but is almost uncorrelated during next consecutive blocks. From (6.4), we can readily obtain

$$P(\boldsymbol{g} \rightarrow \tilde{\boldsymbol{g}}) \leq \left[\left(\frac{E_s}{16N_0}\right)^{l_\eta} d_{P2}^2(l_\eta)\right]^{-2}, \tag{6.6}$$

where $d_{P2}^2(l_\eta) = \prod_{k\in\eta}(|g_{2k} - \tilde{g}_{2k}|^2 + |g_{2k+1} - \tilde{g}_{2k+1}|^2)$ denotes the product of distance sum over two symbol intervals of length l_η. Define this as the *product-sum distance* over span two symbol intervals [8],[39]. And l_η is the number of elements in η, called the *effective length* of the error event over span two symbol intervals [8],[39].

Let P_e denote the error event probability. By using union bound, an upper bound of P_e is expressed as $P_e \leq \sum_{\boldsymbol{g}} \sum_{\tilde{\boldsymbol{g}}\neq\boldsymbol{g}} P(\boldsymbol{g})P(\boldsymbol{g} \rightarrow \tilde{\boldsymbol{g}})$, where $P(\boldsymbol{g})$ is the a priori probability of transmitted sequence $\boldsymbol{g}$.

At high SNR, those terms with the smallest l_η and smallest $d_{P2}^2(l_\eta)$ will dominate the error event probability. Denote $L_\eta = \min(l_\eta)$, which can be called the *effective code length over span two symbol intervals* (ECL_2), then the error event probability is approximated as

$$P_e \approx \Xi(L_\eta, d_{P2}^2(L_\eta)) \frac{1}{\left(\frac{E_s}{16N_0}\right)^{2L_\eta} \left(d_{P2}^2(L_\eta)\right)^2}, \tag{6.7}$$

where $\Xi(l_\eta, d_{P2}^2(l_\eta))$ is the average number of error events with the span-2 effective length l_η [8],[39] and the product-sum distance over span two symbol intervals $d_{P2}^2(l_\eta)$.

The error event probability asymptotically varies as the negative $2L_\eta$ power of SNR. The TCM design criteria in this case are therefore to maximize ECL_2 and the minimum $d_{P2}^2(L_\eta)$ at high SNR in Rayleigh fading channel. Denote the minimum $d_{P2}^2(L_\eta)$ as $MPSD_2$ for simplicity.

Note that the design criteria derived from (6.5) and (6.6) are exactly the same as that of TCM concatenated with STBC and with perfect CSI [8],[39]. Therefore, optimal TCM schemes designed with STBC in perfect CSI channels are also optimal for DSTBC in unknown CSI channels. Also, note that E_s/N_0 terms in (6.5) and (6.6) are divided by 16 while they are divided by 8 in [8]. This indicates 3-dB inferior performance in an unknown channel compared to a perfect CSI channel, as expected.

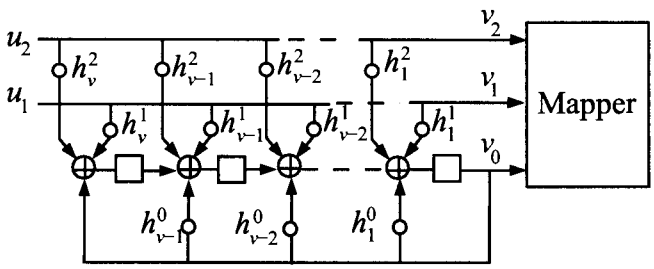

Figure 6.2. *Rate-2/3 Ungerboeck systematic code encoder [5]*

6.4 Quasiregular Code

To reduce the code search space, we will concentrate on a special class of trellis codes called *quasiregular codes*. A code is quasiregular if its distance property can be computed only by assuming that a specific codeword has been sent (e.g. all-zero sequence) [40]. The distribution of the distance between codewords depends on each correct codeword but we can compute the code distance spectrum from an average state error diagram (see [40] for more details). Ungerboeck's systematic code (Fig. 6.2) has been proved to be quasiregular with respect to Euclidean distance and product distance in [40] and [42], respectively.

Let v_1,v_2 be two signal selectors (binary n-tuple before mapping to a symbol) from TCM encoder during two symbol intervals, e_1,e_2 be corresponding selector errors and s_0,s_1,s_2 be the associated trellis states during two symbol intervals. Define the error polynomial over span two symbol intervals as

$$P_{s_0 s_1 s_2, e_1 e_2}(x) \triangleq \sum_{v_1 v_2} p(v_1 v_2 | s_0) x^{f(M(v_1), M(v_1+e_1), M(v_2), M(v_2+e_2))}, \tag{6.8}$$

where $f(\cdot)$ is some distance metric which has additive property on the trellis, $p(v_1 v_2|s_0)$ is the probability of selector v_1, v_2 given initial state s_0 and $M(\cdot)$ is the constellation mapping function. Here we define $f(\cdot)$ as

$$\ln\left(|M(v_1) - M(v_1+e_1)|^2 + |M(v_2) - M(v_2+e_2)|^2\right). \tag{6.9}$$

Similar to [40], a trellis code is quasiregular with respect to product-sum distance over span two symbol intervals if its error polynomial over span two symbol intervals does not depend on any state pairs (s_0, s_2).

Suppose the distance metric $f(\cdot) = |M(v_1) - M(v_1 + e_1)|^2 + |M(v_2) - M(v_2 + e_2)|^2$. We can readily find the error polynomial over span two symbol intervals from

$$P_{s_0 s_1 s_2, e_1 e_2}(x) = P_{s_0 s_1, e_1}(x) \cdot P_{s_1 s_2, e_2}(x), \tag{6.10}$$

where $P_{s_0 s_1, e_1}(x)$ and $P_{s_1 s_2, e_2}(x)$ are the error polynomial (over span one) defined in [40].

Therefore, we can state that if a code has its error polynomial over span one which does not depend on any state pairs, its error polynomial over span two symbol intervals will not depend on any state pairs either. Then we replace the distance metric with (6.9) without affecting the dependency of state pairs and the code will be quasiregular with respect to product-sum distance over span two symbol intervals. So, we can conclude that Ungerboeck's systematic code, whose error polynomial over span one does not depend on any state pairs, is quasiregular with respect to the product-sum distance over span two symbol intervals.

6.5 Search Results and Simulation Performance

We performed a computer search by modifying Larsen's algorithm [40] to find optimal rate-2/3 8-PSK Ungerboeck's systematic codes. First, we maximize ECL_2. Among the codes that have the same ECL_2, we find the codes that have maximum $MPSD_2$. In all cases, parallel transition must be avoided. Table 6.1 shows the search results and comparison with TCM codes designed for AWGN [41] and fading channels [42]. The codes shown are optimal in terms of ECL_2 and $MPSD_2$ although several codes are found to achieve the same ECL_2 and $MPSD_2$. Note that the value $MPSD_2$ is computed with the unit energy 8-PSK constellation.

For 4-, 8- and 16- state codes, they are found to be the same as those in [8],[39]. For 8- and 16-state codes, they actually correspond to Ungerboeck's codes. The new codes

achieve a clear improvement over existing codes when the number of state is greater than 16.

Fig. 6.3 and 6.4 show bit error rate (BER) performances of some TCM schemes in perfect-interleaved Rayleigh fading channels. The block length is 130 symbols. We neglect error bits occurring near the end of the frame. Solid lines correspond to differential coherent receiver cases while dash lines correspond to coherent receiver cases. We can see 3-dB performance degradation of differential coherent receiver compared to coherent receiver. The codes in Fig. 6.3 are 4-state TCM schemes from Ungerboeck [41], Jamali/Le-Ngoc [43] and Wilson/Leung [44], which have $MPSD_2$ equal to 4, 4 and 4.59, respectively. Ungerboeck's code [41] is inferior to Jamali/Le-Ngoc's code [43] because it has parallel transitions. In Fig. 6.4, a new 32-state TCM code, t5, has 0.8-dB gain to f5 (optimal code design for fading channels) and 5-dB gain to g5 (optimal code design for AWGN channels), at BER 10^{-5}. The slopes of t5 and f5 are steeper than g5 because t5 and f5 have $ECL_2 = 2$ and g5 has $ECL_2 = 1$. Fig. 6.3 and 6.4 clearly illustrates the dominant effects of ECL_2 and $MPSD_2$ to the code performance.

We compare our results with trellis coded unitary space-time modulation (TCUSTM) [45]. At BER 10^{-4}, t5 has about 4-dB gain compared to 256-state TCUSTM (Fig. 5 [45]) while the former sustains spectral efficiency 2 bps/Hz and the latter provides 1 bps/Hz. This improvement comes at possibly higher complexity and at the expense of inherit constellation expansion of DSTBC. However, to find the optimal trellis structure for TCUSTM seems to be more difficult than our approach, especially with a large number of states. If we compare our results with a turbo code concatenated with differential unitary space-time modulation [46], it seems that the latter has greater performance. However, it requires a larger block length and higher decoding complexity due to iterative demodulation and decoding.

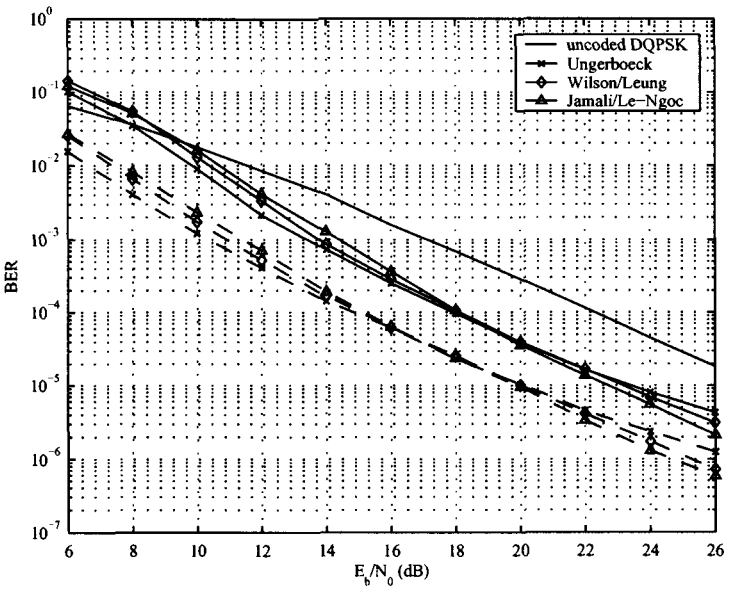

Figure 6.3. *Rate-2/3 8-PSK 4-state TCM concatenated with DSTBC with perfect interleaving on Rayleigh fading channels, two transmit antennas and one receive antenna. Solid lines correspond to differential coherent receiver cases. Dashed lines correspond to coherent receiver cases.*

6.6 Summary

In this chapter, we have derived the design criteria for TCM with differential space-time block code in unknown Rayleigh fading channels. These new design criteria, are *effective code length over span two symbol intervals* and minimum *product-sum distance over span two symbol intervals*. The concept of quasiregularity is extended to the new design criteria. Several new rate-2/3 8-PSK TCMs are found and shown to outperform the optimal codes design for AWGN channel and Rayleigh fading channel without transmit diversity. The codes presented here can be used with STBC in perfectly known fading channels.

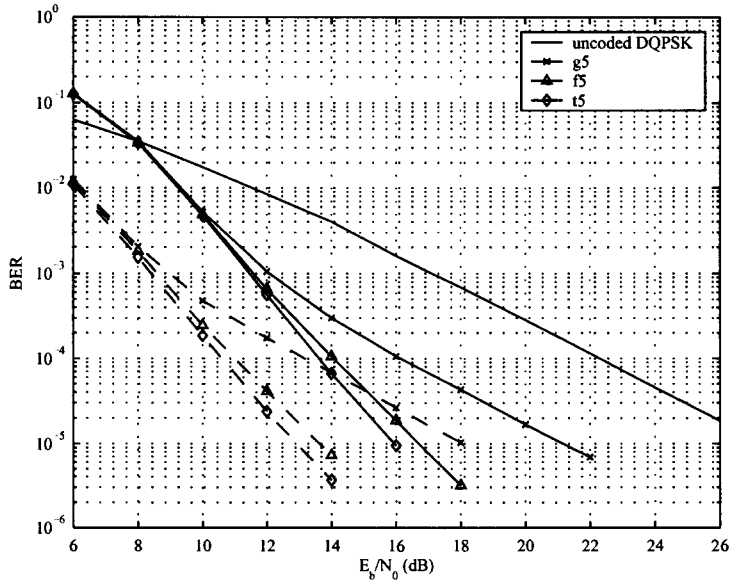

Figure 6.4. *Rate-2/3 8-PSK 32-state TCM concatenated with DSTBC with perfect interleaving on Rayleigh fading channels, two transmit antennas and one receive antenna. Solid lines correspond to differential coherent receiver cases. Dashed lines correspond to coherent receiver cases.*

Table 6.1. *Rate-2/3 8-PSK Systematic Ungerboeck Codes*

ν	Code	$h^0(D)$	$h^1(D)$	$h^2(D)$	ECL_2	$MPSD_2$
3	t3	11	02	04	1	6
	g3	11	02	04	1	6
	f3	11	02	04	1	6
4	t4	23	04	16	2	8
	g4	23	04	16	2	8
	f4	23	04	16	2	8
5	t5	65	34	04	2	15.51
	g5	45	16	34	1	6
	f5	43	14	36	2	6.69
6	t6	101	030	004	2	16
	g6	103	030	066	2	12
	f6	103	036	154	2	14
7	t7	303	144	124	2	59.31
	g7	277	054	122	2	18.34
	f7	223	076	314	2	21.66
8	t8	425	070	360	3	36.69
	g8	435	072	130	2	16
	f8	673	336	164	3	7.83
9	t9*	1335	150	360	3	48
	g9	1007	164	260	2	16
	f9	1413	756	244	3	7.83
10	t10*	2445	726	620	3	62.06
	g10	2003	164	770	2	14.04
	f10	3303	1676	504	3	36.2

ν is the number of memories; tx is the new code found

gx is the code designed for AWGN channels [41]

fx is the code designed for fading channels [42]

* search not complete

Chapter 7

Future Works and Extensions

Although space-time coding and modulation were born in 1998 and there have been many research papers published in recent years, this research area is still in a growing stage. There are still a lot of unsolved problems as mentioned in the recent special issues of IEEE Journal Selected Areas on Communications, April 2003 and IEEE Transactions on Information Theory, October 2003. The research area of differential space-time codes accompanied with an efficient decoding scheme is growing fast and very popular. A few interesting extensions are classified as follows.

7.1 The Extension to More than Two Transmit Antennas

All the receiver algorithms in this thesis have been derived for a specific DSTBC based on Alamouti's transmission matrix. As already mentioned, the algorithms can be applied to other types of DSTBC for two transmit antennas with trivial modifications. However, the extension to more than two transmit antennas leads to a more complex problem. Since the receivers are exponentially complex with respect to the number of transmit antennas, a large number of trial symbols must be required in the decoding. In addition, the algorithms themselves have to be modified to accommodate nonsquare transmission matrix since a full-rate STBC does not exist for more than two transmit antennas. For DSTBC with $\mathcal{N}$ transmit antennas, the linear predictor embedded in the receiver is expected to be $\mathcal{N}$-step linear predictor.

The assumption of fixed channel gains during a transmission block will have more influence on DSTBC with higher numbers of transmission antennas. The degradation due to this assumption will be distinct and will not be negligible. This raises a question of whether an optimal receiver for DSTBC which takes into account the time-varying channel gains within a transmission block can be found.

For the concatenated coding system with $\mathcal{N}$ transmit antennas, the design criterion for non-interleaved TCM for DSTBC is expected to be free distance while the design criteria for perfect-interleaved case are expected to be effective length and product-sum distance over span $\mathcal{N}$. Many more new optimal TCM concatenated with DSTBC for $\mathcal{N}$ transmit antennas are still to be discovered.

7.2 Optimal Receiver for DSTBC on Fading Time-Varying Channels

Although the multistage receiver presented in Chapter 5 tries to deal with the time-varying channel gains within a transmission block, it can not be claimed as an optimal receiver. Recent contributions which point out and try to solve this problem are [47] and [48]. They propose a Viterbi receiver and decision-feedback receiver which take into account the time-varying channel gains within a transmission block. The performance of their new receivers is significantly improved and they are claimed to be optimal. However, the receivers only work with a specific type of DSTBC, so-called G-diagonal. For other types of DSTBC, the design of an optimal receiver still remains a challenging problem. In addition, the optimal receiver which takes the spatial correlation into account is obviously the one to be explored.

7.3 Receiver for DSTBC on Frequency-Selective Fading Channels

In practice, the frequency-selective fading characteristic usually appears and it causes severe performance degradation if intersymbol-interference (ISI) is not properly mitigated. Conventional equalization methods may be applied but it will be complicated for multiple antenna system since training symbols are needed for each transmit antenna. Blind equalization in multiple antenna system may be a viable option for DSTBC. This is a non-trivial problem since DSTBC constellations may not have constant modulus property to be exploited in the blind equalization.

Recent approaches consider the combination of orthogonal frequency division multiplexing (OFDM) and multiple transmit antennas to mitigate the effects of ISI. Since OFDM inherently transforms a frequency-selective fading channel to a frequency-flat fading channel, then equalization is performed easily in the frequency domain. For DSTBC system, DSTBC incorporated with OFDM modulation type have been considered in [49], [50] where equalization has done by differential decoding in the frequency domain. Time domain equalization of DSTBC has been proposed in [49] to avoid the disadvantages of OFDM with increased complexity. Other approaches may be possible and there still exists a large research gap in this problem.

7.4 Iterative Decoding for DSTBC

In the concatenated coding with DSTBC system, since DSTBC can also be considered as a recursive inner code, the concatenated coding scheme is a serial concatenated code in which iterative decoding is possibly applied. Noncoherent iterative decoding without CSI has been applied successfully in single antenna systems [51],[52]. For multiple antenna systems, there have been a few efforts recently to apply iterative decoding with DSTBC system. The first effort was presented in [53] where BCJR-typed [54] symbol level iterative

decoding is applied to a concatenation of convolutional code and DSTBC. A similar idea has been presented in [55] including a more detailed analysis. Bit level iterative decoding with hard decision feedback has recently been applied with bit-interleaved DSTBC in [35] where good performance is obtained with relatively low complexity. Two more recent approaches apply soft-output Viterbi algorithm to iterative decoding of DSTBC in [56] and [57]. All the performance curves of iterative decoding (without CSI) of DSTBC in the above papers approach or even outperform the performance of coherent detection with perfect CSI. However, time-varying channel gains within a transmission block are still not taken into account in the iterative decoding. This gap might be possible to considered by a multistage receiver in this thesis or other new approaches.

Bibliography

[1] V. Tarokh, N. Seshadri, and A. R. Calderbank, "Space–time codes for high data rate wireless communication: Performance criterion and code construction," *IEEE Transactions on Information Theory*, vol. 44, no. 2, pp. 744–765, March 1998.

[2] S. M. Alamouti, "A simple transmit diversity technique for wireless communications," *IEEE Journal on Selected Areas in Communications*, vol. 16, no. 8, pp. 1451–1458, October 1998.

[3] V. Tarokh and H. Jafarkhani, "A differential detection scheme for transmit diversity," *IEEE Journal on Selected Areas in Communications*, vol. 18, no. 7, pp. 1169–1174, July 2000.

[4] B. M. Hochwald and W. Sweldens, "Differential unitary space–time modulation," *IEEE Transactions on Communications*, vol. 48, no. 12, pp. 2041–2052, December 2000.

[5] B. L. Hughes, "Differential space–time modulation," *IEEE Transactions on Information Theory*, vol. 46, no. 7, pp. 2567–2578, November 2000.

[6] P. Fan, "Multiple–symbol detection for transmit diversity with differential encoding scheme," *IEEE Transactions on Consumer Electronics*, vol. 47, no. 1, pp. 96–100, February 2001.

[7] E. Chiavaccini and G. M. Vitetta, "Further results on Tarokh's space–time differential technique," in *Proc. IEEE International Conference on Communications (ICC)*, vol. 3, 28 April - 2 May 2002, pp. 1778–1782.

[8] Y. Gong and K. B. Letaief, "Analysis and design of trellis coded modulation with transmit diversity for wireless communications," in *Proc. IEEE Wireless Communications and Networking Conference (WCNC)*, vol. 3, pp. 1356–1361.

[9] V. Tarokh, H. Jafarkhani, and A. R. Calderbank, "Space–time block codes from orthogonal designs," *IEEE Transactions on Information Theory*, vol. 45, no. 5, pp. 1456–1467, July 1999.

[10] W. Su and X.-G. Xia, "Two generalized complex orthogonal space–time block codes of rates 7/11 and 3/5 for 5 and 6 transmit antennas," *IEEE Transactions on Information Theory*, vol. 49, no. 1, pp. 313–316, January 2003.

[11] H. Jafarkhani and V. Tarokh, "Multiple transmit antenna differential detection from generalized orthogonal designs," *IEEE Transactions on Information Theory*, vol. 47, no. 6, pp. 2626–2631, September 2001.

[12] T. L. Marzetta and B. M. Hochwald, "Capacity of a mobile multiple–antenna communication link in Rayleigh flat fading," *IEEE Transactions on Information Theory*, vol. 45, no. 1, pp. 139–157, January 1999.

[13] B. L. Hughes, "Optimal space–time constellations from groups," *IEEE Transactions on Information Theory*, vol. 49, no. 2, pp. 401–410, February 2003.

[14] A. Shokrollahi, B. Hassibi, B. M. Hochwald, and W. Sweldens, "Representation theory for high-rate multiple–antenna code design," *IEEE Transactions on Information Theory*, vol. 47, no. 6, pp. 2335–2367, September 2001.

[15] M. O. Damen, H. E. Gamal, and N. C. Beaulieu, "Linear threaded algebraic space–time constellations," *IEEE Transactions on Information Theory*, vol. 49, no. 10, pp. 2372–2388, October 2003.

[16] Z. Hong and B. L. Hughes, "Differential transmit diversity for PSK constellations," in *Proc.* 34^{th} *Annual Conference on Information Sciences and Systems, Princeton University, NJ*, 15-17 March 2000.

[17] K. Feher, "MODEMS for emerging digital cellular-mobile radio system," *IEEE Transactions on Vehicular Technology*, vol. 40, no. 2, pp. 355–365, May 1991.

[18] D. Divsalar and M. K. Simon, "Multiple symbol differential detection of MPSK," *IEEE Transactions on Communications*, vol. 38, no. 3, pp. 300–308, March 1990.

[19] C. Gao and A. M. Haimovich, "Multiple–symbol differential detection for space–time block codes," in *Proc.* 36^{th} *Annual Conference on Information Sciences and Systems, Princeton University, NJ*, 20-22 March 2002.

[20] F. Edbauer, "Bit error rate of binary and quaternary DPSK signals with multiple differential feedback detection," *IEEE Transactions on Communications*, vol. 40, no. 3, pp. 457–460, March 1992.

[21] G. M. Vitetta and D. P. Taylor, "Maximum likelihood decoding of uncoded and coded PSK signal sequences transmitted over Rayleigh flat-fading channels," *IEEE Transactions on Communications*, vol. 43, no. 11, pp. 2750–2758, November 1995.

[22] B. D. Hart and D. P. Taylor, "Maximum–likelihood synchronization, equalization, and sequence estimation for unknown time-varying frequency-selective Rician channels," *IEEE Transactions on Communications*, vol. 46, no. 2, pp. 211–221, February 1998.

[23] D. Makrakis, P. T. Mathiopoulos, and D. P. Bouras, "Optimal decoding of coded PSK and QAM signals in correlated fast fading channels and AWGN: A combined

envelope, multiple differential and coherent detection approach," *IEEE Transactions on Communications*, vol. 42, no. 1, pp. 63–75, January 1994.

[24] R. Schober and L. H.-J. Lampe, "Noncoherent receivers for differential space–time modulation," *IEEE Transactions on Communications*, vol. 50, no. 5, pp. 768–777, May 2002.

[25] C. Ling and X. Wu, "Linear prediction receiver for differential space–time modulation over time-correlated Rayleigh fading channels," in *Proc. IEEE International Conference on Communications (ICC)*, vol. 2, 28 April-2 May 2002, pp. 788–791.

[26] B. H. Park, K. J. Kim, S. Y. Kwon, and K. C. Whang, "Multistage decision-directed channel estimation scheme for DS–CDMA system with M–ary orthogonal signaling," *IEEE Transactions on Vehicular Technology*, vol. 49, no. 1, pp. 43–49, January 2000.

[27] F. Adachi, "Adaptive differential detection using linear prediction for M-ary DPSK," *IEEE Transactions on Vehicular Technology*, vol. 47, no. 3, pp. 909–918, August 1998.

[28] R. Schober and W. H. Gerstacker, "Decision–feedback differential detection based on linear prediction for MDPSK signals transmitted over Ricean fading channels," *IEEE Journal Selected Areas in Communications*, vol. 18, no. 3, pp. 391–402, March 2000.

[29] M. Schwartz, W. R. Bennett, and S. Stein, *Communication Systems and Techniques.* New York: McGraw-Hill, 1966.

[30] A. D. Wunsch, *Complex Variables with Applications.* Addison-Wesley, 1983.

[31] ETSI, "Digital cellular telecommunications system (phase 2+); channel coding," *ETSI TS 100 909*, vol. 8.6.0, (2000-11).

[32] J. Hagenauer, E. Offer, and L. Papke, "Iterative decoding of binary block and convolutional codes," *IEEE Transactions on Information Theory*, vol. 42, no. 2, pp. 429–445, March 1996.

[33] P. Robertson, E. Villebrun, and P. Hoeher, "A comparison of optimal and sub–optimal MAP decoding algorithms operating in the log domain," in *Proc. IEEE International Conference on Communications (ICC)*, vol. 2, 18-22 June 1995, pp. 1009–1013.

[34] J. Ventura-Traveset, G. Caire, E. Bliglieri, and G. Taricco, "Impact of diversity reception on fading channels with coded modulation-Part I: coherent detection," *IEEE Transactions on Communications*, vol. 45, no. 5, pp. 563–572, May 1997.

[35] L. H.-J. Lampe and R. Schober, "Bit-interleaved coded differential space–time modulation," *IEEE Transactions on Communications*, vol. 50, no. 9, pp. 1429–1439, September 2002.

[36] S. M. Kay, *Modern Spectral Estimation.* Prentice Hall, 1987.

[37] G. Caire and E. Viterbo, "Upper bound on the frame error probability of terminated trellis codes," *IEEE Communications Letters*, vol. 2, no. 1, pp. 2–4, January 1998.

[38] S. M. Alamouti, V. Tarokh, and P. Poon, "Trellis–coded modulation and transmit diversity: Design criteria and performance evaluation," in *Proc. IEEE International Conference on Universal Personal Communications (ICUPC)*, vol. 1, October 1998, pp. 703–707.

[39] Y. Gong and K. B. Letaief, "Concatenated space–time block coding with trellis coded modulation in fading channels," *IEEE Transactions on Wireless Communications*, vol. 1, no. 4, pp. 580–590, October 2002.

[40] M. Rouanne and D. J. Costello, "An algorithm for computing the distance spectrum of trellis codes," *IEEE Journal on Selected Areas in Communications*, vol. 7, no. 6, pp. 929–940, August 1989.

[41] G. Ungerboeck, "Channel coding with multilevel/phase signals," *IEEE Transactions on Information Theory*, vol. IT-28, pp. 55–67, January 1982.

[42] C. Schlegel and D. J. Costello, "Bandwidth efficient coding for fading channels: code construction and performance analysis," *IEEE Journal on Selected Areas in Communications*, vol. 7, no. 9, pp. 1356–1368, December 1989.

[43] H. Jamali and T. Le-Ngoc, *Coded modulation techniques for fading channels.* Boston, MMA:Kluwer, 1994.

[44] S. G. Wilson and Y. S. Leung, "Trellis–coded phase modulation on Rayleigh channels," in *Proc. IEEE International Conference on Communications (ICC)*, June 1987, pp. 21.3.1–21.3.5.

[45] I. Bahceci and T. M. Duman, "Trellis coded unitary space–time modulation," in *Proc. IEEE Global Telecommunications Conference (Globecom)*, vol. 2, 25-29 November, pp. 1108–1112.

[46] A. Steiner, M. Peleg, and S. Shamai(Shitz), "Turbo coded space–time unitary matrix differential modulation," in *Proc. IEEE Vehicular Technology Conference (VTC)*, vol. 2, 6-9 May 2001, pp. 1352–1356.

[47] C. Ling, K. H. Li, and A. C. Kot, "Noncoherent sequence detection of differential space–time modulation," *IEEE Transactions on Information Theory*, vol. 49, no. 10, pp. 2727–2734, October 2003.

[48] ——, "On decision-feedback detection of differential space–time modulation in continuous fading," *Submitted to IEEE Transactions on Communications*, October 2003.

[49] S. N. Diggavi, N. Al-Dhahir, A. Stamoulis, and A. R. Calderbank, "Differential

space–time coding for frequency-selective channels," *IEEE Communications Letters*, vol. 6, no. 6, pp. 253–255, June 2002.

[50] H. Li, "Differential space–time-frequency modulation over frequency-selective fading channels," *IEEE Communications Letters*, vol. 7, no. 8, pp. 349–351, August 2003.

[51] G. Colavolpe, G. Ferrari, and R. Raheli, "Noncoherent iterative (turbo) decoding," *IEEE Transactions on Communications*, vol. 48, no. 9, pp. 1488–1498, September 2000.

[52] L. H.-J. Lampe and R. Schober, "Iterative decision-feedback differential demodulation of bit-interleaved coded MDPSK for flat Rayleigh fading channels," *IEEE Transactions on Communications*, vol. 49, no. 7, pp. 1176–1184, July 2001.

[53] A. V. Nguyen and M. A. Ingram, "Iterative demodulation and decoding of differential space–time block codes," in *Proc. IEEE Vehicular Technology Conference (VTC)*, vol. 5, 24-28 September 2000, pp. 2394–2400.

[54] L. Bahl, J. Cocke, F. Jelinek, and J. Raviv, "Optimal decoding of linear codes for minimizing symbol error rate," *IEEE Transactions on Information Theory*, vol. 20, pp. 284–287, March 1974.

[55] C. Schlegel and A. Grant, "Differential space–time turbo codes," *IEEE Transactions on Information Theory*, vol. 49, no. 9, pp. 2298–2306, September 2003.

[56] K. J. Han and J. H. Lee, "Iterative decoding of a differential space–time block code with low complexity," in *Proc. IEEE Vehicular Technology Conference (VTC)*, vol. 3, 6-9 May 2002, pp. 1322–1325.

[57] J. Yuan, X. Shao, and Y. Hong, "Differential space–time block codes with iterative detection," in *Proc. IEEE International Symposium on Information Theory (ISIT)*, 29 June-4 July 2003, p. 61.

[58] M. J. Barrett, "Error probability for optimal and suboptimal quadratic receivers in rapid Rayleigh fading channels," *IEEE Journal on Selected Areas in Communications*, vol. 5, no. 2, pp. 302–304, February 1987.

Appendix A

Derivation of Pairwise Error Probability of DSTBC with Viterbi Receiver

This appendix derives a pairwise error probability (PEP) of DSTBC with Viterbi receiver. Let $\Phi(\xi)$ be a characteristic function of a Gaussian quadratic form which can be represented as

$$\Phi_{\boldsymbol{z}}(\xi) = \frac{1}{\det[I - j2\xi \boldsymbol{R}_{\boldsymbol{r}}\boldsymbol{Y}]} = \prod_{\forall\, \mathrm{eig}_n(\boldsymbol{R}_{\boldsymbol{r}}\boldsymbol{Y})\neq 0} (1 - j2\xi \mathrm{eig}_n(\boldsymbol{R}_{\boldsymbol{r}}\boldsymbol{Y}))^{-1} \tag{A.1}$$

The PEP (4.13) is repeated here with manipulations.

$$\begin{aligned} P(\boldsymbol{\mathcal{D}}_L \to \tilde{\boldsymbol{\mathcal{D}}}_L) &= \int_0^\infty \frac{1}{2\pi} \int_{-\infty}^{\infty} \Phi_{\boldsymbol{z}}(\xi)\exp(-j\xi\kappa)d\xi d\kappa \\ &= \frac{1}{2\pi}\int_{-\infty}^{\infty} \Phi_{\boldsymbol{z}}(\xi) \int_0^\infty \exp(-j\xi\kappa)d\kappa d\xi \\ &= \frac{1}{2\pi}\int_{-\infty}^{\infty} \Phi_{\boldsymbol{z}}(\xi) \int_{-\infty}^{\infty} u(\kappa)\exp(-j\xi\kappa)d\kappa d\xi \\ &= \frac{1}{2\pi}\int_{-\infty}^{\infty} \Phi_{\boldsymbol{z}}(\xi) \left[\frac{1}{j\xi} + \frac{1}{2}\delta\left(\frac{\xi}{2\pi}\right)\right] d\xi \\ &= \frac{1}{2} + \frac{1}{2\pi}\int_{-\infty}^{\infty} \frac{\Phi_{\boldsymbol{z}}(\xi)}{j\xi} d\xi \end{aligned} \tag{A.2}$$

$u(\kappa)$ is a unit-step function. Let $\mathcal{P}$ denote a set of nonzero eigenvalues of $\boldsymbol{R}_{\boldsymbol{r}}\boldsymbol{Y}$. The characteristic function (A.1) is written as

$$\Phi_{\boldsymbol{z}}(\xi) = \prod_{p_i \in \mathcal{P}} \frac{jp_i^{-1}}{2\xi + jp_i^{-1}} \tag{A.3}$$

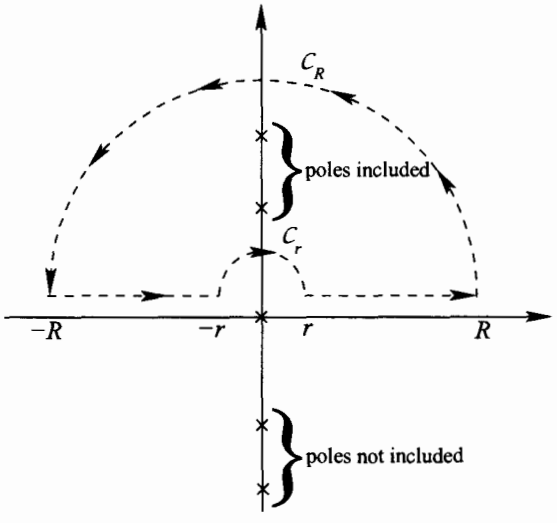

Figure A.1. *Contour integral C. The cross points are poles of $F(\varsigma)$*

Then, the PEP (A.1) is expressed as

$$P(\boldsymbol{\mathcal{D}}_L \to \tilde{\boldsymbol{\mathcal{D}}}_L) = \frac{1}{2} + \frac{1}{2\pi}\int_{-\infty}^{\infty}\left[\prod_{p_i\in\mathcal{P}}\left(\frac{jp_i^{-1}}{2\xi + jp_i^{-1}}\right)\right](j\xi)^{-1}d\xi \tag{A.4}$$

To evaluate the integral in (A.4), we follow the approach in [58] where the integral has been evaluated for the performance of quadratic receivers in Rayleigh fading channels. Let $F(\xi) = \left[\prod_{p_i\in\mathcal{P}}\left(\frac{jp_i^{-1}}{2\xi+jp_i^{-1}}\right)\right](j\xi)^{-1}$. The set of the poles of $F(\xi)$ is $\{0, -jp_i^{-1}/2$ where $p_i \in \mathcal{P}\}$. The infinite integral in (A.4) is represented as a contour integral

$$\begin{aligned}\int_{-\infty}^{\infty} F(\xi)d\xi &= \lim_{r\to 0, R\to\infty}\oint_C F(\varsigma)d\varsigma \\ &= \lim_{r\to 0, R\to\infty}\left[\int_{C_R} F(\varsigma)d\varsigma + \int_{-R}^{-r} F(\varsigma)d\varsigma + \int_{C_r} F(\varsigma)d\varsigma + \int_{r}^{R} F(\varsigma)d\varsigma\right]\end{aligned} \tag{A.5}$$

where the contour C is shown in Fig. A.1. The variable ξ has been redefined as ς to accommodate complex values in the contour integral. Now, the following Residue theorem is applied [30].

$$\oint_C F(\varsigma)d\varsigma = 2\pi j \cdot \sum_{\varsigma_n \in \text{poles of } F(\varsigma) \text{inside} C} \text{Res}\left[F(\varsigma), \varsigma_n\right] \tag{A.6}$$

where $\text{Res}[F(\varsigma), \varsigma_n]$ is the residue of $F(\varsigma)$ at ς_n computed as [30]

$$\text{Res}[F(\varsigma), \varsigma_0] = \lim_{\varsigma \to \varsigma_0} [(\varsigma - \varsigma_0)F(\varsigma)], \text{if } \varsigma_0 \text{ is a first-order pole} \quad (A.7)$$

$$\text{Res}[F(\varsigma), \varsigma_0] = \lim_{\varsigma \to \varsigma_0} \frac{d}{d\varsigma} [(\varsigma - \varsigma_0)^2 F(\varsigma)], \text{if } \varsigma_0 \text{ is a second-order pole} \quad (A.8)$$

Using (A.7), we obtain $\text{Res}[F(\varsigma), 0] = -j$.

When $F(\varsigma)$ is a rational function and the order of its denominator is more than the order of its nominator at least two, the integral along the arc with radius close to infinity is zero [30](Eq.6.5-10). Therefore, the integral of the larger arc C_R is evaluated as

$$\lim_{R \to \infty} \int_{C_R} F(\varsigma) d\varsigma = 0. \quad (A.9)$$

The integral of the smaller arc C_r when $r \to 0$ contributes half of the closed contour around the origin in the clockwise direction [58] which is expressed as

$$\lim_{r \to 0} \int_{C_r} F(\varsigma) d\varsigma = -\frac{1}{2} \cdot 2\pi j \cdot \text{Res}[F(\varsigma), 0] = -\pi. \quad (A.10)$$

Therefore, from (A.5), (A.9) and (A.10) The integral of the characteristic function can be evaluated as

$$\int_{-\infty}^{\infty} F(\varsigma) d\varsigma = \pi + 2\pi j \cdot \sum_{\varsigma_n in u.h.p.} \text{Res}[F(\varsigma), \varsigma_n] \quad (A.11)$$

and the poles to be included lie on the upper half plane (u.h.p.) (See Fig. A.1)

For DSTBC, the nonzero poles of the characteristic function $F(\varsigma)$ fall into two cases

Case 1: All nonzero poles of $F(\varsigma)$ are distinct. Each pole is a first-order pole and its residue is

$$\begin{aligned} \text{Res}[F(\varsigma), -jp_i/2] &= \lim_{\varsigma \to -jp_i/2} (\varsigma + jp_i^{-1}/2) \left[\prod_{p_i \in \mathcal{P}} \left(\frac{jp_i^{-1}/2}{\varsigma + jp_i^{-1}/2} \right) \right] (j\varsigma)^{-1} \\ &= j \cdot \prod_{p_j \in \mathcal{P}, p_j \neq p_i} \frac{1}{1 - p_j/p_i}. \end{aligned} \quad (A.12)$$

Using the above result in (A.11) and (A.4), the PEP can be expressed as

$$P(\boldsymbol{\mathcal{D}}_L \to \tilde{\boldsymbol{\mathcal{D}}}_L) = 1 - \sum_{p_i \in \mathcal{P}, p_i < 0} \prod_{p_j \in \mathcal{P}, j \neq i} \frac{1}{1 - p_j/p_i}. \quad (A.13)$$

Case 2: There are $2 \times (L-1)$ distinct nonzero eigenvalues, each with multiplicity two. Let $\tilde{\mathcal{P}}$ denote a set of *distinct* nonzero eigenvalues of $\boldsymbol{R}_{\boldsymbol{r}}\boldsymbol{Y}$. Each pole $p_i \in \tilde{\mathcal{P}}$ is a second-order pole and its residue is

$$\text{Res}\left[F(\varsigma), -jp_i/2\right] = \lim_{\varsigma \to -jp_i/2} (\varsigma + jp_i^{-1}/2)^2 \left[\prod_{p_i \in \tilde{\mathcal{P}}} \left(\frac{jp_i^{-1}/2}{\varsigma + jp_i^{-1}/2}\right)^2\right] (j\varsigma)^{-1}. \quad \text{(A.14)}$$

After some manipulation, the residue in (A.14) is evaluated as

$$\text{Res}\left[F(\varsigma), -jp_i/2\right] = 2j \sum_{j \in \tilde{\mathcal{P}}, j \neq i} \frac{1}{1 - p_i/p_j} \prod_{j \in \tilde{\mathcal{P}}, j \neq i} \frac{1}{(1 - p_j/p_i)^2} + j \prod_{j \in \tilde{\mathcal{P}}, j \neq i} \frac{1}{(1 - p_j/p_i)^2}. \quad \text{(A.15)}$$

Using the above result in (A.11) and (A.4), the PEP can be expressed as

$$P(\boldsymbol{\mathcal{D}}_L \to \tilde{\boldsymbol{\mathcal{D}}}_L) = 1 - \sum_{p_i \in \tilde{\mathcal{P}}, p_i < 0} \left(\prod_{p_j \in \tilde{\mathcal{P}}, p_j \neq p_i} \frac{1}{\left(1 - \frac{p_j}{p_i}\right)^2} + \frac{2}{\prod_{p_j \neq p_i} \left(1 - \frac{p_j}{p_i}\right)^2} \cdot \sum_{p_j \neq p_i} \frac{1}{\left(1 - \frac{p_i}{p_j}\right)} \right). \quad \text{(A.16)}$$